BUILDING A RED SEQUENCE IN COSMOLOGICAL HYDRODYNAMIC SIMULATIONS

by

Jared M. Gabor

A Dissertation Submitted to the Faculty of the

DEPARTMENT OF ASTRONOMY

In Partial Fulfillment of the Requirements
For the Degree of

DOCTOR OF PHILOSOPHY

In the Graduate College

THE UNIVERSITY OF ARIZONA

2011

THE UNIVERSITY OF ARIZONA
GRADUATE COLLEGE

As members of the Dissertation Committee, we certify that we have read the dissertation prepared by Jared M. Gabor entitled "Building a Red Sequence in Cosmological Hydrodynamic Simulations" and recommend that it be accepted as fulfilling the dissertation requirement for the Degree of Doctor of Philosophy.

_____ Date: 22 August 2011
Romeel Dave'

_____ Date: 22 August 2011
Chris Impey

_____ Date: 22 August 2011
Desika Narayanan

_____ Date: 22 August 2011
Rodger Thompson

_____ Date: 22 August 2011
Ann Zabludoff

Final approval and acceptance of this dissertation is contingent upon the candidate's submission of the final copies of the dissertation to the Graduate College.

I hereby certify that I have read this dissertation prepared under my direction and recommend that it be accepted as fulfilling the dissertation requirement.

_____ Date: 22 August 2011
Dissertation Director: Romeel Dave'

STATEMENT BY AUTHOR

This dissertation has been submitted in partial fulfillment of requirements for an advanced degree at The University of Arizona and is deposited in the University Library to be made available to borrowers under rules of the Library.

Brief quotations from this dissertation are allowable without special permission, provided that accurate acknowledgment of source is made. Requests for permission for extended quotation from or reproduction of this manuscript in whole or in part may be granted by the head of the major department or the Dean of the Graduate College when in his or her judgment the proposed use of the material is in the interests of scholarship. In all other instances, however, permission must be obtained from the author.

SIGNED: Jared M. Gabor

Acknowledgments

Thanks to everybody. You know who you are.

TABLE OF CONTENTS

TABLE OF CONTENTS — *Continued*

TABLE OF CONTENTS — *Continued*

LIST OF FIGURES

ABSTRACT

Despite years of study, the origins of red galaxies are not fully understood in a cosmological context. We develop new models for quenching star-formation and producing red galaxies in cosmological hydrodynamic simulations.

We start with phenomenological models applied in post-processing to previously-run simulations. We focus separately on mergers and hot haloes – akin to "quasar mode" and "radio mode" feedback – as the drivers shutting down star-formation. With appropriate parameter choices, each model can produce a reasonably good match observed color-magnitude diagrams and red galaxy luminosity functions at redshift zero. We uncover some difficulties with these models in general, including red galaxy stellar populations that appear too blue by 0.1 magnitudes in $g - r$ due to a metallicity deficit.

Building on the post-processing models, we develop quenching models for simulations that run on-the-fly. Again, we test merger quenching and hot halo quenching separately. We model merger feedback as > 1000 km s^{-1} winds motivated by observations of post-starburst galaxies, and we model hot halo feedback by continuously adding thermal energy to circum-galactic gas in haloes dominated by gas above $250,000$ K. Merger quenching temporarily shuts down star-formation, but merger-remnant galaxies typically resume star-formation with $1-2$ Gyrs thanks to accretion of new fuel from the IGM. Hot halo quenching successfully produces a realistic red sequence, providing a good match to the observed red galaxy luminosity function.

Despite some minor difficulties with hot halo quenching, we examine its effects in more detail. Specifically, we study the evolution of the simulated red sequence over time. We find that galaxies with stellar mass $\sim 10^{11} M_{\odot}$ are the

first to populate the red sequence at $z \gtrsim 2$, with significantly fewer red galaxies around $10^{10} M_{\odot}$ until $z \approx 0$. We show that massive galaxies grow substantially after moving onto the red sequence, primarily through minor mergers. We also examine the relationship between quenching and environment.

CHAPTER 1

INTRODUCTION

Ever since Hubble (1926), galaxies have been separated into two broad classes. Hubble initially classified galaxies according to their morphological appearance into spirals and ellipticals. Observations over the better part of a century have shown that this morphological classification correlates with other galaxy properties: optical color, mean stellar age, star-formation rate, gas content, and local environment (Schweizer & Seitzer, 1992; Strateva et al., 2001; Blanton et al., 2003; Kauffmann et al., 2003; Bell et al., 2004b; Dressler, 1980). Theoretical advances over the decades have developed into a mature industry that tries to explain the origins of galaxies, yet we still don't fully understand what processes lead to the two broad categories of galaxies. In this thesis we contribute to this understanding using cosmological hydrodynamic simulations.

1.1 A brief history of galaxy models

Two alternative ideas emerged from early debates about galaxy formation: monolithic collapse and hierarchical structure formation. In monolithic collapse, a cloud of gas forms in the primordial universe and collapses under gravity to form a galaxy over cosmic history (Eggen et al., 1962). In the hierarchical scenario, small galaxies form first then merge to build up larger and larger galaxies over time (Searle & Zinn, 1978).

As an understanding of cosmology improved, the hierarchical scenario gained favor with the (Λ) Cold Dark Matter (ΛCDM) model (Peebles, 1982; Blumenthal et al., 1984; Davis et al., 1985), and detailed analytic models of galaxy formation emerged (Rees & Ostriker, 1977; Silk, 1977; White & Rees, 1978; White & Frenk,

1991). These models form a basis for our current picture of galaxy formation. Initial density fluctuations (imprinted at recombination on the Cosmic Microwave Background) in the early universe grew under the influence of self-gravity (Press & Schechter, 1974), dominated by collisionless dark matter. The dark matter halos formed in this way played host to a proportion of gas that was able to cool via radiation, to collapse, and to form stars. As time went on, halos merged with one another to form ever larger structures.

The advent of fast computers enabled simulations of these processes. N-body gravitational simulations capture the growth of galaxy-sized structures and larger, which is dominated by gravity. Simulations visually revealed the large scale topography of the universe, including voids, filaments, sheets, and nodes where filaments intersect (Davis et al., 1985; White et al., 1987). Gravitationally bound, ellipsoidal, virialized dark matter halos form along filaments, with the largest present-day galaxy clusters forming at nodes. Since precision cosmology has nailed down most relevant parameters within a few percent (e.g. Komatsu et al., 2009), the dark matter dynamics are thought to be very robust. The greatest remaining uncertainties are in the more-complex baryonic physics.

With thousands of simulated halos from N-body simulations, theorists analytically model the behavior of gas and stars to come up with a statistical representation of the full galaxy population (in so-called semi-analytic models, or SAMs White & Frenk, 1991; Cole, 1991; Kauffmann et al., 1993; Cole et al., 1994). SAMs are relatively fast to compute, allowing for a broad, even statistical, exploration of parameter space. With enough input physics (including gas cooling, angular momentum conservation, star-formation, stellar and AGN feedback), they have successfully matched a variety of galaxy population observables from mass functions to black hole scaling relations (De Lucia et al., 2004; Bower et al., 2006;

Croton et al., 2006; Somerville et al., 2008). On the downside, the simplified models entering SAMs sometimes do not provide much physical insight into physical processes, and they can allow multiple acceptable fits to the data. For an example relevant to this thesis, consider "radio mode" AGN feedback. Different SAMs use different prescriptions, but they all effectively offset gas cooling in massive hot halos, and this leads to improved matches to color distributions and mass functions of galaxies (Bower et al., 2006; Croton et al., 2006; Cattaneo et al., 2006; Somerville et al., 2008).

A more computationally expensive approach involves calculating the gas dynamics along with the dark matter (e.g. Carlberg, 1984; Lake & Carlberg, 1988; Katz, 1989; Katz et al., 1992, 1996). Advantages with this technique include a full accounting of the distribution of gas, local calculation of baryonic physics like cooling and star-formation, and a lesser reliance on physical simplifications (e.g. spherical symmetry). These simulations must still rely on analytic prescriptions for things like star-formation and feedback (e.g. Katz et al., 1996; Springel & Hernquist, 2003; Oppenheimer & Davé, 2006), but they can be applied at the resolution limit rather than for a galaxy as whole as in SAMs. The computational tradeoff is a significant one, since parameters cannot be fully explored. In this work we use cosmological hydrodynamic simulations.

Another important approach has been the simulation of individual galaxy systems at high resolution. Perhaps the most famous and fruitful examples of this approach are galaxy merger simulations (Toomre & Toomre, 1972; White, 1978; Barnes, 1988; Hernquist, 1989; Barnes, 1990; Barnes & Hernquist, 1992; Cox et al., 2004; Bournaud et al., 2004; Springel et al., 2005; Cox et al., 2006b,a; Moster et al., 2011). In the hierarchical scenario of galaxy formation mergers, being frequent and perhaps the dominant mode of galaxy growth, play a critical role. Early

N-body work showed that spectacular tails observed in some "multiple galaxies" can be explained through the interaction process (Toomre & Toomre, 1972). Later simulations including gas dynamics and star formation indicate that mergers may induce starbursts and quasars, and transform disks into bulges (Barnes, 1990; Di Matteo et al., 2005; Springel et al., 2005; Bournaud et al., 2007; Teyssier et al., 2010).

Recent work suggests that the role of hierarchical merging may have been overstated, but monolithic collapse is not quite right either. In cosmological simulations, most galaxies are fed by cold streams of gas along filaments that are not virialised (Kereš et al., 2005, 2009; Dekel et al., 2009). Matter fuels galaxies smoothly and continuously, more so than in clumps or galaxies. Mergers still happen of course, and they may have dramatic results in transforming galaxies, but they do not dominate galaxy growth.

1.2 Why are red galaxies red?

As galaxy models have improved, coming closer to matching various observational constraints, one major theme has been to understand the galaxy bimodality first observed by Hubble. Star-forming disk galaxies are readily understood as the result of gas accumulation, dissipative cooling, and angular momentum conservation (Mo et al., 1998). Even an initially spherical gas cloud with nonzero angular momentum will tend to collapse under gravity into a disk. Radiative cooling allows the gas to lose energy but not angular momentum, so as it is drawn into smaller orbits it must continue to rotate in a preferred direction. Once the gas becomes dense enough it fragments and collapses to form stars. Simulations show that all halos are accreting new gas from the IGM (Kereš et al., 2009), so disk galaxies effectively never exhaust the available fuel for star-formation – the fuel

is constantly replenished. What remains, then, is to explain the elliptical galaxies, which have little rotation, little cold gas, and little star-formation.

Mergers have long been thought to transform galactic disks into ellipticals (e.g., Barnes, 1989, , see other references above). Although this depends on the relative masses, the orbital parameters, and the gas contents of the progenitors, it seems to be a robust theoretical conclusion. Since mergers are naively more likely when galaxies are closer together, they might help explain the correlation between morphology and local galaxy density (Zwicky, 1942; Dressler, 1980; Postman & Geller, 1984). Gas-rich major mergers may also induce starbursts and AGNs that both consume and expel the cold gas in the remnant, leaving behind a galaxy with no star-formation that is fated to redden as its stars age (e.g. Springel et al., 2005).

While mergers are the best explanation for transforming disks into spheroids, they may not be necessary to quench star-formation and turn galaxies red. As suggested by some SAMs (and as this thesis will argue), quenching by mergers may not be sufficient to explain the red galaxy population either, mainly because galaxies are constantly accreting new fuel from the IGM (Croton et al., 2006; Bower et al., 2006). An alternative quenching mechanism has been associated with the formation of hot, virialized halos of gas around massive galaxies (Dekel & Birnboim, 2006; Birnboim et al., 2007).

Since the early analytic galaxy formation models, hot gas coronae have been expected to form around galaxies. Conceptually, the gravitational potential energy of gas at a distance is converted into thermal energy when that gas is drawn to the center of a halo's potential well. One can imagine a gas cloud accreting onto an existing galaxy: the cloud, initially far away, will accelerate under the galaxy's gravitational pull. Once it reaches the galaxy, it will be traveling at a high speed

and create a powerful shock with gas in the galaxy. The shock ultimately thermalizes the cloud's kinetic energy, and the system can then be described by the virial theorem. This is the concept of the virial shock.

Radiative gas cooling complicates this picture by allowing energy to escape the system. Based on the halo densities and accretion rates in an ΛCDM universe, the cooling rates in small halos exceed the heating rate due to the virial shock. Simulations suggest that gas entering such halos is never heated up substantially, and never virialized. In more massive halos ($\gtrsim 10^{12} M_{\odot}$) the heating exceeds cooling, so that a reservoir of virial-temperature gas builds up (Birnboim & Dekel, 2003; Kereš et al., 2005, 2009). This forms a hot gaseous halo, or hot corona, around the galaxy. This process is thought to be the origin of million-Kelvin X-ray emitting gas in massive galaxy groups and clusters.

By shock-heating any in-falling gas at roughly the virial radius, the hot gas corona helps prevent, or at least stall, gas from getting onto galaxies to provide fuel for star-formation. In detail, cooling is still happening in these halos (especially if they have high central densities), and the cooling gas ought to be deposited on the central galaxy and fuel star-formation. This is related to the classic cooling flow problem in galaxy clusters (e.g. Fabian et al., 1984). If there is some heating source in the central regions of hot halos that can help maintain the gas in a hot state, it will prevent re-fueling of the galaxy. The galaxy will eventually consume any remaining fuel for star-formation and "starve." The required heating source is not immediately clear, but a radio AGN seems to be the most likely culprit (Burns, 1990; Binney & Tabor, 1995; McNamara et al., 2000; Fabian et al., 2003; Voit & Donahue, 2005; Fabian et al., 2006; Croton et al., 2006; Randall et al., 2010).

1.3 This work

Thus we have two main candidate quenching mechanisms, neither of which is properly implemented in cosmological hydrodynamic simulations. Simulations with large enough volumes to statistically sample the galaxy population cannot resolve the detailed structure of individual galaxies, so a proper treatment of gas conditions in galaxy mergers is presently impossible. The build-up of hot coronae around massive galaxies is a natural result of hydrodynamic simulations, yet in our simulations massive galaxies tend to grow too massive and continually form stars. Furthermore, we rely on sub-resolution models for star-formation and feedback, and critical uncertainties remain in such models (especially for the latter). Accretion and feedback by supermassive black holes remains highly uncertain, and only limited models have been tested in cosmological models (Di Matteo et al., 2008; Booth & Schaye, 2009, 2010).

In this thesis we test simplified models for quenching star-formation in cosmological hydrodynamic simulations. We focus on the two quenching mechanisms discussed above: quenching associated with major mergers, and quenching associated with hot gaseous halos. We avoid invoking AGN feedback directly, for several reasons. It is not clear that AGNs are the dominant heating source in either quenching mechanism. Furthermore, uncertainties in AGN physics make it difficult to determine the accuracy of any model. Instead, we focus on simplified models and extreme cases, taking a heuristic approach by asking what it takes to get a reasonable red sequence.

Chapter 2 serves as a series of plausibility tests for various quenching models in the simulations. We apply quenching prescriptions in post-processing (after a full simulation has run), which affords a degree of speed and adaptability. This approach can be seen as a bridge between hydrodynamic simulations and

SAMs. The basic result is that there are sufficient numbers of major mergers, and sufficient numbers of galaxies in massive hot halos, for either quenching mechanism to plausibly result in the observed luminosity functions at low-redshift. In Chapter 3 we construct quenching models that run on-the-fly during the simulations. By incorporating quenching into the simulations we get a full accounting of the gas. We show in this chapter that merger quenching alone does not succeed in producing a realistic red sequence because galaxies accrete new fuel for star-formation even after being quenched in a merger. A simple hot gas quenching model, on the other hand, produces red galaxies in numbers that match observations at $z = 0$. In Chapter 4 we examine the build-up over cosmic time of the red sequence in our favored hot gas quenching model. This highlights some qualitative trends for models like this, including that the first red galaxies tend to be the most massive galaxies in the universe at $z \gtrsim 2$, these red galaxies grow substantially over time via minor mergers with satellite galaxies, and low-mass red galaxies are necessarily in dense environments.

CHAPTER 2

HOW IS STAR FORMATION QUENCHED IN MASSIVE GALAXIES?

The bimodality in observed present-day galaxy colors has long been a challenge for hierarchical galaxy formation models, as it requires some physical process to quench (and keep quenched) star formation in massive galaxies. Here we examine phenomenological models of quenching by post-processing the star formation histories of galaxies from cosmological hydrodynamic simulations that reproduce observations of star-forming galaxies reasonably well. We consider recipes for quenching based on major mergers, halo mass thresholds, gas temperature thresholds, and variants thereof. We compare the resulting simulated star formation histories to observed $g - r$ colour-magnitude diagrams and red and blue luminosity functions from SDSS. The merger and halo mass quenching scenarios each yield a distinct red sequence and blue cloud of galaxies that are in broad agreement with data, albeit only under rather extreme assumptions. In detail, however, the simulated red sequence slope and amplitude in both scenarios are somewhat discrepant, perhaps traceable to low metallicities in simulated galaxies. Merger quenching produces more massive blue galaxies, earlier quenching, and more frosting of young stars; comparing to relevant data tends to favor merger over halo mass quenching. Although physically-motivated quenching models can produce a red sequence, interesting generic discrepancies remain that indicate that additional physics is required to reproduce the star formation and enrichment histories of red and dead galaxies.

2.1 Introduction

Galaxies in the local universe broadly fall into two main categories: blue star-forming disks typically found in lower-density environments, and red and "dead" ellipticals found in galaxy clusters. Some of the earliest extragalactic research revealed the two main morphological categories (e.g. Hubble, 1926), and later work uncovered relationships between morphologies and larger scale environments (Oemler, 1974; Davis & Geller, 1976; Dressler, 1980). More recent work employing data from large surveys has solidified a picture of galaxy bimodality, showing distinct divisions in galaxy colour (Strateva et al., 2001; Baldry et al., 2004; Balogh et al., 2004), which serves as a proxy for star formation rate per unit stellar mass. Surveys such as the Sloan Digital Sky Survey (SDSS) have characterized the statistics of red and blue galaxies to remarkable precision. Red spheroids dominate the massive galaxy population (with stellar masses above $\sim 10^{10.5} M_{\odot}$), while less massive galaxies tend to be star-forming disks (Kauffmann et al., 2003c), with luminosity functions showing that the relative fraction of red galaxies grows with luminosity. Surveys pushing to higher redshifts have robustly demonstrated that galaxy bimodality exists out to redshift $z = 1$ (Bell et al., 2004b; Weiner et al., 2005; Willmer et al., 2006), and possibly to $z = 2$ and beyond (Kriek et al., 2008; Taylor et al., 2009; Brammer et al., 2009). The properties and evolution of massive galaxies is one of the best-studied observational areas of extragalactic astronomy (e.g. Faber et al., 2007).

2.1.1 Why Is Quenching Needed?

Despite the accumulating wealth of data, the physical origin of the bimodality in galaxy properties remains poorly understood. Red passive galaxies evolve from blue star-forming ones, in the sense that galaxies dominated by old stars to-

day must have built up their stellar mass through star formation at early epochs. Early theories of galaxy formation proposed that primordial clouds of gas collapsed under gravity to form rotating discs that harbor star formation (e.g. Eggen et al., 1962). In hierarchical models, smaller galaxies then merge to build up larger ones (e.g. White & Rees, 1978). Such mergers are thought to be capable of transforming spirals into ellipticals through well-understood dynamical processes (Toomre & Toomre, 1972; Mihos & Hernquist, 1996), but it is less clear why this also results in a colour transformation from blue and star-forming to red and dead. Recent efforts to measure the global mass build-up of the red galaxy population over cosmic time strongly suggest this type of transformation. The total stellar mass in red galaxies has grown by roughly a factor of two since z$\sim$1, whereas blue galaxies have changed little (Bell et al., 2004b; Faber et al., 2007). Furthermore, evidence suggests the transition from blue to red is rapid, ~ 1 Gyr (Bell et al., 2004b; Blanton, 2006).

These data call for some mechanism(s) that "quench," or quickly shut off, star formation. Given the correlation between morphology and colour, such mechanisms (or related ones) must also lead to morphological transformation of disk-dominated galaxies into bulge-dominated ones, either through disruption or disk fading and bulge growth. Requiring that the star formation quenching occurs rapidly likely excludes the possibility that galaxies simply consume all of their available fuel supply. Even without the rapid quenching requirement, analytic arguments suggest that the dense central regions of hot halos should cool rapidly onto galaxies in so-called cooling flows, which are not observed. Furthermore, simulations show that (barring new physics) filaments in the intergalactic medium can also continuously feed galaxies with fresh supplies of cold gas (Kereš et al., 2009; Brooks et al., 2009). This implies that feedback associated with

star formation is unlikely to quench galaxies, since red and dead galaxies have no star formation yet must remain quenched over the majority of cosmic time. Hence some additional physical process is required to quench star formation.

2.1.2 Mechanisms that quench star formation

There have been a number of mechanisms proposed to provide quenching. Each mechanism either heats gas to the point where it cannot collapse to form stars ("preventative" feedback) or expels gas that would otherwise form stars ("ejective" feedback) (Kereš et al., 2009a). In this work, we focus on quenching in massive central galaxies, so we do not address mechanisms that may quench star formation in small satellite galaxies such as ram pressure or tidal stripping and "strangulation" (Gunn & Gott, 1972; Balogh et al., 2000).

One well-studied mechanism is virial shock heating of intergalactic gas falling into a galactic dark matter halo. As gas falls in toward the central galaxy, its gravitational energy converts to heat. In halos with masses above $\sim 10^{12}$ $M_{\odot}$, radiative cooling cannot keep up with gravitational heating, and a halo of hot virialized gas forms near the virial radius (Birnboim & Dekel, 2003; Kereš et al., 2005; Dekel & Birnboim, 2006). This hot halo shocks in-falling cold gas immediately to the viral temperature. Although it may succeed for $\sim$2 Gyr, virial shock heating alone cannot quench all star formation, since the hot halo gas should cool via radiation and condense to form stars in the centers of massive halos (Birnboim et al., 2007). Additional heating of the hot halo, perhaps by an active galactic nucleus (AGN; e.g. Croton et al., 2006) or gravitational heating due to clumpy accretion (Birnboim et al., 2007; Dekel & Birnboim, 2008; Dekel et al., 2009) could potentially prevent such cooling.

As alternatives to virial shock heating, various types of galaxy interactions show promise for transforming galaxies. High-velocity encounters between galax-

ies may cause minor distortions and disk heating. Major galaxy mergers tend to transform disks to ellipticals (Toomre & Toomre, 1972; Springel et al., 2005; Cox et al., 2006a), and the resulting shocks and intense star formation winds may expel or heat cold star-forming gas through shocks or feedback from supernovae (e.g. Cox et al., 2006b). Simulations show, however, that processes like supernova feedback are not enough to sufficiently stifle star formation (Springel et al., 2005). As with virial shock heating, some additional energy input is required.

A popular culprit to supply the necessary energy is the supermassive black hole thought to reside at the center of most massive galaxies (cf. Kormendy & Richstone, 1995; Richstone et al., 1998). When the black hole accretes material, the resulting AGN injects energy into its surroundings (e.g. McNamara et al., 2006), supplying the necessary heating and/or expulsion of gas. Croton et al. (2006) propose that cooling and accretion of hot halo gas triggers low-luminosity AGN at the centers of massive elliptical galaxies, visible as radio lobes. This so-called "radio mode" feedback adds enough energy to the surrounding hot halo to prevent further cooling and star formation.

In a merger-driven quenching scenario, Di Matteo et al. (2005) and Hopkins et al. (2006), among others, suggest that powerful AGN induced by galaxy mergers dump energy into the remnants of the gaseous galactic disk, effectively superheating and expelling it to prevent further star formation. This "quasar mode" feedback operates only in the aftermath of major mergers of gas-rich galaxies. An additional benefit of this high accretion rate mode, for which the phenomenon was originally investigated, is that it explains the existence of quasars and the relationships between black hole mass and bulge properties.

Observational evidence provides some support for a connection between AGN and galaxy evolution. Correlations between black hole mass and bulge properties

like mass and velocity dispersion helped motivate the concept of AGN fueling and self-regulation via feedback (Magorrian et al., 1998; Ferrarese & Merritt, 2000; Gebhardt et al., 2000; Tremaine et al., 2002). Furthermore, in both the local and distant universe, AGN have been associated with a transition in galaxies from blue to red (Sánchez et al., 2004; Silverman et al., 2008; Schawinski et al., 2009) and from disk-dominated to bulge-dominated (Kauffmann et al., 2003a; Grogin et al., 2005; Gabor et al., 2009).

A handful of alternative mechanisms have recently emerged that do not invoke AGN. Dekel et al. (2009) suggest that smooth cosmic gas accretion provokes instabilities in a galactic disk by building up its mass, whereas clumpy accretion suppresses instabilities via gravitational stirring. Clumps transfer gravitational energy to the disk, effectively heating it and suppressing star formation. Other mechanisms, such as cosmic ray heating (e.g. Mathews, 2009) and self-annihilation of dark matter particles (Totani, 2005), have not enjoyed as ample consideration in the recent literature.

2.1.3 Hierarchical models of red and dead galaxies

Several of these quenching mechanisms have been incorporated into semi-analytic models (SAMs) of hierarchical galaxy formation. These models start with pure N-body simulations of dark matter, then use the resulting dark matter halo population and merger history to build baryonic galaxies within them using physically-motivated prescriptions. SAMs enable great speed and flexibility to explore parameter space and compare the resulting observables to data, but the large numbers of assumptions and free parameters they employ make interpretation a challenge.

Empirically-constrained SAMs have enjoyed success at reproducing observations of massive galaxies at low redshift. The SAM of Croton et al. (2006)

based on the Millennium Simulation (Springel et al., 2005b) established a red sequence through mergers and disk instabilities, but required AGN feedback to prevent additional star-forming gas from cooling onto the most massive galaxies. This model successfully reproduced luminosity functions derived from 2dFGRS (Madgwick et al., 2002). Bower et al. (2006) improved on the "Durham" SAM (Cole et al., 2000; Benson et al., 2002; Baugh et al., 2005), which forms bulges as the result of strong disk instabilities, by incorporating black hole feedback in quasi-statically cooling halos. Along with matching low-redshift luminosity functions and colour distributions, the improved Durham model matches observed luminosity functions, mass functions, and the cosmic star formation rate density at redshifts $z < 2$ (Pozzetti et al., 2003; Drory et al., 2003). Taking a more analytical approach, Hopkins et al. (2008) adopt dark matter halo mass functions from simulations, populate halos with galaxies using halo occupation distribution models, and estimate merger rates among galaxies. By assuming that major mergers convert star-forming disk galaxies into spheroidal quiescent galaxies, these models are found to match mass functions and the integrated stellar mass density of quenched galaxies.

Overall, the general scenario that has enjoyed the most success is as follows: A major merger causes a transformation from a spiral to bulge-dominated system, while concurrently feeding a central black hole that shines briefly as a quasar and emits a small fraction of its accreted mass-energy back into the galaxy. This causes a rapid truncation of star formation by driving a large fraction of star-forming gas from the galaxy, forming a red and dead elliptical. After the transformation, eventually a cooling flow forms, allowing low angular momentum gas to feed the black hole. This triggers a low-luminosity AGN which deposits energy into the surrounding hot gaseous halo. This shuts off the cooling flow, which in turn

shuts off the AGN, and the cycle restarts. SAMs incorporating this scenario can explain observed correlations between galaxy morphology, colour, stellar age, bulge mass, and black hole mass.

Recently, the growth of and feedback from black holes have been incorporated into hydrodynamic cosmological simulations (Di Matteo et al., 2008; Booth & Schaye, 2009). At substantial computational expense, these simulations combine with N-body dynamics the complex three-dimensional dynamics of gas inflow and outflow responsible for establishing galaxy properties. Such simulations employ parameters for sub-grid physical processes associated star formation, galactic winds, and feedback from black holes, but bypass many additional parameters for treating gas dynamics as are required in SAMs.

Simulations incorporating AGN feedback have showed early promise by reproducing properties of the black hole and AGN and galaxy populations (Colberg & Di Matteo, 2008; Croft et al., 2009; Degraf et al., 2010; Booth & Schaye, 2009), along with the global cosmic star formation history (Schaye et al., 2009). However, the implementation of AGN feedback is quite heuristic, and some assumptions such as spherical input of AGN feedback energy seem dubious at face value. Hence like with SAMs, it is premature to regard these models as fully physical descriptions of black hole and galaxy co-evolution.

In this paper, we take an approach that might be considered as a hybrid between simulations and SAMs. We begin with galaxy star formation histories (SFHs) taken from cosmological hydrodynamic simulations, and then apply quenching recipes by post-processing the SFHs to see which recipe(s) best match observations of massive galaxies. This retains the rapid computational flexibility of SAMs by allowing us to explore parameter space without re-running expensive simulations, while still employing star formation histories of galaxies that are

described by fully hydrodynamic simulations up until quenching. We compare our simulated quenched galaxies to observed colour-magnitude diagrams and luminosity functions in the local universe, focusing on the massive (and bright) galaxy population since these are well-observed, since the largest discrepancies in existing models are found there, and since it is where the bimodality is most pronounced. This approach avoids any explicit reference to the physical mechanisms of quenching, e.g. it does not explicitly account for growth and feedback from black holes, and instead focuses on asking the question: Which aspects of galaxy and halo evolution govern quenching in massive galaxies?

Our paper is organized as follows. §2.2 describes our base cosmological hydrodynamic simulation employed in this work. §2.3 details how we post-process the SFHs under various proposed quenching mechanisms. We then compare the resulting galaxy properties to data as described in §2.4. Our results, in §2.5, suggest that several quenching mechanisms can indeed qualitatively reproduce a red sequence, but they all fail to exactly match observations in sometimes subtle ways. We devote much of our discussion in §2.6.4 to understanding the failures of these models, with an eye toward what new aspects may be required to improve agreement. Finally, we summarize in §2.7.

2.2 Simulations

2.2.1 Input physics

We run simulations using a modified version of the N-body + Smoothed Particle Hydrodynamics (SPH) code GADGET-2 (Springel, 2005) described in Oppenheimer & Davé (2008). In essence, SPH is a Lagrangian implementation of hydrodynamics where particles represent fluid elements, and each particle's density and temperature are determined by kernel averages over its nearest neighbors.

GADGET-2 computes gravitational forces between particles using a tree-particle-mesh algorithm, and employs an entropy-conserving SPH formulation to compute pressures and densities of the gas. The code tracks three distinct types of particle — dark matter, gas (or SPH), and star — including positions, velocities, and masses, as well as temperatures, densities, and metallicities as appropriate.

GADGET-2 incorporates a mechanism for gas particles to spawn star particles stochastically. This mechanism, based on an analytic two-phase model of the interstellar medium with cold dense clouds embedded in a diffuse ionized gas (Springel & Hernquist, 2003), operates on scales not resolved by the simulations. The model assumes that each gas particle that is sufficiently dense to be Jeans unstable contains a hot ambient medium, cold clouds, and stars which form within the cold clouds, and the phases exchange mass, energy, and metals via condensation and supernovae energy input (McKee & Ostriker, 1977). The resulting star formation rate (SFR) in the cold clouds is calculated assuming a Schmidt (1959) law. A gas particle with a positive SFR will spawn a star particle with a mass, M_*, with some probability determined by the SFR. Any newly spawned star particle inherits the position, velocity, and metallicity of its parent gas particle, whose mass is reduced by M_*. We use $M_* = 0.5 M_{\rm gas}$, the initial mass of a gas particle. On average, a gas particle can spawn up to two star particles, but this varies because gas particles can acquire additional gas mass from nearby stellar evolution (see below). Springel & Hernquist (2003) have reduced this model to a single free parameter: the characteristic time-scale over which cold clouds convert into stars at the threshold density, which is set to 2.1 Gyrs in order to match the observed Kennicutt relation (Kennicutt, 1998).

Galactic outflows driven by star formation are implemented in a similarly stochastic fashion. Our model, first introduced by Springel & Hernquist (2003),

ejects star-forming particles from galaxies by kicking them with a velocity v_w. The probability for ejection is set by the mass loading factor η (i.e. the mass loss rate relative to the star formation rate) times the star formation probability for that particle. The simulation used here employs our favored momentum-driven wind scalings (Murray et al., 2005) as described in Oppenheimer & Davé (2006) and Oppenheimer & Davé (2008), and motivated by observations of local winds by Martin (2005) and Rupke et al. (2005). In these scalings, v_w is proportional, and η is inversely proportional, to the galaxy circular velocity. We also decouple the winds hydrodynamically until they reach a density 0.1 times the critical density for star formation (up to a maximum duration of 20 kpc/v_w) in order to mock up chimneys through which outflowing gas can escape but that are poorly treated by the spherically-averaging SPH algorithm. Both outflows and star formation are to be regarded as Monte Carlo prescriptions, in which individual events are not by themselves meaningful; resolution convergence tests (e.g. Finlator et al., 2006) have shown that once 64 star particles are formed within a galaxy, then its star formation history is fairly stable and well-resolved. We use this as our galaxy (stellar) mass resolution limit.

More recent improvements in Oppenheimer & Davé (2008) include a sophisticated chemical enrichment model, Type Ia supernovae, and stellar mass loss. We track carbon, oxygen, silicon, and iron individually, with yields taken from various works. Type Ia SNe rates are taken from Scannapieco & Bildsten (2005), with a prompt and delayed component, and these inject energy and metals (predominantly iron) into surrounding gas. We also track mass loss from AGB stars (using models of Bruzual & Charlot, 2003, ; BC03), injecting metal-enriched mass (but no energy) to the nearest three gas particles. Generally, these "delayed feedback" mechanisms become more important at later epochs, which will be less of a con-

cern for us in this work since the quenching of star formation in massive galaxies typically occurs relatively early on.

The momentum-driven outflow scalings, together with hydrodynamic decoupling, have resulted in our simulations broadly matching a wide range of galaxy and intergalactic medium properties. These include the chemical enrichment of the $z \sim 2-6$ IGM (Oppenheimer & Davé, 2006, 2008), the galaxy mass-metallicity relation (Davé et al., 2007; Finlator & Davé, 2008), and high-z galaxy luminosity functions (Davé et al., 2006; Finlator et al., 2007). As such, while our model is not an ab initio description of galactic outflows, it appears to modulate the SFHs of star-forming galaxies in broad accord with observations. Hence our simulations provides a plausible starting point for studying the quenching of star formation across cosmic time.

2.2.2 Simulation parameters

The simulation we employ here begins at redshift $z = 99$ with 512^3 dark matter particles and 512^3 gas particles in a cube of comoving side length $l_{\rm box} = 96h^{-1}$ Mpc with periodic boundary conditions, and is evolved to $z = 0$. The volume of this simulation allows us to sample large galaxies in high-density environments (with halo mass up to $\sim 10^{14.5} M_\odot$), while also providing the dynamic range to resolve galaxies well fainter than the knee of the luminosity function. With a mass resolution of $1.2\times10^8\ M_\odot$ per gas particle, we can resolve galaxies with stellar masses $\geq 3.8\times10^9 M_\odot$. We employ a WMAP-5 concordance cosmology (Komatsu et al., 2009) with $H_0 \equiv 100h = 70$ km s^{-1} Mpc^{-1}, matter density $\Omega_m = 0.28$, baryon density $\Omega_b = 0.046$, a cosmological constant with $\Omega_\Lambda = 0.72$, root mean square mass fluctuation at separations of 8 Mpc $\sigma_8 = 0.82$, and a spectral index of $n = 0.96$.

2.2.3 Simulation outputs and analysis tools

We configure GADGET-2 to output simulation "snapshots" at 108 redshifts, starting at $z = 30$ and ending at $z = 0$. The proper time between snapshots ranges from ~ 50 Myr at $z \sim 6$ to ~ 330 Myr at $z \sim 0$. The snapshots contain information for each dark matter, gas, and star particle in the simulation, including position, velocity, mass, metallicity (for gas and star particles), density and temperature (for gas particles), and time of formation (for star particles). We also store auxiliary information such as star formation rates and carbon, oxygen, silicon, and iron abundances.

From this basic information we identify and extract properties of dark matter halos and galaxies. We use SKID (Spline Kernel Interpolative DENMAX; http://www-hpcc.astro.washington.edu/tools/skid.html) to identify gravitationally-bound groups of star-forming gas and star particles that comprise a galaxy. Halos are identified using a spherical overdensity (SO) algorithm. Beginning at the most bound particles within SKID-identified galaxies, halos are expanded radially until they reach the virial overdensity threshold. Smaller halos whose centers lie within the virial radius of larger ones are subsumed, while halos whose virial regions overlap but whose centers lie outside each others' virial regions divvy up the particles according which center is closer as scaled by their virial radii. In the end, each halo has at least one galaxy by construction, and each particle belongs to not more than one halo. From these identified galaxies and halos, we calculate quantities such as masses, star formation rates, and metallicities by summing over all member particles.

The star particles within a SKID galaxy are tagged with formation time and metallicity, and hence provide a series of single stellar populations (SSPs) from which one can construct the star formation and chemical enrichment history of

each galaxy. This allows us to calculate galaxy spectra using the high-resolution grid in the stellar population synthesis models of Bruzual & Charlot (2003). We then measure photometric magnitudes by convolving the galaxy spectra with broad-band filter curves. The code optionally computes extinction due to dust in the galaxy; we explore the effects of different dust models in §2.5.5. Since we mainly focus on red sequence galaxies where dust extinction is negligible (e.g. Lauer et al., 2005), our dust prescription does not strongly impact our results.

2.3 Post-processed quenching

For each simulated galaxy we compile a star formation history to $z = 0$. Hence we can test models for quenching by modifying that SFH in post-processing, based on some set of prescribed rules. This approach allows us to assess to first order the feasibility of a wide range of quenching mechanisms in a short amount of time, without the additional computational costs associated with building those mechanisms directly into the simulations. To describe our quenching models in detail, we first present a general explanation of the quenching process, and then give examples of the implementation for each quenching mechanism.

Since we determine properties like galaxy stellar masses and broad-band luminosities from groups of simulated star particles, we can mimic the effects of quenching simply by removing star particles from consideration when extracting these bulk properties. Thus, at each snapshot, we examine the conditions under which each new star particle formed. If these conditions match the quenching condition, then we flag that star particle to indicate that it never should have formed. With this flag, we track the quenched star particle through all subsequent time steps. Finally, when we extract a galaxy's stellar mass and luminosity (at any particular output time step), we ignore any star particles which have been

flagged as quenched.

This method has the obvious disadvantage that any gas which forms into a quenched star particle will be locked up in that phantom star particle (i.e. a star particle that never should have formed), rather than remaining in its gaseous state to be tracked dynamically by the simulation. Furthermore, the additional feedback energy associated with quenching could have an impact on the surrounding gas that subsequently forms stars, which our post-processing technique cannot account for. Physically, one can view this material as having been heated or expelled in such a way so that it is unable to return to a cool star-forming state within a Hubble time, and also does not interact significantly with other infalling gas or galaxies. Clearly this cannot be true in detail, but this approach can still give useful first-order insights. Hence while this method has the advantage of computational flexibility and speed, a fully self-consistent quenching mechanism must be incorporated into the simulations dynamically in order to properly assess all effects; this is under development.

We study quenching mechanisms that have been recently considered in the literature. Namely, we specify conditions under which star formation should be quenched using three different models: (i) quenching induced by galaxy mergers, (ii) quenching by virial shock heating in massive dark matter halos, and (iii) quenching due to the inability of gas shocked above a critical temperature and/or expelled in a wind to cool. For each of these mechanisms, we define a quenching condition based on an event or property that we can extract from the simulations. Then we ignore star particles whose formation satisfies the quenching condition, as described above. We refer to this as quenching the star particle.

2.3.1 Quenching via galaxy mergers

As mentioned above, various works have suggested that feedback from intense star formation and AGN activity induced by galaxy mergers can heat and expel the cold gas from merger remnants, rapidly halting star formation. We apply this hypothesis to the simulations by quenching star formation in galaxy merger remnants. To do this, we first identify remnants of major mergers by tracing growth in galaxy stellar mass. For each galaxy in a given output time step t_c, we identify its most massive progenitor galaxy in the most recent time step t_p ($t_c > t_p$, and these times represent the age of the universe at the corresponding time step). If the galaxy and its progenitor have stellar masses M_* and M_p, respectively, then a major merger occurred in the last timestep if $M_* = M_p(1 + 1/r)$, where r is the critical mass ratio that separates major and minor mergers. We use the typical value $r = 3$ (Dasyra et al., 2006; Woods et al., 2006; Hopkins et al., 2008) and a more extreme $r = 4$, and also require that the remnant be well-resolved in our simulation, with $M_* > 3.84 \times 10^9 M_\odot$. Note that since galaxies also grow by star formation, this merging criterion can be considered conservative in the sense that the actual merger ratio is probably higher (i.e. r is larger) than the assumed value.

Motivated by recent work suggesting that remnants of galaxy mergers may re-form into star-forming disks (Springel & Hernquist, 2005; Robertson et al., 2006; Governato et al., 2007, 2009; Hopkins et al., 2009), we incorporate an additional parameter, $f_{\rm gas}$. We assume that any merger remnant with a gas fraction $M_{\rm gas}/(M_{\rm gas} + M_{\rm stars}) > f_{\rm gas}$ re-forms into a disk galaxy, and therefore is not quenched. If a galaxy meets the quenching conditions, then we set its most recent merger time, $t_{\rm merge} = t_p$. We track $t_{\rm merge}$ for all galaxies through the evolution of the simulation. At any given time step, galaxies inherit $t_{\rm merge}$ from their most massive progenitors of the previous time step. Note that in some cases, merger

remnants that are absorbed by larger galaxies can effectively lose their remnant status; this is fairly rare except at the earliest epochs.

After identifying merger remnant galaxies, we quench any star particle that forms in such a galaxy at a time $t_{\rm form} > t_{\rm merge}$ Since the simulations track the time of formation $t_{\rm form}$ for each star particle and our tools match star particles to galaxies, we can easily identify those star particles to be quenched. Our model assumes that, barring a subsequent merger with a larger galaxy, a merger remnant will never recover from whatever quenching process occurs. That is, we maximally halt all future star formation, ignoring the possibility that cold gas later accretes onto the remnant to rejuvenate star formation. A more physically accurate model might account for the initial heating of gas in the galaxy during the merger, then permit cooling as part of the subsequent evolution. Some authors (e.g. Croton et al., 2006) have proposed that heating due to an intermittent AGN prevents later cooling and star formation; we implicitly assume that such a process operates to keeps merger remnants quenched.

2.3.2 Halo Mass Quenching

Some authors (Birnboim et al., 2007; Dekel & Birnboim, 2008; Dekel et al., 2009) have proposed that hot gas in massive dark matter halos can halt the accretion of gas onto galaxies, cutting off the fuel for star formation. As gas falls toward the center of the dark matter potential well, gravitational energy converts to thermal energy, heating the gas to temperatures near the virial temperature. In halos with masses $M_h \lesssim 10^{11.4-12} M_\odot$, rapid cooling prevent the virial shock from being supported, but in halos above that mass a stable hot gas envelope can form (Birnboim & Dekel, 2003; Kereš et al., 2005, 2009). The virial shock rapidly heats any further infalling gas, stifling accretion of cold gas onto galaxies and thus quenching star formation. This mechanism effectively quenches star formation in dark matter

halos with $M_h > M_c$, where $M_c \sim 10^{12} M_\odot$.

The X-ray emission from intracluster gas around massive galaxies indicate that the gas is cooling at rates of tens or hundreds of $M_\odot$ per year. However, young stars and reservoirs of cool gas where the cooling flow might be deposited have not been observed (the cooling flow problem; see Peterson & Fabian, 2006, for review), suggesting that an additional long-term heating mechanism acts near the halo center. Low-luminosity AGN could in principle provide this heating (Croton et al., 2006), but the details of the heating process are poorly understood. Some works suggest that AGN jets generate pressure waves or magnetic fields within intracluster gas to isotropize energy input (e.g. Ruszkowski et al., 2004a,?; Brüggen et al., 2005), though it is not clear that such processes can operate in more typical-sized halos.

Birnboim et al. (2007) suggest a scenario in which dark matter halos that reach M_c abruptly form a rapidly expanding shock, heating the supply of infalling gas and quenching star formation for ~ 2 Gyrs. Eventually the shock slows, the halo stabilizes, and $\sim 10^{11} M_\odot$ of gas quickly cools and initiates a starburst, followed by a long-term quiescence. This can quench star formation in galaxies residing in groups, but galaxies in massive clusters require additional heating from AGN or clumpy accretion to prevent recurrent star formation.

In this paper, we explicitly avoid reference to any particular physics of halo quenching, but are rather interested in generally testing whether quenching based on some halo mass threshold can match observations of passive galaxies. We therefore adopt a simple approach in which no stars can form in halos above M_c. To model this process in the simulations, we first identify all dark matter halos with $M_h > M_c$ in a given output time step. Then we quench any star particle which formed in one of those halos within the most recent time step. Again, since

the simulations and analysis tools track the time of formation and corresponding dark matter halo of each star particle, we can straightforwardly identify star particles to be quenched. We treat M_c as a free parameter when comparing with observations, testing plausible values in the range $M_c = 10^{11.5-12.5} M_\odot$.

This procedure implicitly quenches star formation in all galaxies in the dark matter halo, including both dominant (or central) and satellite galaxies. Therefore, when a small galaxy falls into a massive halo, we immediately truncate its star formation rather than allowing a slow decline like that expected for "strangulation" (e.g. Simha et al., 2009). Although the abruptness of this truncation does not reflect realistic galaxy infall to clusters (Balogh et al., 2000), we are primarily interested in the population of massive central galaxies that dominate the bright end of the red sequence today. We discuss variants of this mechanism, including quenching only central galaxies, in §2.5.4.

2.3.3 Quenching of hot mode and wind mode

Galaxies in simulations show two main paths in density-temperature space for acquiring gas to fuel star formation (Binney, 1977; Birnboim & Dekel, 2003; Kereš et al., 2005): Hot mode, in which gas heats to near the virial temperature of the halo before cooling to form stars; and cold mode, in which gas never gets significantly above $\sim 10^5$ K and radiates most of its gravitational potential energy in Lyman alpha emission (Fardal et al., 2001; Yang et al., 2006). Recently, Oppenheimer et al. (2010) introduced recycled wind accretion, or "wind mode", as a third accretion path. Wind mode constitutes gas that was previously ejected from a galaxy, and has been re-accreted to form stars, and in our simulations with plausible outflows models it dominates the cosmic accretion budget, particularly in massive galaxies, at $z \lesssim 1$.

In either the hot mode or wind mode cases, it is conceivable that the gas

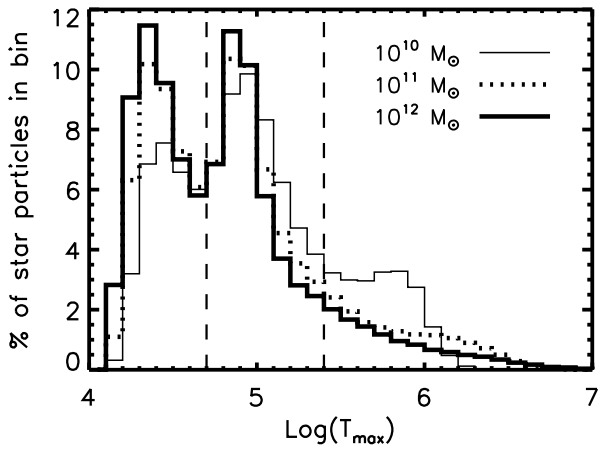

Figure 2.1 Distribution of $T_{\rm max}$ for simulated star particles in galaxies with stellar masses in three mass bins: 10^{10}–$10^{10.1}, 10^{11}$ – $10^{11.1}, 10^{12}$–$10^{12.1} M_{\odot}$. All masses show two distinct peaks, with a low shoulder or tail to high temperatures. Vertical dashed lines show our two separate choices of the critical $T_{\rm max}$ above which star particles will be quenched.

should never re-accrete. This could be owing to some heat source that keeps hot halos energized, as hypothesized in Kereš et al. (2005) and Dekel & Birnboim (2006), or else it could be because there are numerical difficulties in handling two-phase media and cold clumps in SPH (Agertz et al., 2007) by which accretion is over-estimated. Indeed, Kereš et al. (2009) found that the amount of hot mode accretion in entropy-conserving SPH is far less than in previous version of SPH, highlighting the numerical uncertainties involved. Oppenheimer et al. (2010) also speculates that wind mode should never re-accrete, again owing to numerical issues of cold clumps moving through hot halo gas. It is conceivable that, since hot mode and wind mode are preferentially more important in larger systems, that simply removing such accretion modes could yield a bimodality with a clear red sequence.

Our simulations track a parameter $T_{\rm max}$ corresponding to the highest temperature achieved by that particle in its history before entering a galaxy. The simulations stop updating $T_{\rm max}$ for gas particles ejected from galaxies via winds, even if they are heated above the previous maximum value. When a gas particle stochastically spawns a star particle, the star particle inherits its parent's $T_{\rm max}$ at the time of spawning, retaining it for the remainder of the simulation. We thus track the maximum temperature achieved by the gas which formed any given star particle. To quench hot mode, we simply assume that any gas particle heated above some critical temperature, T_c, can never cool to form stars. For this mechanism, we simply identify and quench any star particles with $T_{\rm max} > T_c$.

Figure 2.1 shows the distribution of $T_{\rm max}$ for all star particles in galaxies in three different stellar mass bins: $M_* = 10^{10}, 10^{11}, 10^{12} M_\odot$. Each distribution shows two distinct peaks (at $\log T \simeq 4.4$ and 4.9) and a tail to higher temperatures. The low-temperature peak is from gas that has never been substantially

heated, and the high-temperature peak comes from warmer gas that then cools to form stars. The peaks are associated with hydrogen cooling and helium cooling, respectively (cf. Sutherland & Dopita, 1993). Mild shocks during accretion likely heat the warm component, while the colder component somehow avoids such shocks. Somewhat counter-intuitively, Kereš et al. (2009) found that both low and high mass galaxies form predominantly through cold mode, and that intermediate mass systems ($M_{\rm baryon} \approx 5 \times 10^{10} M_{\odot}$) have the highest hot mode fraction. In the high mass case, it is because large galaxies assemble from lower-mass galaxies that formed early on mainly via cold mode accretion. Based on this plot, we explore critical values of $\log T_c = 4.7, 5.4$ (shown as vertical dashed lines), though it turns out that the results are not very sensitive to this choice.

Since most of the high-temperature gas is heated via virial shocks, one might expect these results to mimic those of the virial shock heating prescription in §2.3.2. In many halos, however, cold flows of gas from the IGM (particularly at early epochs) can penetrate the hot envelope to feed the central galaxy directly, so the quenching is not complete (Kereš et al., 2005, 2009). Our results in §2.5.3 indeed suggest that cold flows are a significant factor in ongoing star formation in massive galaxies.

Quenching wind mode is also straightforward, since we track which gas particles have been ejected in a wind, and this information is passed on to spawned star particles (see Oppenheimer et al., 2010, for implementation details). Certainly, it is the case that at least some material that participated in an outflow (particularly at early epochs when outflows were most prominent) is likely to have fallen back into a galaxy at late times. Here, we make the most extreme assumption that none of it ever falls back.

2.4 Observational Constraints

The ultimate goal of this study (and others like it) is to build a model for galaxy evolution that matches observed global distributions of galaxy properties. Accordingly, we compare the results of our simulations to well-studied quantities of the low-redshift ($z < 0.1$) galaxy population, primarily based on measured luminosities. We focus on colour-magnitude diagrams (CMDs) and luminosity functions (LFs). Of course, a litany of other observations could provide additional detailed constraints, such as luminosity- and colour-dependent correlation functions (Zehavi et al., 2005; Weinmann et al., 2006; Cooper et al., 2006; Phleps et al., 2006; Cooper et al., 2007; Coil et al., 2008; Brown et al., 2008; Williams et al., 2009; Cooper et al., 2009), properties of post-starburst galaxies (Zabludoff et al., 1996; Quintero et al., 2004; Blake et al., 2004; Balogh et al., 2005; Yang et al., 2008), the total star formation history of the universe (e.g. Hopkins & Beacom, 2006; Thompson et al., 2001, 2006), the star formation intensity distribution of galaxies (Thompson, 2002), and other observations of galaxy properties at higher redshifts. Given the challenges that even low-redshift CMDs and LFs present to our models, we defer more detailed comparisons to future work.

We use the Value-Added Galaxy Catalog (VAGC; Blanton et al., 2005) of the Sloan Digital Sky Survey (Adelman-McCarthy et al., 2008; Padmanabhan et al., 2008) for comparison to our simulations. The DR6 version of the VAGC includes k-corrected absolute magnitudes in the SDSS ugriz + JHK bands for more than 2.6 million galaxies, including a special low-redshift sample of ∼170,000 galaxies with distances of 10 h^{-1} Mpc to 150 h^{-1} Mpc (redshifts roughly 0.003 to 0.05). Because the low-redshift sample's volume is roughly comparable to (though larger than) the volume of our simulations, we use it (rather than the full VAGC) to provide observational constraints on our models. We convert the reported absolute

magnitudes (which use $h = 1$) to our preferred cosmology (with $h = 0.70$) with $M_{h=.7} = M_{h=1} + 5\log(0.7)$. Colors are then straightforward, and we compute luminosity functions using the $1/V_{\rm max}$ method (Schmidt, 1968) and the $V_{\rm max}$ values presented in the VAGC.

Because it effectively traces stellar mass, we plot r-band absolute magnitudes in most of our plots, and we use $g-r$ colors for CMDs. We compare observations with results from our simulation snapshots at $z = 0.025$, chosen to fall in the middle of the observed low-redshift VAGC range, though the simulation results are insignificantly different at $z = 0$. We refer to redshift 0.025 as $z \approx 0$, or "low-redshift," throughout the remainder of the paper.

Stellar masses for galaxies in SDSS (including those in VAGC) were determined by Kauffmann et al. (2003), using template fits to spectra including the effects of dust extinction. We cross-correlate these publicly available data with the VAGC catalog to obtain stellar masses for our comparison galaxy sample.

2.5 Results

To begin, we illustrate the current state of galaxy formation in cosmological hydrodynamics simulations without quenching in Figure 2.2. This shows CMDs (top) and LFs (bottom) for our simulations compared with observations from SDSS. We separate blue galaxies from red using a solid line drawn in the CMD, and we show a best-fit to the SDSS red sequence as a dot-dashed line (see below). Our mass resolution produces a diagonal envelope in the bottom right of the CMD panel, corresponding roughly to $r \sim -20$. This cutoff affects the blue galaxy LF fainter than $r \sim -20.5$, although the red galaxy LF is not impacted within our plotting range, brighter than $r = -20$. This simulation fails to produce massive red and dead galaxies as observed. Almost all galaxies occupying the red

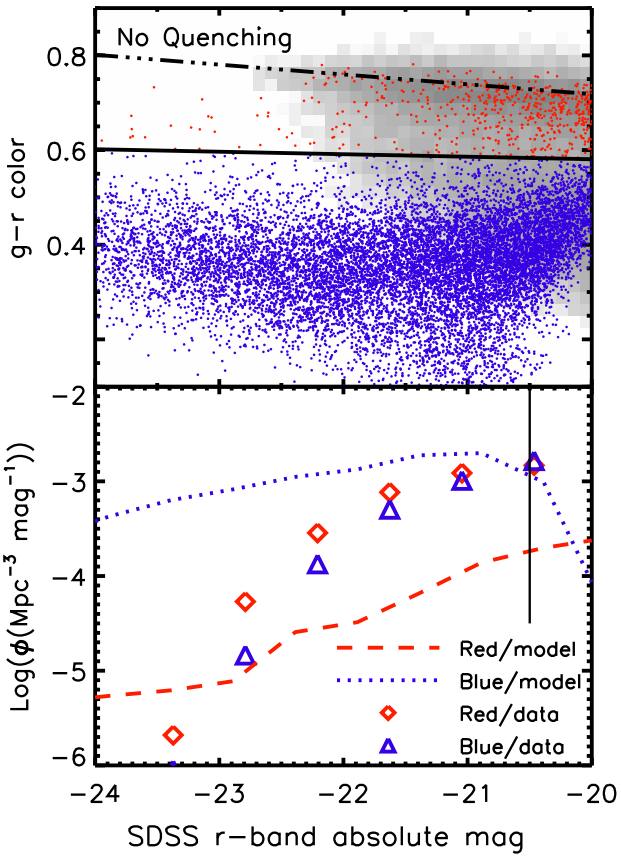

Figure 2.2 Colour-magnitude diagram in $g-r$ vs. r (top panel) and r-band luminosity functions (bottom panel) for our original simulation without quenching, compared to data from the SDSS VAGC. The solid line separates blue and red galaxies in the simulations, and the dot-dashed line shows a best-fit to the SDSS red sequence (see §2.5.1). Greyscale in top panel shows SDSS VAGC galaxy density scaled logarithmically, and colour-coded points show simulated galaxies. In bottom panel, symbols represent SDSS VAGC data, split into blue (blue triangles) and red (red diamonds) galaxies. Lines show simulated luminosity functions for blue (blue dotted) and red (red dashed) galaxies. Our mass resolution cutoff corresponds to a diagonal envelope in the CMD at about $r = -20$, and the cutoff affects our luminosity functions fainter than $r \sim -20.5$ (vertical solid line). Without quenching, our simulation produces too many bright blue galaxies, and almost no bright red ones.

sequence regime are low-mass satellites that have been quenched primarily via strangulation (see e.g. Simha et al., 2009), with just a few massive systems that are a red extension of the blue cloud, without evidence for a distinct bimodality.

We reiterate that this simulation includes strong galactic outflows from star-forming galaxies. Clearly, even such fairly energetic feedback is insufficient to quench star formation in massive galaxies. Galaxies almost always have supplies of gas to fuel new star formation, Galaxies accrete cold gas from the IGM through filaments of the cosmic web (cf. Kereš et al., 2009), and hot gas in galactic halos may cool onto the central galaxies. In our simulations, much of the accreting gas today is recycled from earlier galactic winds expelled from the galaxy (Oppenheimer et al., 2010). This illustrates that some other physical process must quench star formation in massive galaxies.

When calculating galaxy magnitudes, we neglect the effects of dust to highlight the intrinsic red sequence, i.e. the red sequence made up solely of galaxies with old stellar populations. Red galaxies without ongoing star formation contain little enough dust that we can neglect dust effects on colors for the intrinsic red sequence. Although dust tends to redden star-forming galaxies from the blue cloud, observations suggest only ~ 10–20% of the red sequence comes from such galaxies (Bell et al., 2004a; Brammer et al., 2009). In §2.5.5 we will explore dust effects on the population of star-forming blue cloud galaxies.

In the following three sections, we present CMDs and LFs for merger-based quenching, halo mass quenching based on a critical halo mass, and accretion mode quenching. We focus on the intrinsic red sequence successfully generated in the first two models, exploring some properties of the red galaxy populations formed. Because of its sensitivity to dust, we defer discussion of the blue cloud to §2.5.5.

2.5.1 Merger quenching

Figure 2.3 shows the results of our merger quenching prescription with a mass ratio of 3:1 ($r = 3$) with $f_{\rm gas} = 0.6, 1$ (top two panels) and $r = 4$ with $f_{\rm gas} = 1$ (third panel). CMDs in all cases exhibit a distinct red sequence with a shallow but nonzero slope, and a tail of bright red galaxies, qualitatively in agreement with observations. However, the LF for the $f_{\rm gas} = 0.6$ case shows a significant excess of very bright red galaxies, which is only partly mitigated in the $f_{\rm gas} = 1$ case. Note that these are quite high gas fractions: Disk galaxies like the Milky Way today have gas fractions well below 0.6, and even at high-z one has to go to $M_* <\sim 10^{10} M_\odot$ to get typical gas fractions as high as 50% (Erb et al., 2006). Our results prefer *never* re-forming a star-forming disk once a major merger happens. Since hydrodynamic simulations without AGN clearly show that a disk re-forms even with more modest gas fractions (e.g. Robertson et al., 2006; Governato et al., 2009), this implies that for this quenching mechanism to work, something must heat or eject all the gas such that it not only stops forming stars at that time, but prevents the re-formation of a gaseous disk.

In the third panel we make the model even more extreme by quenching star formation after all 1:4 mergers, regardless of gas content. This has only a minor impact on the resulting CMD (relative the 1:3 case). It decreases the number of very bright galaxies, which mitigates the discrepancy there, at the expense of worsening the agreement for moderately bright galaxies.

The LF shows a related problem that all merger models fail to produce a sufficiently sharp knee at a characteristic magnitude M^* as seen in the data. The model can reasonably match the number of galaxies at the low-luminosity end, but it over-produces bright galaxies and under-produces galaxies at $\sim L^*$. This is a fairly generic problem in this scenario, present even in our most extreme case,

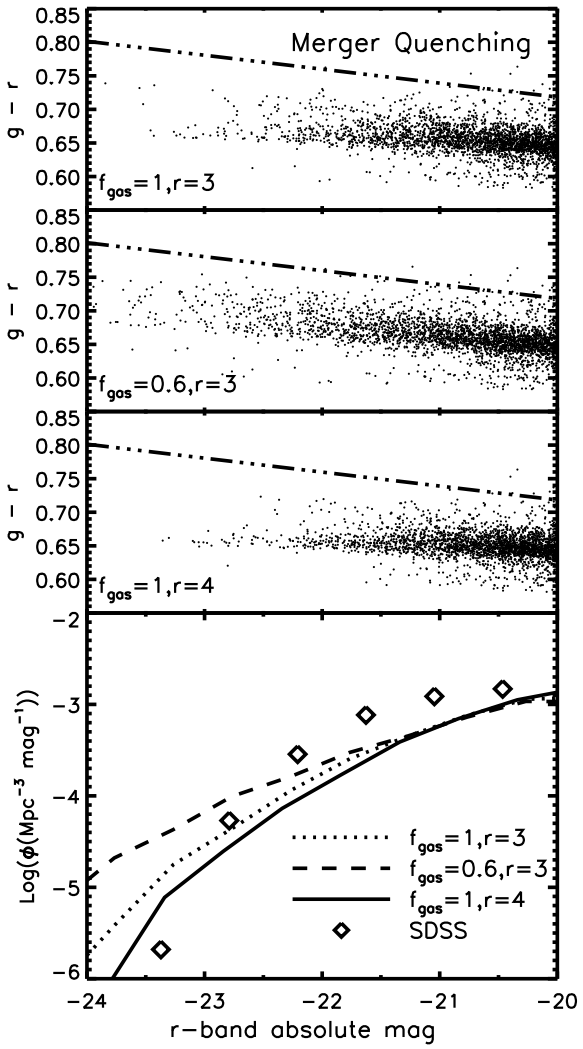

Figure 2.3 Merger quenching colour-magnitude diagrams (top 3 panels) and luminosity functions (bottom) for intrinsic (dust-free) red sequence galaxies. As indicated in the lower left of the panels, the CMDs correspond to merger quenching with a gas fraction thresholds of $f_{\rm gas} = 0.6$ and 1, above which merger remnants re-form into star-forming disks. In the third panel we count 1:4 $r = 4$) mergers as major, quenching star formation in the remnant. The dot-dashed line shows the best-fit to the SDSS VAGC red sequence. In the bottom panel, we show luminosity functions for red galaxies for each of the three quenching models (lines), along with the true red sequence from the SDSS VAGC (diamonds). All models over-produce bright galaxies, and under-produce fainter ones.

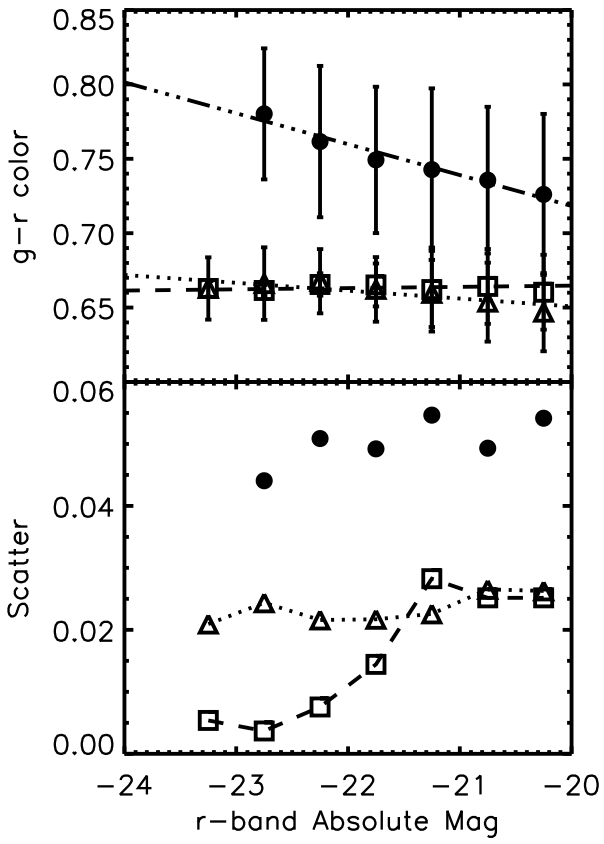

Figure 2.4 Slope and scatter of the red sequence, for SDSS data (circles) and two simulations: one with merger quenching with $f_{\rm gas} = 1$ and $r = 3$ (triangles), and another with halo mass quenching with $M_c = 10^{12} M_\odot$ (squares). Our models produce red sequences that have shallow slopes, $g - r$ colors that are too blue, and smaller scatter compared to the true red sequence.

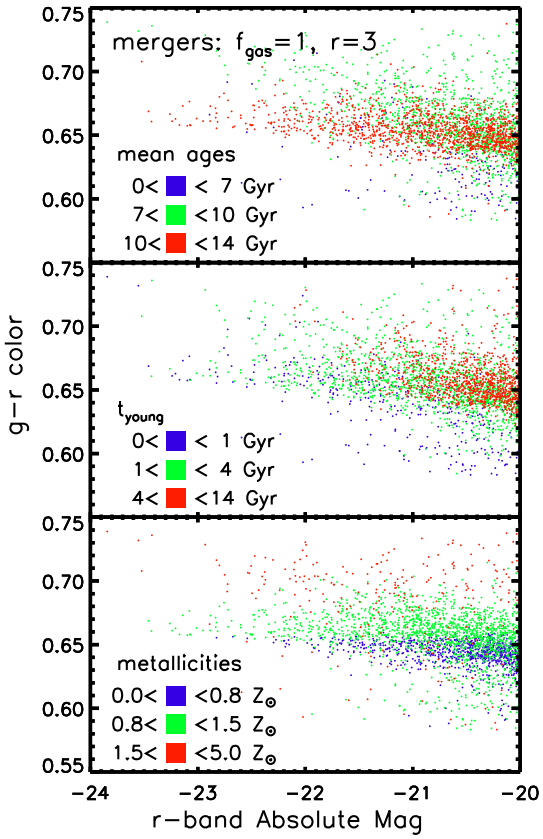

Figure 2.5 A closer look at the CMD red sequence resulting from 3:1 mergers with $f_{\rm gas} = 1$. Galaxies are colour-coded by r-band luminosity-weighted mean stellar ages (top panel); $t_{\rm young}$, the age of the youngest (most recently formed) star particle (middle panel); and r-band luminosity-weighted mean stellar metallicities (bottom panel). For reference, solar metallicity is $Z_{\odot} \simeq 0.012$. Although the brightest red sequence galaxies generally have old stellar populations, they have traces of young stars ($t_{\rm young} < 1$ Gyr). A distinct gradient in metallicity creates most of the spread in $g - r$ colour.

arising because mergers occur at a wide range of masses and only weakly pick out a characteristic scale around $\sim L^*$.

Merger quenching (along with all our quenching models) exhibit what we call the "blueness problem": the red sequence is too blue by $\sim$0.1 magnitudes in $g-r$ colour. This corresponds to $\sim 10\%$ error in the flux ratio between the two bands. We explore several possible explanations for this problem in §2.6.2, which likely has an origin in the overall calibration of galaxy metallicities. Since it occurs in all quenching models, we cannot use this blueness problem to constrain quenching mechanisms.

To more quantitatively compare the slope, scatter, and average colour, we perform linear fits to the simulated and real red sequences. We first separate the red sequence from the blue cloud using a constant $g-r$ colour, 0.65 for real galaxies and 0.55 for simulated ones. Various reasonable choices of this separator, including those with nonzero slope chosen simply by eye, yield similar results. After dividing the absolute magnitudes into bins of width 0.5, we calculate the mean, median, and standard deviation of $g-r$ colour within each bin for galaxies above our separator. We fit the median points to a straight line, as shown in the top panel of Figure 2.4 for SDSS galaxies and our 3:1, $f_{\rm gas} = 1$ merger model. Along with highlighting the blueness problem, the figure shows that the simulated red sequence slope is somewhat too shallow, at least in this quenching model. Note (in Figure 2.3) that the model with lower $f_{\rm gas}$ produces a steeper slope, and a smaller blueness problem, albeit failing more spectacularly in the LF comparison.

In the lower panel of Figure 2.4, we plot the scatter as a function of absolute magnitude. The observed scatter is ~ 0.05 magnitudes, but part of that is observational uncertainties. Cool et al. (2006) estimated that the intrinsic scatter in $g-r$

is 0.035 mag, at least for the most luminous ($> 2.2L^*$) galaxies. This is still larger than the scatter in our simulations, which is good because our quenching prescription makes the maximal assumption of zero star formation since the time of quenching. Early-type galaxies today do appear to have a small "frosting" of star formation (Trager et al., 2000; Yi et al., 2005), which would tend to increase the scatter. However, the simulated scatter is not significantly smaller than observed, so there is scant little room for additional scatter from frosting.

Figure 2.5 explores the red sequence produced in the 3:1, $f_{\rm gas} = 1$ merger quenching model in greater detail. We select this as our preferred merger quenching model since it yields the least deviations from the observed red galaxy LF. The top panel shows the r-band luminosity-weighted mean stellar age; the middle panel shows the simulated galaxies in colour-coded bins of $t_{\rm young}$, the age of the youngest star particle in the galaxy; and the bottom panel shows the r-band luminosity-weighted mean stellar metallicity. The metallicities shown are absolute mass fractions of elements heavier than helium, where solar metallicity is $Z_\odot \approx$0.012 (Asplund et al., 2005).

At the brightest end, the galaxies have old stellar populations on average. Less massive galaxies show a wider spread in age, and perhaps counter-intuitively, the intermediate-age galaxies are redder than the oldest galaxies. There are some small (i.e. $\sim L^*$) galaxies that are fairly young, having just been quenched onto the red sequence. The middle panel shows that even the brightest galaxies generally have some quite young stars (< 1 Gyr old). This is because they live in the largest halos that are still assembling at the present day, and hence they recently subsumed galaxies that were recently forming stars (i.e. unquenched galaxies); we discuss this further in §2.6. In metallicity, the red sequence shows a gradient where the reddest galaxies are the most metal rich, and this occurs at all lumi-

nosities. This reflects the well-known fact from population synthesis models that metallicity is the primary determinant of colour in old stellar populations. Here we can see why intermediate age systems are redder than the oldest systems: They generally have higher metallicities, having formed stars up until a later cosmic epoch.

2.5.2 Halo mass quenching

Figure 2.6 shows CMDs and LFs for halo mass quenching, analogous to Figure 2.3 for mergers. We show results for three values of the critical cutoff mass, M_c = $10^{11.5}, 10^{12}$, and $10^{12.5} M_{\odot}$. As with mergers we obtain a distinct red sequence in qualitative agreement with data. The slope is slightly shallower than in the merger case, essentially zero, as shown in Figure 2.4, and the scatter around the red sequence drops to nearly zero for the brightest galaxies, in contrast to merger quenching where the scatter is independent of luminosity. The blueness problem is present at roughly the same level as in merger quenching.

In halo mass quenching, most red galaxies tend to clump in a relatively small range of absolute magnitude. For $\log M_{\rm c}$=12.5 this clumping occurs around $r = -22$ (and stellar mass $\sim 10^{11} M_{\odot}$), and scales with halo mass for the other M_c cases. Variations in star formation and merging histories smear out this clumping somewhat, but this general feature remains; no such feature is seen in the data. The bright end of the red sequence grows large through dry mergers after the quenching process, and faint galaxies are mostly satellites. The dark matter halos of central galaxies tend to achieve the critical mass when the galaxies have a particular stellar mass, and then move from the blue cloud to the red sequence. Thus, at all epochs, galaxies tend to move onto the red sequence at an effective critical stellar mass or absolute magnitude that corresponds to the critical halo mass. Variations in the time of quenching and metallicities then cause significant

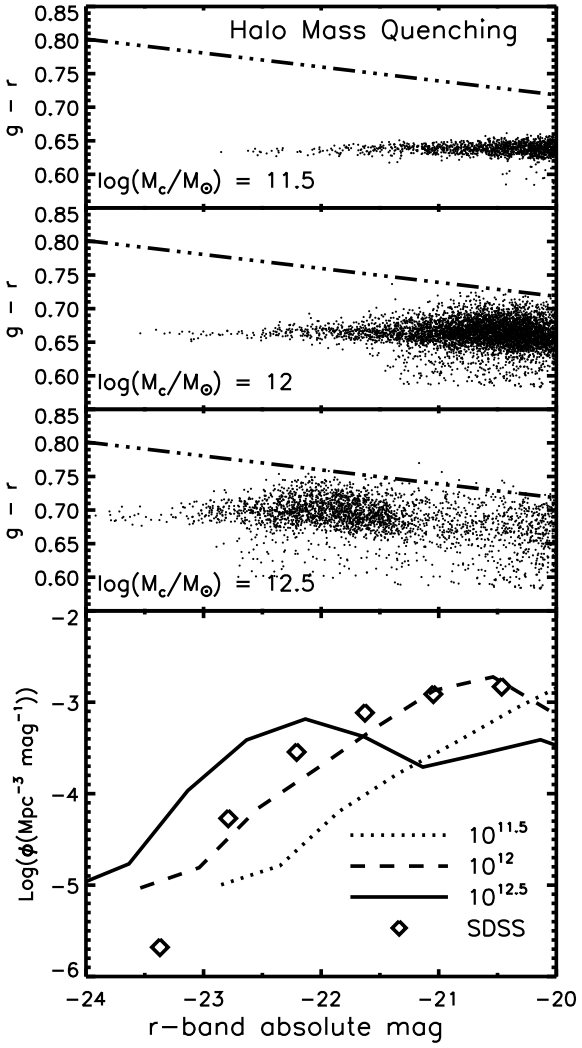

Figure 2.6 Halo mass quenching CMDs and LFs, analogous to Figure 2.3. We quench star formation in halos above the critical mass, M_c, for three values $M_c = 10^{11.5}, 10^{12}$, and $10^{12.5} M_\odot$. Galaxies tend to enter the red sequence in a clump defined by a characteristic r-band absolute magnitude (or stellar mass) associated with M_c (e.g. $r \sim -22$ for $M_c = 10^{12.5}$). The luminosity functions (bottom panel) show an unobserved uptick at the brightest bins for all three cases. The model with $M_c = 10^{12} M_\odot$ yields the best match to the SDSS luminosity function.

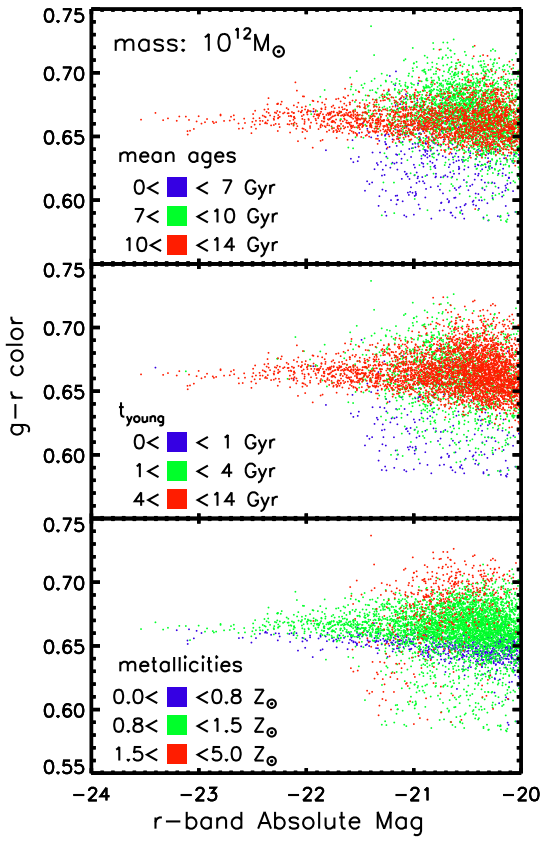

Figure 2.7 A closer look at the CMD red sequence resulting from halo mass quenching with a critical mass of $10^{12}M_\odot$. Colour coding is the same as in figure 2.5. Unlike in our merger quenching model, the brightest galaxies include no young stars.

vertical scatter in $g - r$ colour for these clump galaxies. At a fixed stellar mass, galaxies early in the universe (high redshift) have lower metallicities than those later on (low redshift) (Erb et al., 2006; Maiolino et al., 2008), so galaxies that move onto the red sequence later have higher metallicities.

The LF is quite sensitive to M_c: $M_c = 10^{12} M_\odot$ fits the luminosity functions best, with the other cases far under-predicting or over-predicting the number of bright galaxies. The CMD clump is evident in the LF as well. Even in the generally best-fitting $M_c = 10^{12} M_\odot$ case there is a tail of bright galaxies that leads to an excess in the luminosity function at $r < -23$, just as in merger quenching. Overall, the luminosity function produces a slightly steeper drop-off than the merger quenching models, although a characteristic knee is still less pronounced than in the data.

Figure 2.7 shows the red sequence in more detail for the best-fitting $\log M_c = 12$ case, with galaxies colour-coded by mean stellar age, $t_{\rm young}$, and mean stellar metallicity (from top to bottom). Like in merger quenching (cf. Figure 2.5), we find that the most massive galaxies have old stellar populations. Unlike in merger quenching, these old massive galaxies do not contain any young stars. Each of these galaxies, lying at the centre of a cluster, tends to merge only with smaller galaxies that have already been quenched a while ago because they live in the same dark matter halo above the critical halo mass. Thus, when the central galaxies grow through accretion of satellites, they do not obtain any stars younger than 1 Gyr.

The metallicity panel shows that the highest metallicity systems are generally the smallest (and reddest) systems. The large, old systems typically have fairly low metallicities. Qualitatively, this explains why the red sequence slope is basically zero; the age and metallicity gradients cancel each other. The tight

correlation between luminosity and metallicity directly translates into a scatter in the red sequence that goes from nearly zero at the brightest end to fairly large at the faint end, as seen in Figure 2.4.

2.5.3 Accretion mode quenching

Figure 2.8 shows results of $T_{\rm max}$ (i.e. hot mode) and wind mode quenching. The top two panels show CMDs for two different threshold temperatures, $10^{4.7}$ K and $10^{5.4}$ K. These are chosen as the bimodality separation in $T_{\rm max}$ in our simulations and the (no wind, no metal cooling) simulations of Kereš et al. (2009), respectively. The third panel shows the extreme case of quenching both hot mode with a $10^{4.7}$ K threshold, *and* quenching all wind mode as well.

Quenching hot mode alone does not produce a red sequence; it is not bimodal, and the number densities of red galaxies are far too small at all but the largest masses. This is because cold mode, either pristine or in the form of recycled winds, continues to provide significant accretion at late times. Hence the idea that simply keeping gas hot in a hot halo reproduces a red sequence does not appear to be viable, since it takes only a fairly small amount of ongoing star formation to make a galaxy blue.

Quenching both hot *and* wind mode produces something that looks like a red sequence, with an amplitude, slope, and scatter that is (coincidentally) comparable to the merger quenching case. However, the red galaxy LF continues to have the wrong shape; it is roughly just a constant factor higher than in the hot mode-only quenching case. Oppenheimer et al. (2010) anticipate this failure of wind-mode quenching, finding that *allowing* wind mode accretion leads to the best-matching stellar mass functions below the turnover mass M^*. Kereš et al. (2009) highlighted a numerical problem in GADGET-2 in which cold clumps form owing to thermal instabilities that then rain down ballistically onto the cen-

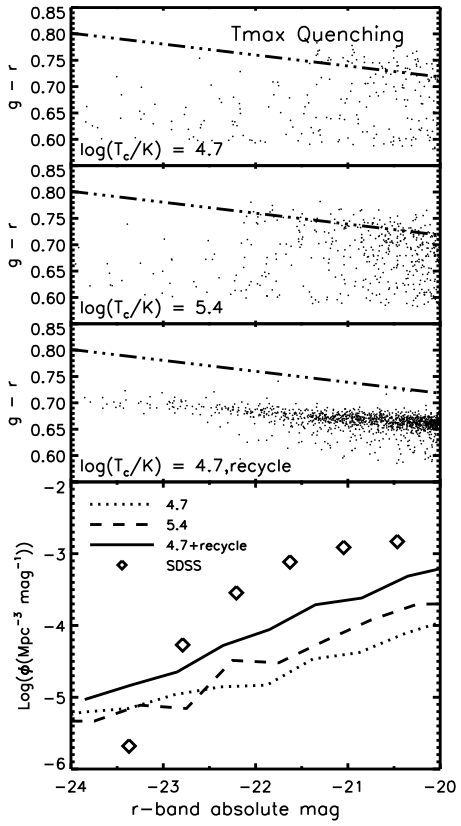

Figure 2.8 $T_{\rm max}$ CMDs and LFs, analogous to Figures 2.3 and 2.6. We quench star formation from gas particles that achieved a maximum temperature above a critical value, T_c, for $T_c = 10^{4.7}$ and $10^{5.4}$ K. These first models fail to produce a substantial red sequence because at all masses, galaxies accrete fresh cold gas from the intergalactic medium and form it into stars. Although this model may suppress global star formation, it fails to suppress *all* the star formation in a given galaxy. In the third panel we show a model where, along with a $T_{\rm max} = 10^{4.7}$ threshold, we also quench star formation from any gas particles that were recycled from a galactic wind. Although this model shows a reasonable red sequence in the CMD, it strongly suppresses the formation of blue cloud galaxies (not shown).

tral galaxy; the trouble is that the clumps always occur near the resolution limit, even as the resolution varies substantially. Hence this cold drizzle may be a numerical artifact, although Kereš & Hernquist (2009) used very high-resolution simulations to show that at least some of it is likely to be real.

Accretion mode quenching appears to be the least promising of our various quenching mechanisms, so we do not elaborate on these results any further. In the discussion we examine some implications of its failure (§2.6.4).

2.5.4 Variants on quenching models

After considering our basic models with few free parameters, we attempted several variations on our quenching models to try to improve agreement with observations. In the end there were no obvious successes, though the results illustrate some interesting trends.

As discussed above, halo mass quenching leads to characteristic clumping in the red sequence not observed in nature. This clumping arises from the sharp critical dark matter halo mass cutoff. While observational uncertainties could smear out the clumping, we investigate two more physically-motivated reasons why the critical mass cutoff might not be so sharp.

Physically, the halo mass threshold is representative of the mass scale above which a stable hot halo forms. Preventative feedback mechanisms can operate more effectively in the presence of a hot halo (Kereš et al., 2005; Dekel & Birnboim, 2006). However, there is non-trivial scatter between halo mass and hot gas fraction (e.g. see Kereš et al., 2009). Hence we tried a model variant in which we quench galaxies in halos with a hot gas fraction $f_{\rm hot} = M_{\rm hot}/(M_{\rm hot} + M_{\rm cold})$ above a critical fraction. We attempted models with critical fractions 0.2, 0.4, 0.6, and 0.8, which correspond roughly to halo masses $10^{11.5}$–$10^{12.3} M_\odot$ but with a scatter of $\sim$0.2–0.3 dex. The results are shown in Figure 2.9 (with the CMD in the top

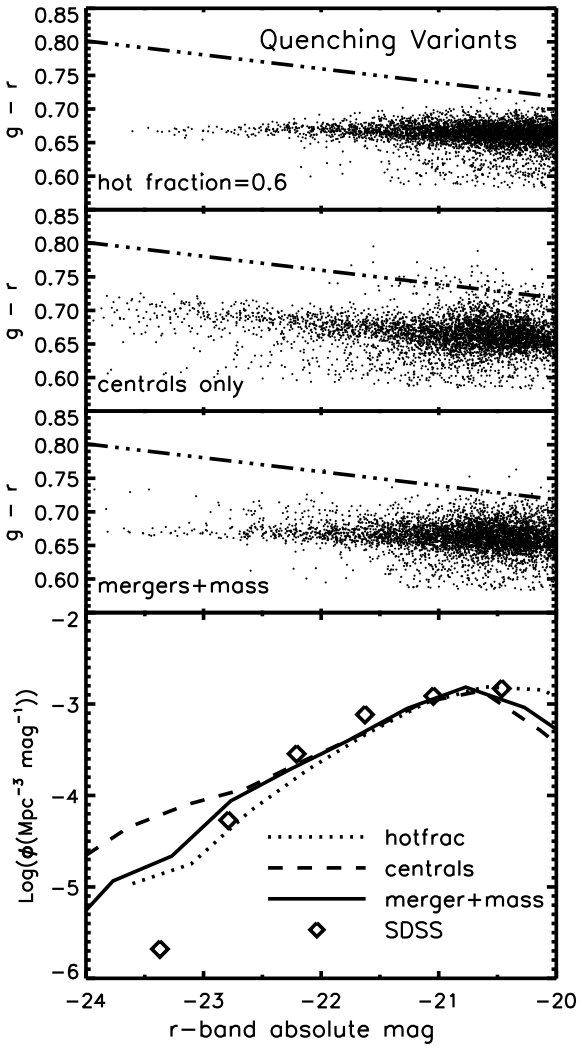

Figure 2.9 Red Galaxy CMDs and LFs for variants of our quenching models. The top panel shows the red sequence created by quenching star formation in haloes with a hot gas fraction above 0.6, the second panel shows halo mass quenching where only central galaxies undergo quenching, and the the third panel shows a model where both a merger *and* a halo mass above $10^{12} M_{\odot}$ are required to quench star formation. Although these models show promise at matching the LF at $r > -22$, they share the problems of our simpler models at the bright end: an excess of bright galaxies.

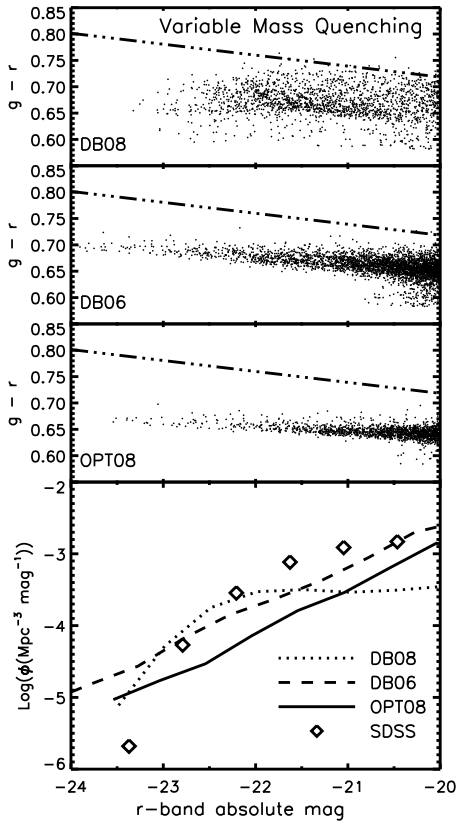

Figure 2.10 Red galaxy CMD and LF for variable mass halo mass quenching. Instead of a constant critical halo mass above which shocks quench star formation, the critical mass varies with redshift. The top panel uses a model from Dekel & Birnboim (2008) where the critical mass required to sustain a hot halo increases with cosmic time. This model yields a dearth of galaxies fainter than $r = -22$. In the other two models, cold flows are assumed to penetrate hot haloes at high redshift due to the higher relative densities of cosmic filaments. This effectively causes the the critical mass above which quenching occurs to decrease with cosmic time. We show two different versions of the critical mass as a function of redshift, based on Dekel & Birnboim (2006) and Ocvirk et al. (2008), which differ only by the metallicity assumed for cosmic gas. These models exhibit a nearly-constant slope in the LF.

panel), for a critical hot gas fraction of 0.6. This variant smooths out the characteristic absolute magnitude or stellar mass at which blue galaxies move to the red sequence, yielding a less clumped red sequence. However, the slope and scatter (and trends with luminosity) remain essentially unchanged. Also, the LF still shows the excess of very bright galaxies as noted in the halo mass quenching case. Hence besides the aesthetic appeal of removing the clump in the CMD, it does not fare any better (or worse) than halo mass quenching.

As another variant, we examined a scenario in which we quench only in central galaxies of halos, not satellite galaxies. This is shown in Figure 2.9 (second panel) for a critical mass of $10^{12} M_{\odot}$. The CMD in this model shows greater scatter in the red sequence and a much flatter luminosity function slope than our preferred model where satellites are quenched as well. Galaxies are able to build up more mass before ending up on the red sequence, and massive central galaxies end up merging with more massive satellites than in the preferred model. This failure is disappointing, as most scenarios of halo mass quenching only quench the central galaxy, and observations favor a more gradual quenching of satellites (e.g. Weinmann et al., 2009). Indeed, SAMs that quench satellite galaxies in halos have difficulties reproducing the colour distributions of satellites (Weinmann et al., 2006; Baldry et al., 2006), which is a drawback that is shared by our original halo mass quenching scenario. We do note that the red sequence slope seems to be in better agreement with data, as larger galaxies acquire larger (unquenched) satellites that are more metal-rich.

We also investigated a hybrid model that requires both a major merger and a critical halo mass for quenching. That is, we quench only if a major merger occurs inside a halo with mass $> 10^{12} M_{\odot}$ (here we assume $f_{\rm gas} = 1$). Physically, this model mimics the action of a hot halo to prevent post-merger gas accretion from

the IGM, perhaps by continued energy injection from an AGN. In our original quenching model, such post-merger accretion is always prevented, but here we only prevent accretion in larger halos that can support a virial shock. This model is perhaps closest to what is envisioned in current ideas for quasar plus radio mode quenching, in which a merger initially transforms the galaxy into an elliptical and quenches star formation, but only when the resulting halo is sufficiently large to form a virial shock does the resulting halo gas stay hot e.g. via low-level AGN activity.

Figure 2.9, third panel, shows the results of this model. The results are fairly similar to halo mass quenching, showing that it is this aspect that is the limiting factor for quenching; mergers are frequent enough that it does not add a stringent criterion. The red sequence shows slightly more scatter than in halo mass quenching, and there is no evidence for clustering at a particular r-band magnitude; the slope is still incorrect, and (as always) the blueness problem persists. The LF is also similar to the halo mass quenching case, with an excess of very bright galaxies and a possible dearth of $\sim L^*$ systems. This model may, in fact, be the best-fitting model as well as the most physically-motivated, but the results are qualitatively very similar to those of our simpler models.

Finally, we consider three variants of halo mass quenching where the critical halo mass varies with redshift. The first is motivated by Dekel & Birnboim (2008), who argue that the critical halo mass for quenching owing to gravitational clump heating varies slightly with redshift due to the evolving cosmic density of gas (see their Figure 3). In this scenario, the quenching mass varies from $M_c \simeq 10^{11.8} M_\odot$ at $z = 3$ to $M_c \simeq 10^{12.8} M_\odot$ at $z = 0$. For $z > 3$ we use the lower value, $M_c = 10^{11.8} M_\odot$. Figure 2.10, top panel, shows the results. The shape of the LF is affected most strongly, as there is now a significant dearth of red galaxies

fainter than $r \simeq -22$. The high M_c at late times makes the fainter end of the red sequence similar to the fixed $M_c = 10^{12.5} M_\odot$ case, i.e., it does not populate the red sequence enough. We do note that it produces a larger red sequence slope that is in better agreement with data, although the scatter is larger. Overall, this model does not fare as well as our favored halo mass quenching model with a constant $M_c = 10^{12} M_\odot$, although it does illustrate that varying the quenching mass with epoch can produce notable changes in the red sequence (at the aesthetic expense of introducing more parameters).

In another paper, Dekel et al. (2009a) argue that M_c evolves with redshift in the opposite sense, namely that $M_c \approx 10^{11.7} M_\odot$ out to $z = 1.5$, but at higher redshifts it increases rapidly owing to the ability of cold streams to penetrate through hot halos at early epochs (see their Figure 5, and also Dekel & Birnboim 2006). From an eyeball estimate of their conjectured hot halo mass limit in the presence of cold streams, we take $M_c = 10^{11.7} M_\odot$ for $z < 1.5$, and $\log M_c \simeq 1.2z + 9.9$ for $z > 1.5$. We also show a variation from Ocvirk et al. (2008) where gas in cosmic filaments is assumed to have a lower metallicity than Dekel & Birnboim (2006) assume. In this formulation, $M_c \simeq 10^{11.5}$ for $z < 3$, and $\log M_c \simeq 1.4z + 7.3$ for $z > 3$. The lower panels of Figure 2.10 show the results in these cases: A red sequence is produced, but the CMDs have a very small colour scatter, and more dramatically the LFs are power laws! The LFs of the two parametrizations differ primarily in their normalization. These models exacerbate the problem of producing a knee in the LF over constant-M_c models.

None of these quenching model variants stands out as obviously superior to the others. Since the simple models perform as well as the variants, and because they involve simpler prescriptions, we use merger quenching with $f_{gas} = 1$ and $r = 3$ and halo mass quenching with $M_c = 10^{12} M_\odot$ as our preferred models. For

the remainder of the paper, we focus on these two models.

2.5.5 The Blue Cloud

So far we have focused on the red sequence. Our merger and halo mass quenching models also produce a star-forming blue cloud of galaxies that is separated from the red sequence, as shown in the left panels of Figures 2.11 and 2.12. Here we examine the properties of the blue cloud in these scenarios.

Computing the observed luminosities of blue cloud galaxies is complicated by uncertainties in dust extinction. Our simulation tracks metallicity, which is correlated with dust extinction. There are also empirical correlations between UV or blue-band luminosity and extinction. Since in general the bright blue galaxies are quite metal-rich, the exact form and nature of the assumed extinction makes a significant difference in their resulting brightness and colors. We only apply an extinction correction to blue galaxies, leaving quenched galaxies unaffected. Also, we employ Calzetti et al. (2000) reddening law where the optical depth due to dust varies as wavelength $\lambda^{-0.7}$.

We first tried employing a correlation between metallicity and extinction from SDSS, including scatter, as described in Finlator et al. (2006). However, we found that the resulting blue cloud had a very large scatter, and a substantial number of previously blue galaxies ended up redder than the red sequence. It is possible that second parameter correlations exist in metallicity versus extinction that are not accounted for, but we did not explore this further.

Our preferred method, i.e. one that produced a blue cloud similar to observed, uses an empirical correlation between UV luminosity and dust extinction given by Wang & Heckman (1996), also described in Finlator et al. (2006). This prescription moves bright blue galaxies more than dimmer ones, so that the bluest galaxies are not necessarily the brightest ones. The resulting overall shape of the

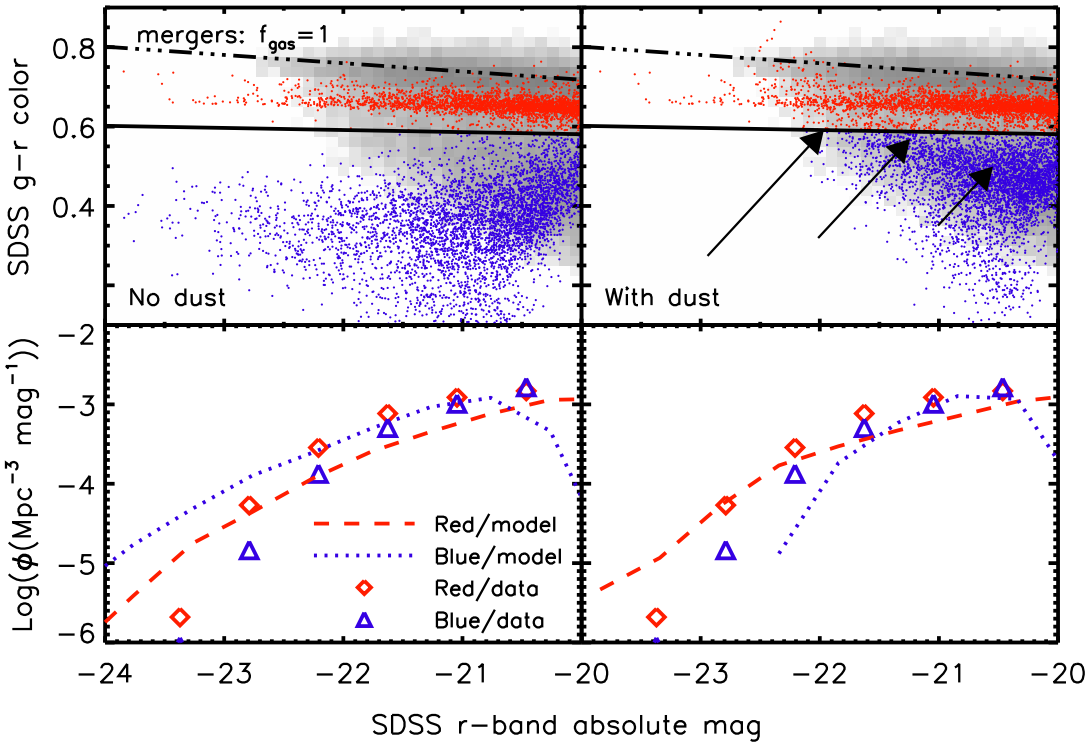

Figure 2.11 Dust comparison of CMDs and LFs for merger quenching with $f_{\rm gas} = 1$. Our dust model (right panels) shifts bright blue galaxies up and to the right in the CMDs, introducing contaminants to the bright end of the red sequence. Arrows illustrate the change in position (from tail to head) due to dust for three galaxies, with star-formation rates ≈3, 9, and 15 $M_\odot$ yr^{-1} (right to left). The luminosity functions reflect the increase in bright red galaxies due to contamination, as well as the suppression of bright blue ones.

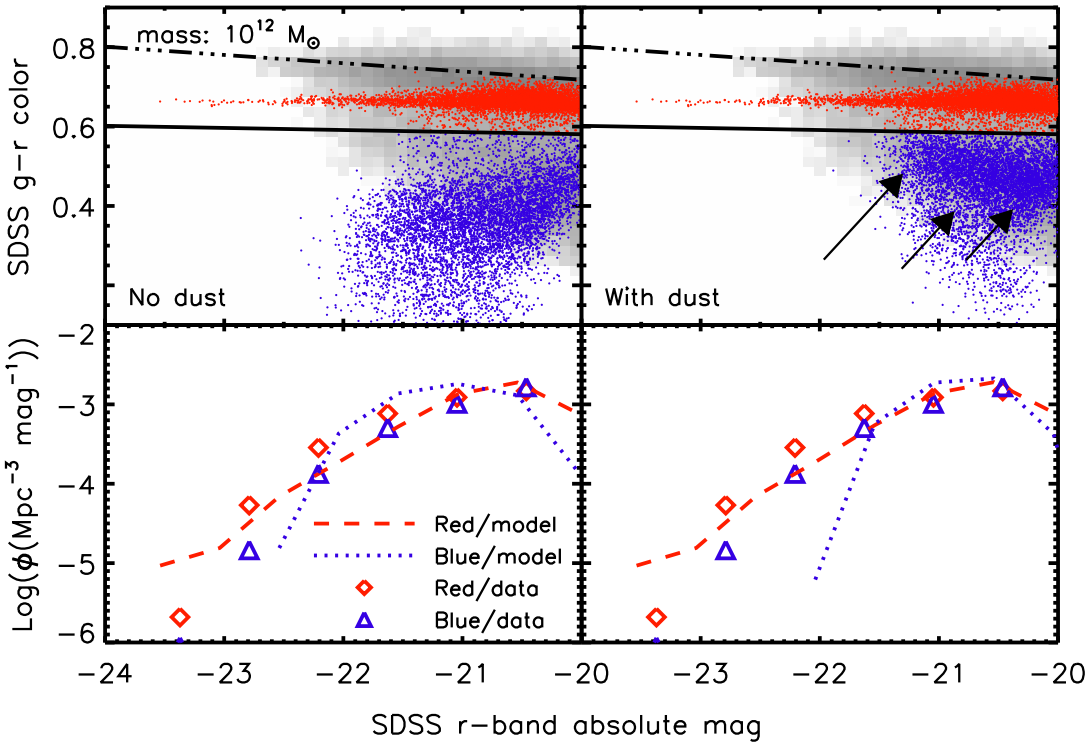

Figure 2.12 Dust comparison of CMDs and LFs for halo mass quenching with $M_c = 10^{12} M_\odot$. Arrows show the change in position for three galaxies, with star-formation rates ≈2, 4, and 7.5 $M_\odot$ yr^{-1} (right to left). Even without dust (left panels), this model does not produce exceptionally bright blue galaxies: once blue galaxies attain a critical stellar mass corresponding to M_c, they move to the red sequence. Our dust model (right panels) suppresses the bright blue galaxies, leading to a steep cutoff in the blue galaxy luminosity function.

blue sequence matches the observed SDSS blue sequence reasonably well.

Figure 2.11 compares CMDs and LFs for our merger quenching model with and without dust. Without dust, the brightest blue galaxies in the universe would have r-band luminosities brighter than the brightest red galaxies, and they would be ~ 0.3 magnitudes bluer than the red sequence in $g-r$. With dust applied, the brightest star-forming galaxies are scattered into the red sequence, making up $\sim$6% of red sequence galaxies; this is reasonably consistent with observational estimates (cf. Bell et al., 2004a; Brammer et al., 2009). Furthermore, the dust obscuration ensures that massive blue galaxies are not brighter than the red sequence. The luminosity functions reflect this difference markedly. In the no-dust case, blue galaxies dominate over the bright end of the red sequence, but the presence of dust shifts the bright blue objects to lower luminosities.

Figure 2.12 compares the dust and no-dust cases for halo mass quenching. Even the no-dust case lacks bright blue galaxies like those seen in the merger model and in observations, and once dust is included the problem becomes significantly more severe. As discussed in §2.5.2, once galaxies attain a stellar mass corresponding to the critical halo mass, they move out of the blue cloud and onto the red sequence. Application of the dust prescription pushes blue cloud galaxies up and right in the figure, creating a diagonal envelope. Since dust tends to move the brightest galaxies the most, the dearth of blue galaxies intrinsically brighter than $r \sim -22$ leads to fewer intrinsically blue interlopers on the red sequence ($< 2\%$).

As an aside, we note an interesting study by Maller et al. (2009) of galaxy orientation in relation to dust obscuration, and its impact on derived galaxy properties. Notably, they find that structural parameters like axis ratio and Sérsic index significantly impact measured colors and magnitudes, and they find an average

of 0.2-0.3 magnitudes of extinction in the SDSS g and r bands. This study predicts considerably more bright blue galaxies than are generally inferred from studies that do not take into account orientation-dependent effects. We do not account for such effects in our work, as we use a simple dust screen model to account for obscuration.

While such comparisons are illustrative, the sensitivity to the exact extinction prescription used makes robust interpretation of the discrepancies difficult. As an alternative approach, we can perform the comparison versus stellar mass functions rather than luminosity functions. The stellar masses derived by Kauffmann et al. (2003c) implicitly account for dust extinction on a galaxy-by-galaxy basis, albeit with some assumptions about the reddening law. Baldry et al. (2008) show that these masses, determined by comparing star formation history templates based on the BC03 models to absorption features in the galaxy spectra, yield similar mass functions to other mass derivations using photometry, different population synthesis models, or different spectral features.

In Figure 2.13 we show stellar mass functions (the number of galaxies per Mpc^3 per logarithmic stellar mass bin), separated into red and blue galaxies, for merger quenching, halo mass quenching, and SDSS galaxies. When dividing our simulated galaxy sample into red and blue, we do not use our dust prescription, so that Figure 2.13 shows the mass functions for intrinsically blue and red galaxies. Given the small level of contamination of actively star-forming galaxies on the red sequence, this choice does not significantly impact the results.

In our models, the red galaxy mass functions behave similarly to the luminosity functions, as expected since for these galaxies r-band absolute magnitude is a good tracer of stellar mass. The red mass functions do not have a sharp knee, and the slope for halo mass quenching is slightly steeper than that for merger quench-

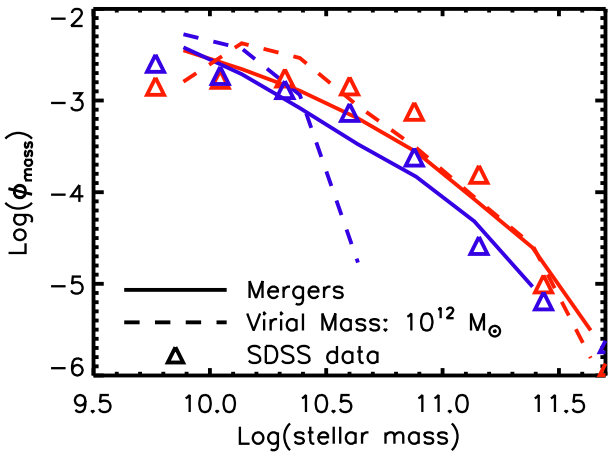

Figure 2.13 Stellar mass functions for merger quenching (solid lines), halo mass quenching (dashed lines), and SDSS data (symbols). We split the galaxy populations into blue and red, as indicated by the colour of the lines. For merger quenching, the shape of the blue galaxy mass function tracks that of red galaxies, roughly in agreement with observations. Halo mass quenching, however, yields a sharp cutoff in the blue galaxy mass function.

ing. In fact, above M^* (the characteristic stellar mass in a Schechter function fit, $\approx 10^{10.7} M_\odot$), the red galaxy mass functions in the two models are remarkably similar.

The blue galaxy mass functions reveal a crucial difference between our halo mass and merger quenching models. Halo mass quenching produces a precipitous drop in the blue mass function above $\sim 10^{10.5} M_\odot$, a critical stellar mass corresponding to the critical halo mass $10^{12} M_\odot$. Mergers, in contrast, yield a blue stellar mass function whose shape traces that of the red stellar mass function (but with slightly lower normalization) for massive galaxies. The merger scenario markedly better reproduces the observed blue galaxy mass function. At $M_* > 10^{11} M_\odot$ there are fewer blue galaxies, but *not* zero blue galaxies.

The overall conclusion from the stellar mass function comparison is the same as obtained from the luminosity function comparison: The merger quenching model produces red and blue stellar mass functions that broadly agree with data, but the halo mass quenching produces a sharp truncation in the large blue galaxy population that is in disagreement with data. We emphasize that this truncation persists even in our variant quenching models which smear out the clumping associated with a halo mass cutoff (the hot fraction variant). This generic result is difficult to avoid given a relatively tight correlation between halo mass and stellar mass seen in the simulations. Unless this correlation has much greater scatter in nature than in our models, a simple halo mass quenching model will have difficulty matching this data.

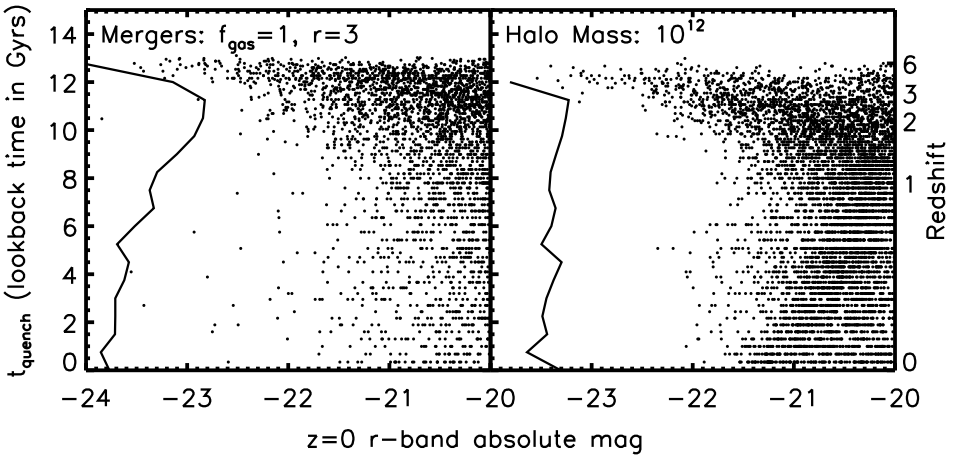

Figure 2.14 Lookback time of initial quenching vs. $z = 0$ r-band absolute magnitude for merger quenching and halo mass quenching. For mergers, $t_{\rm quench}$ is the lookback time of the first major merger. For halo mass quenching, $t_{\rm quench}$ is the lookback time when the galaxy's dark matter halo first exceeded the critical halo mass of $10^{12} M_{\odot}$. Along the y-axis, we show histograms of $t_{\rm quench}$. The brightest galaxies all entered the red sequence at early times ($z > 2$). Merger quenching yields a peak quenching era at $z \approx 3$, whereas a halo mass limit quenches galaxies with a rate nearly constant in time.

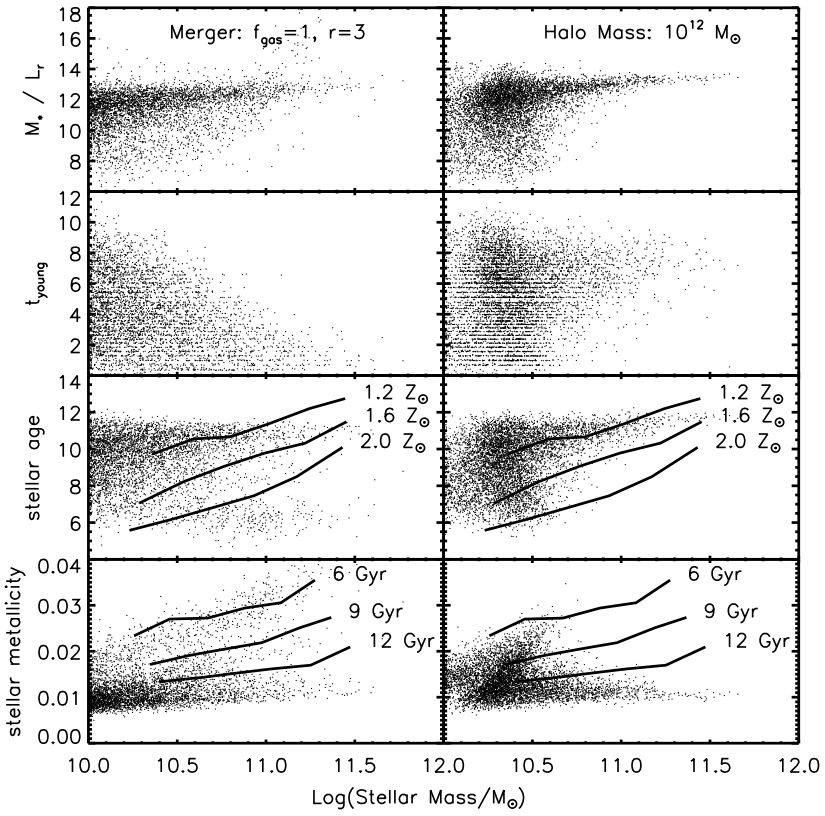

Figure 2.15 Redshift zero r-band mass-to-light ratios, age of the youngest star particle, mean stellar age, and mean stellar metallicity vs. stellar mass for galaxies in the merger quenching (left) and halo mass quenching (right) models. All panels include only red sequence galaxies. In the mean stellar age panels, lines represent the mean stellar age required to get the correct colors of the SDSS red sequence assuming a fixed metallicity along the red sequence of 1.2, 1.6, or 2.0 $Z_{\odot}$ (as labeled on the plot; see text), where $Z_{\odot} \approx 0.012$. The metallicity plot shows analogous lines assuming a constant age along the red sequence of 6, 9, or 12 Gyrs.

2.6 Discussion

2.6.1 Origins of the red sequence

Observations now suggest red and dead galaxies have existed since at least $z \simeq 2$ (Kriek et al., 2008; Williams et al., 2009; Brammer et al., 2009), and the formation time for their stellar populations is quite old. When does the quenching take place in our models?

Figure 2.14 shows the lookback time at which initial quenching occurred for each of the quenched galaxies in our two preferred quenching models. For the brightest red galaxies, quenching occurred at $z \geq 3$ in both models. In halo mass quenching, essentially zero galaxies brighter than $r = -22$ were quenched after $z = 1.5$, whereas in merger quenching a small number of bright galaxies came to the red sequence at late times. In halo mass quenching, red galaxies can only achieve the highest masses via mergers *after* moving to the red sequence because the effective critical stellar mass ($\sim 10^{10.5} M_{\odot}$) is much smaller than the biggest galaxies. In merger quenching, on the other hand, blue galaxies can attain quite high stellar masses and then move onto the red sequence as an already-bright galaxy at late times.

Along the y-axis we show vertical histograms in $t_{\rm quench}$, indicating the quenching rate in terms of the number of newly quenched galaxies as a function of cosmic time. The merger quenching rate peaks at $z \sim 3$, whereas a halo mass threshold quenches at a roughly constant rate over time. Here we caution that the peak in the merger quenching rate is sensitive to our minimum mass for merger quenching, which is set by the simulation resolution. A higher resolution simulation would likely move the peak to higher redshift, since small galaxies could quench earlier. In any case, the peak will remain as a distinguishing feature between merger and halo mass quenching.

For a deeper physical understanding of our model galaxies, we turn to Figure 2.15, where we plot r-band stellar mass-to-light ratios, $t_{\rm young}$ (the age of the youngest star particle), mean stellar age, and mean stellar metallicity vs. stellar mass for our galaxies in our two preferred quenching models. We estimate mass-to-light ratios in solar units by dividing stellar mass by L_r, which is given by $\log(L_r/d\nu) = (r - C)/(-2.5)$. Here r is the galaxy's r-band absolute magnitude, $C = -48.6$ for AB magnitudes (Oke, 1974), and $d\nu = d\lambda(c/\lambda^2)$ is the approximate frequency width of the SDSS r-band filter. We take $\lambda = 6250$ and $d\lambda = 1500$ angstroms for the r-band. In both quenching models, we find a mass-to-light ratio that increases slowly with stellar mass, and is fairly tight above $10^{10.5} M_\odot$ where most galaxies have been quenched for some time. Halo mass quenching displays a clump of M/L just below the quenching (stellar) mass, since these galaxies have recently undergone quenching.

In the second row, we highlight a distinction in the age of the youngest stars between the merger quenching and halo mass quenching models. Massive galaxies in the halo mass quenching model lack any population of young stars: all the galaxies they accrete have old stellar populations, since even satellites that will be accreted later are quenched in massive halos at an early time. Galaxies quenched via mergers, however, include trace populations of young stars. Even though mergers quenched the star formation in these massive galaxies at $z > 2$, they obtain young stars via accretion of younger satellite galaxies.

In the bottom panels of the figure, we examine ages and metallicities to understand why our models do not match the slope and normalization of the real red sequence. We include tracks showing the mean ages and stellar metallicities vs. stellar mass required to reproduce the observed red sequence. Specifically, on the plot of mean stellar age vs. stellar mass, we assume a uniform metallicity for

all red sequence galaxies, and ask: what mean ages would those galaxies need to have to get the correct red sequence colors using the BC03 models? To answer this question, we create a grid of artificial single stellar populations (SSPs) with a variety of masses and randomly chosen metallicites and ages. This grid densely samples the region of the CMD where real red sequence galaxies lie. We then take our fit to the SDSS red sequence from Figure 2.4, and for each absolute magnitude bin we identify all the artificial SSPs which fall within the scatter of the median in $g-r$ and within 0.003 of the assumed metallicity. We compute the mean stellar mass and mean stellar age of these SSPs, and plot as a connected line in the figure. The plotted values have a scatter of $\sim$1 Gyr. We follow an analogous procedure for the tracks in the metallicity vs. stellar mass plots.

These tracks tell us what slope and normalization in age (metallicity) would be required to get the correct red sequence slope, *assuming* the red sequence has a constant metallicity (age). Of course, in real galaxies both age and metallicity may vary with stellar mass, but this is intended to illustrate the general trends. If age gradients along the red sequence are small, then we require a factor $\sim$2 difference in metallicity from the brightest galaxies to those an order of magnitude less massive in order to reproduce the correct slope. If metallicities are roughly constant across the red sequence, then we require variation of 3–4 Gyrs between the bright and faint galaxies for typical galaxy ages. Finally, if a typical age is 10 Gyr, then the simulation metallicities would need to be increased by $\sim \times 2$ in order to match the observed red sequence amplitude. We will discuss the implications of these trends in §2.6.4.

2.6.2 The blueness problem

In all cases our models yield red sequences too blue by about 0.1 magnitudes in $g-r$, an error of $\sim$10% in the luminosity ratio between those bands. For

these galaxies, colors are determined by matching each constituent star particle's metallicity and age to grids from BC03 stellar population synthesis models. While the discrepancy might originate with uncertainties in the population synthesis models (e.g. Charlot et al., 1996; Conroy et al., 2009), we attempted to mitigate this possibility by using the same models as Blanton et al. (2005) for the VAGC. We also tried the updated Charlot & Bruzual models (graciously provided to us by S. Charlot) that employ an updated treatement of thermally pulsating (TP) AGB stars, but these showed very minor difference compared to BC03 for our red sequence galaxies since TP-AGB stars do not contribute significantly to the luminosity in SDSS bands. Hence we explored other possible reasons for the blueness problem.

There are two ways to make a galaxy too blue: give it a younger age, or a lower metallicity. Perhaps our simulations simply have distributions of galaxy ages and metallicies that are wrong. As shown in Figure 2.15, our brightest red galaxies have mean stellar ages > 10 Gyrs. This leaves little room to maneuver, as galaxies cannot get much older given the age of the Universe.

The story is different for metallicity. The tracks in Figure 2.15 suggest that the metallicities of our galaxies are systematically low. Very few galaxies show metallicities above 0.02 (metal mass fraction), but BC03 models require that the most massive galaxies have metallicities significantly above this to explain their red colors. Why might these galaxies be unrealistically metal poor?

As described in Finlator & Davé (2008), metallicities in un-quenched galaxies are determined by an equilibrium between less enriched gas accreted from the IGM and gas enriched by ongoing star formation. Metallicities tend to rise as a galaxy grows in mass, and even at fixed mass galaxies at lower redshift are more metal rich (Davé et al., 2007). Once quenching occurs in our models, the metal-

licities are frozen into the existing star particles. If our simulations quenched galaxies too early, the galaxies would not have built up their metallicities sufficiently.

Another uncertainty is the adopted supernova metal yields. We use a set of yields from various authors, most notably Chieffi & Limongi (2004) yields for Type II supernovae that dominate the stellar metal budget of these galaxies. The yields are not all that well constrained, and it is possible that they are higher than we have assumed. We note that our simulations assume Asplund et al. (2005) abundances, for which solar metallicity is a metal mass fraction of 0.0126, as opposed to the 0.02 fraction that is assumed for solar metallicity in the BC03 models. We assume that the metallicity scale in the BC03 models represents an absolute scale (S. Charlot & A. Bressan, private communication), so that e.g. a simulated galaxy that has "solar" metallicity of 0.0126 is computed using the $0.6Z_{\odot}$ BC03 templates.

Our enrichment and galactic wind models further complicate the interpretation of the metal content of simulated stellar populations. In our simulations, star formation induces both metal enrichment and galactic winds. The winds suppress enrichment of subsequently-forming stars by removing metals from the ISM; this process is poorly contrained observationally, and our model could be overly efficient at metal removal. We note, however, that the ejected metals in our outflow model match observations of IGM enrichment (Oppenheimer & Davé, 2008, 2009), so it is not clear that one can lower the ejected metals substantially. Since, however, most metals end up in the IGM particularly at early times (Oppenheimer et al., 2009), it would not take large changes to the outflow model in order to double the metallicity retained in galaxies.

Our simulations do reproduce the stellar mass–gas phase metallicity relation

for galaxies at $z \approx 2$ (Finlator & Davé, 2008), suggesting that metallicities for star-forming galaxies in our simulation are generally correct. However, systematic uncertainties at the 0.2–0.3 dex level could impact the Finlator & Davé (2008) comparison with data from Erb et al. (2006). These uncertainties emerge from the calibration of metallicities derived from observations (cf. Kewley & Ellison, 2008), and because Finlator & Davé (2008) compared all simulated galaxies to UV-selected observations, which may have higher specific star formation rates and lower metallicities (Ellison et al., 2008). Hence there is plausibly room for $\sim \times 2$ variations in the metallicities of galaxies.

Finally, it is possible that the under-enrichment is related to the star formation history in the simulations. In particular, at least for the merger quenching, one expects that a starburst may be associated with the merger event (e.g. Mihos & Hernquist, 1996). Such a starburst is not explicitly included when we apply our quenching, and it could consume a significant amount of gas to create an enhanced metallicity. However, we note that we only quench galaxies typically well *after* the merger event, since we quench only at fixed time intervals of the simulation snapshots. While our simulations lack the resolution to track the detailed star formation history during the merger, the *integral* of the SFH is typically close to what would be obtained at much higher resolution, since it is primarily limited by the overall gas supply. Hence while there may be a modest impact from this, it is unlikely that it can boost the metal production (or stellar production) by a factor of two.

It is possible that there are some effects in the observations that make the observed galaxies too red. Deriving reliable absolute magnitudes from apparent magnitudes requires several steps and important assumptions. One must use some galaxy template to calculate a galaxy's redshift/distance and k-correction

(Hogg et al., 2002; Blanton & Roweis, 2007) from photometric data. In the VAGC, this is done by creating a suite of star formation histories with corresponding spectra from BC03 models, running a principle components analysis with the data to determine which star formation histories are most representative, then fitting each galaxy's photometric data to the principle components as templates. The complexity of this procedure makes it difficult to independently determine the reliability of the fits or whether the chosen templates are sufficiently representative. Blanton et al. (2005) do estimate uncertainties in reported absolute magnitudes for each galaxy in the VAGC; for g and r, these are typically ~ 0.04 magnitudes. Only systematic uncertainties much larger than these could give rise to the blueness problem, which seem unlikely.

In summary, the blueness problem is likely to reflect some issue with the chemical enrichment level of simulated galaxies. The most obvious explanation is that the yields are somewhat too low, or that our outflow model is too efficient at metal removal. In either case, while the overall metallicities are too low, the relative metallicities are basically correct, which means that predictions for the slope and scatter of the red sequence are robust. However, it cannot be ruled out that this is reflective of a more subtle issue with the star formation or chemical enrichment histories of our simulated galaxies.

2.6.3 Star formation histories

By shutting off star formation in the largest galaxies, quenching mechanisms strikingly impact global star formation. In our simulations without quenching, the most intense star formation occurs in the most massive galaxies, accounting for significant fractions of the of global star-formation rate density.

We show the effects of merger quenching and halo mass quenching on the star formation histories of galaxies of different masses in Figure 2.16. We first

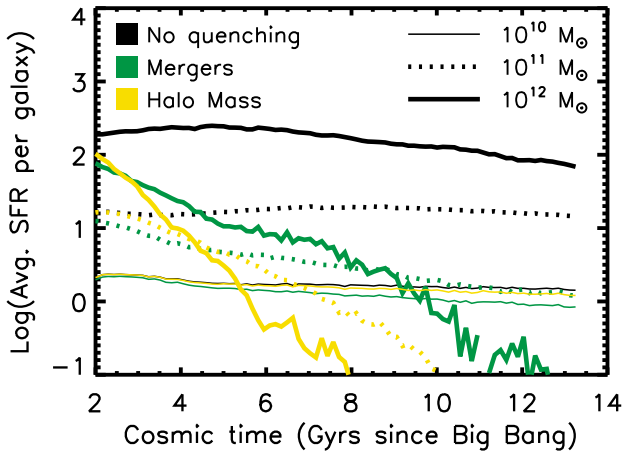

Figure 2.16 Average star formation rates (in $M_\odot$/yr) vs. cosmic time for galaxies in 3 mass bins of width 0.1 dex: $10^{10}, 10^{11}$, and $10^{12} M_\odot$. We sort galaxies into bins by their $z = 0$ stellar mass *in the no-quenching simulation*, then track the mass growth of those same galaxies through cosmic time in the no-quenching (black), merger quenching (green), and halo mass quenching (yellow) cases. By construction, star formation within small galaxies that later merge to form a large galaxy is counted toward the average SFR. Both quenching models strongly suppress star formation in the two massive bins, but only slightly change the low-mass bin. Qualitatively, this behavior mimics the observed "downsizing" of star formation. Halo mass quenching suppresses growth of the most massive galaxies more strongly than merger quenching because in halo mass quenching a massive galaxy's satellites will occupy the same halo, and thus be quenched, well before they merge.

select galaxies from three stellar mass bins, $10^{10}, 10^{11},$ and $10^{12} M_{\odot}$, at $z = 0$ in the simulation with no quenching model applied. The bins have a width of 0.1 dex in stellar mass. We then find the time each star in these galaxies was formed, translating to star-formation rate (in $M_{\odot}$/yr) by averaging over intervals of $\sim$100 Myrs. Dividing by the number of galaxies in each mass bin, we get the average SFR per galaxy as a function of cosmic time. This methodology includes in the SFR any star-formation which occurred in small galaxies that later merged to form a massive galaxy that falls within one of our mass bins.

For the quenching models, we track the same galaxies selected above from the no-quenching simulation, but we ignore the contribution of quenched stars particles to the SFR. We thus show the effects of quenching on specific collections of galaxies, rather than galaxies in given mass bins selected for each model (the quenching models do not produce $10^{12} M_{\odot}$ galaxies).

Both merger quenching and halo mass quenching strongly suppress star formation in massive galaxies, while barely changing the average SFR in the lowest mass bin. This effect naturally leads to "downsizing" with cosmic time (Cowie et al., 1996; Heavens et al., 2004; Juneau et al., 2005), where more star formation occurs in lower-mass galaxies at later times. Halo mass quenching suppresses SFRs more efficiently than mergers because it quenches satellite galaxies which later merge with the central galaxy. In contrast, merger quenching allows satellites to form stars until the final merger. Hence in principle, deriving accurate mean star formation histories from stacked galaxy samples in various mass bins can provide strong constraints on quenching mechanisms.

2.6.4 Successes and failures of quenching models

The most basic result of this paper is that both merger quenching and halo mass quenching successfully recover qualitative aspects of observed local CMDs and

LFs. These quenching models greatly improve upon the results of hydrodynamic simulations that do not have any explicit quenching, which grossly overproduce the abundance of massive blue galaxies and fail to produce hardly any massive red galaxies. At absolute magnitudes $-22.5 < r < -20$, luminosity function results from both models using our favored parameters fall within a factor of ~ 2 of observed luminosity functions from SDSS. The quenching models also yields a qualitatively reasonable colour-magnitude diagram when we apply a dust correction for star-forming galaxies. Qualitatively, the red sequence grows as expected from observations, with the most massive present-day galaxies truncating star formation at $z > 2$, and galaxies around L^* continuing to evolve onto the red sequence to $z = 0$. This leads to mean stellar ages of massive red sequence galaxies that are roughly consistent with observations (Graves et al., 2007, 2009). These are notable successes that show that quenching associated with one or both of these mechanisms is on the right track towards understanding the evolution of massive galaxies.

Models based on quenching hot mode accretion fail to produce a red sequence. This is mainly because even massive galaxies obtain a non-trivial amount of gas via cold mode accretion at the present day (Kereš et al., 2009), which is enough to keep massive galaxies too blue. Hence one must prevent the vast majority of cold gas from entering into massive galaxies, be it pristine of recycled in a wind. Preventing hot and wind mode reaccretion produces a red sequence, but its LF is a power law with no obvious turnover at high masses.

Despite their broad successes, the merger and halo mass quenching model still fail in subtle ways. Investigating these failures critically can help us to identify the underlying physical processes that may be absent from our simulations.

The main failures of the merger quenching model are (a) an excess of very

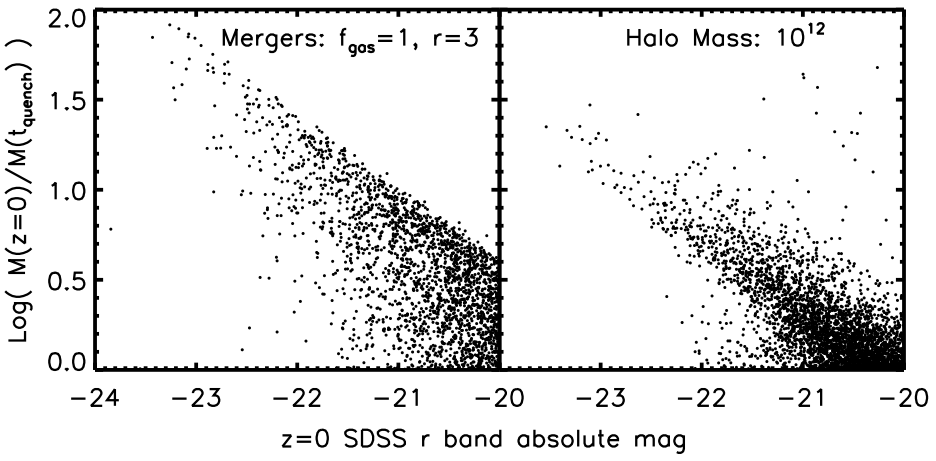

Figure 2.17 Mass growth of quenched galaxies via mergers. The y-axis is the log of the ratio of the stellar mass of quenched galaxies at $z = 0$ to the stellar mass at the time of quenching. The upper envelope in merger quenching arises due to our resolution limit defined by a cut in stellar mass (see §2.3.1). In both merger quenching and halo mass quenching, massive galaxies have obtained most of their stellar mass via mergers since they were quenched.

bright red galaxies, (b) a shallow slope in the red sequence color-magnitude relation, and (c) a shallow slope and a less pronounced knee in the luminosity function (as well as the stellar mass function).

The first problem results at least in part from post-quenching mergers. Quenched galaxies at the centres of massive halos build up stellar mass by accreting satellites. We illustrate the importance of this stellar mass accretion in Figure 2.17, which shows the $z = 0$ stellar mass divided by the stellar mass at the time of quenching as a function of $z = 0$ r-band absolute magnitude. Since we show only quenched galaxies, post-quenching mergers drive all of the mass growth. In both merger quenching and halo mass quenching, the biggest galaxies have grown by factors > 10 via mergers since the time they moved onto the red sequence. How-

ever, the merger quenching is generally larger at a given luminosity, and extends to factors up to ~ 100.

Too much mass is gained through this process, leading to excessively bright galaxies: galaxies brighter than $r = -22.5$ ($M_* > 10^{11} M_\odot$) at $z = 0$ in our model have grown in mass by a median factor of $\sim$3 since $z = 1$. This is inconsistent with observational constraints (Cool et al., 2008). Late-time mergers also explain the presence of young stars. Recent observations suggest no young populations in the brightest red sequence galaxies (Sánchez-Blázquez et al., 2009), although up to $\sim 30\%$ of red sequence galaxies do have $\sim$ 1–3% of their mass in stars < 1 Gyr old (Yi et al., 2005; Schawinski et al., 2007; Kaviraj et al., 2007). It is unclear whether the presence and amount of young stars in our simulated quenched galaxies is inconsistent with these data; we leave a more detailed investigation for the future.

By building up mass with small galaxies, post-quenching mergers may also contribute to the shallow slope of the red sequence colour-magnitude relation produced in the merger model. Stellar metallicities drive the slope of the red sequence, and the mass-metallicity relations (Tremonti et al., 2004; Finlator & Davé, 2008) tell us that massive star-forming galaxies are more metal-rich than their less massive counterparts. If the mass-metallicity effect dominates over the time evolution of metallicity at fixed mass, then a red and dead galaxy built up through accretion of many smaller galaxies will have a lower metallicity than that of a galaxy which grew just as massive through star formation then moved to the red sequence. Any accreted satellites will have a lower metallicity, diluting the total metallicity of the galaxy.

The shape of the luminosity function is more difficult to interpret. Its value in any luminosity bin is determined in a complicated way by the number of galaxies

moving to the red sequence from the blue cloud, and the number of galaxies moving along the red sequence. In principle, decreasing the mass accreted through satellites should steepen the red sequence slope, pushing the too-luminous galaxies to fainter r magnitudes, as well as keeping their metallicities higher.

How might one lower the amount of satellite accretion? One possibility is that the issue is numerical. Simulations with low resolution tend to overmerge dynamical systems owing to stronger tidal forces on satellites whose spatial extents are artificially enlarged by force softening. Another possibility is that much of the satellite mass is actually going into diffuse halo (or intracluster) stars. Conroy et al. (2007) suggests that even fairly sizeable galaxies must be disrupted upon infall into clusters on a fairly short ($\sim$ 2 Gyr) timescale. Both trends suggest that our simulations probably overestimate the growth of the central galaxy, at the expense of intermediate-mass galaxies. Unfortunately, running higher resolution hydrodynamic simulations with sufficient volume to study very massive galaxies is not feasible, unless one performs constrained realizations of dense environments (in which case statistical comparisons become more complicated).

Turning to the halo mass quenching scenario, the main failures are a) an excess of very bright red galaxies, b) essentially zero slope in the red sequence, c) no knee in the luminosity function, and d) a steep mass cut-off for blue galaxies. The first three problems are similar to those for merger quenching. Very bright red galaxies build up to an excess mass even though the satellites they accrete have been quenched. The problem is slightly less severe as in the merger quenching case, likely because satellite galaxies halt their star formation earlier. However, this trend also causes the slightly shallower red sequence slope as compared to merger quenching, because the accreted satellites are less enriched. When galaxies first move to the red sequence, their metallicities are governed by the mass-

metallicity relation. Since all red sequence galaxies arrive with roughly the same mass, they all start with roughly the same metallicity. Subsequent mergers between pairs of red sequence galaxies will then result in a remnant of the same metallicity. This results in almost no trend with metallicity along the bright red sequence ($r < -22$) in this model, as seen in Figure 2.7, which is inconsistent with the rather pronounced slope in the observed red sequence.

The last problem appears more severe and intrinsic to the halo mass quenching scenario. The local universe clearly contains massive, bright blue galaxies; these are absent under this scenario. The difficulty is that the sharp halo mass cut produces a strong truncation of blue galaxies above a certain stellar mass, corresponding to the typical halo mass of truncation. Some blue galaxies are observed to have stellar masses well in excess of $10^{11} M_{\odot}$, which under this scenario would have to live in halos of mass $< 10^{12} M_{\odot}$. This is a remarkably high efficiency of star formation from the available baryonic reservoir of such halos, well above what is inferred from observations at any halo mass (McGaugh et al., 2009). This difficulty for halo mass-based quenching was also was found in a comparison of SAMs to SDSS data by Kimm et al. (2009).

Overall, merger quenching appears to do a reasonable job of producing a red sequence as observed, and the discrepancies may be traceable to numerical issues. Of course a fully realistic model with quenching implemented dynamically within the simulation may alter the results, but the results here provide useful intuition and a starting point for more sophisticated models.

2.6.5 Generic problems in massive galaxy evolution

There are several fairly generic difficulties in understanding quenching in the context of the observed galaxy population and its evolution. These are similar among all models of quenching we have examined, and hint at an underlying

failure in our understanding or our current modeling techniques.

One issue is that there is an intrinsic tension between producing a strong knee in the luminosity or stellar mass function, and having blue galaxies exist in substantial numbers up to the highest stellar masses. The former would imply a very sharp quenching of star formation at a particular mass (stellar or halo), while the latter implies that quenching is a much more gradual function of mass. It is unclear how one can resolve this tension. Neither of our scenarios are able to do so, with merger quenching yielding large blue galaxies, and halo mass quenching producing a more pronounced truncation of the most massive galaxies.

A second issue is that the most massive galaxies are observed to have grown by a surprisingly small amount over the last ~ 10 Gyr (Cool et al., 2008; Banerji et al., 2009). A consequence of this is that we overpredict the bright end of the luminosity function in both our quenching models; this is even the case when the satellites quench immediately upon entering a quenched halo (in disagreement with data). One way to avoid this would be to have fewer or less massive satellites, or to avoid having them fall into the central galaxy. Perhaps more detailed simulations will reveal that our current results are tainted by numerical issues such as a lack of resolution, but even SAMs have shown similar issues. Understanding the dynamical evolution of a collisionless stellar and dark matter halo seems to be an unresolved problem in the context of massive galaxy evolution since $z \sim 1$.

A final issue is one of chemical enrichment, which is perhaps more subtle owing to current uncertainties in supernova yields and outflows. Nevertheless, it appears that our current simulations have difficulty enriching massive galaxies to observed levels, and perhaps more significantly, have trouble preferentially enriching massive red galaxies to levels approximately twice that of $\sim L^*$ sys-

tems. This has traditionally been a difficulty of hierarchical models that assemble the massive end of the red sequence by dry mergers with lower-mass systems, as this will tend to decrease the average stellar metallicities of the most massive system. Hence either massive galaxies must be preferentially enriched to begin with, which is seemingly contradictory to the ideas that they quench early on when galaxies of a given stellar mass have lower metallicity, or else the satellites they acquire must be quite metal-rich, which causes tension with trying to limit the amount of late-time growth. There is the further problem of understanding why α-enhancement grows with galaxy velocity dispersion (Graves et al., 2007), which again seems to place some stringent conditions on massive galaxy evolution (Arrigoni et al., 2009). Given the sensitivity of the exact shape and amplitude of the red sequence to metallicity, it is clear that a full understanding of massive galaxies will require understanding both their star formation and chemical enrichment histories.

2.7 Summary and Conclusion

By combining cosmological SPH simulations with simple post-processing prescriptions for the quenching of star formation, we test several proposed quenching mechanisms associated with major mergers, halo mass quenching, and quenching of hot and recycled wind accretion modes. We compared the galaxy populations resulting from these scenarios with observations of the $z \sim 0$ universe from SDSS. With reasonable parameter choices, our merger and halo mass quenching models vastly improve upon existing simulations by suppressing the excessive growth of massive blue galaxies and creating a well-defined bimodality in galaxy colors. However, even these models fail to match observations in detail, providing clues towards key issues in the modeling of massive galaxy eveolution.

Our main results are:

- Merger quenching and halo mass quenching successfully produce a red sequence distinct from the blue cloud, with luminosity functions roughly consistent with those observed.

- Quenching of hot mode accretion alone does not produce a viable red sequence, showing that late time accretion continues via cold mode in massive galaxies. Further quenching wind mode accretion produces a red sequence, but a highly discepant luminosity function.

- Our preferred merger quenching model rules out the re-formation of disks after gas rich mergers, because such re-formation leads to the build up of too many massive galaxies.

- The halo mass quenching model is quite sensitive to the threshold halo mass: $M_c \approx 10^{12} M_\odot$ yields the best match to the red galaxy luminosity function.

- Both of these models yield an excess of bright red galaxies due to mergers after the quenching process, and both yield somewhat too few galaxies around $\sim L^*$; these problems are more severe in the merger-based model.

- Both models yield red sequences with too shallow slopes in the colour-magnitude diagram, likely due to near-constant mean stellar metallicity along the red sequence.

- In both models, the red sequence is too blue by ~ 0.1 magnitudes, likely owing to simulated galaxies being too metal-poor by $\sim \times 2$ compared to real galaxies.

- In both models, the brightest red sequence galaxies are quenched at redshifts > 2, in general agreement with observed estimates.

We also identified some features that distinguish the merger quenching model from halo mass quenching:

- Massive galaxies quenched via mergers include trace populations of young stars, whereas halo mass quenched galaxies do not. This is true only if satellites in addition central are quenched, but if this is not the case then the massive end of the LF is grossly overpopulated.

- Merger quenching yields a population of very massive blue galaxies, with a mass function shape similar to that of red galaxies. Halo mass quenching creates a cutoff for blue galaxies at a stellar mass $\sim 10^{10.5} M_{\odot}$ associated with the $M_c = 10^{12} M_{\odot}$.

- For resolved galaxies ($M_* > 3.4 \times 10^9 M_{\odot}$), the rate of galaxies quenched via mergers peaks at $z \approx 3$, whereas halo mass quenching occurs at an approximately constant rate.

- The luminosity function for red sequence galaxies created via merger quenching has a shallower (bright end) slope than that for halo mass quenching.

Overall, the merger quenching model seems to fare somewhat better than halo mass quenching, particularly in terms of the blue galaxy mass function, though it still has significant discrepancies versus data. The generic failures in both models in terms of the shallow red sequence slope, the lack of a pronounced knee at L^*, and the excess of massive galaxies reflect that there may be generic failures of the manner in which we quench galaxies here. It is possible that some of the issues are numerical, but it could be that the quenching feedback processes actually

impact subsequent galaxy evolution in a manner not accounted for by the post-processing technique we employ here.

These results give us general intuition about how the red sequence is formed, as well as highlight the key issues that must be tackled by models. A concerted effort along both observational and theoretical fronts will be required to fully decipher the implications of these various trends. In future work, we plan to implement physical models for quenching within simulations dynamically. By identifying halos and merger events on the fly in our simulations, and quenching as appropriate, we can realistically track the feedback from quenching that influences subsequent star formation in galaxies. Given the evidence of the present study we favor quenching mechanisms involving major mergers, but this is unlikely to be the entire story. This work is but an early step towards understanding the origin and evolution of the fundamental bimodality in today's galaxy population.

CHAPTER 3

QUENCHING MASSIVE GALAXIES WITH ON-THE-FLY FEEDBACK IN COSMOLOGICAL HYDRODYNAMIC SIMULATIONS

Massive galaxies today typically are not forming stars despite being surrounded by hot gaseous halos with short central cooling times. This likely owes to some form of "quenching feedback" such as merger-driven quasar activity or radio jets emerging from central black holes. Here we implement heuristic prescriptions for these phenomena on-the-fly within cosmological hydrodynamic simulations. We constrain them by comparing to observed luminosity functions and color-magnitude diagrams from SDSS. We find that quenching from mergers alone does not produce a realistic red sequence, because $1-2$ Gyr after a merger the remnant accretes new fuel and star formation reignites. In contrast, quenching by continuously adding thermal energy to hot gaseous halos quantitatively matches the red galaxy luminosity function and produces a reasonable red sequence. Small discrepancies remain – a shallow red sequence slope suggests that our models underestimate metal production or retention in massive red galaxies, while a deficit of massive blue galaxies may reflect the fact that observed heating is intermittent rather than continuous. Overall, injection of energy into hot halo gas appears to be a necessary and sufficient condition to broadly produce red and dead massive galaxies as observed.

3.1 Introduction

Observations show a distinct bimodality in galaxy colors (Strateva et al., 2001; Baldry et al., 2004; Balogh et al., 2004; Bell et al., 2004b; Weiner et al., 2005; Willmer et al., 2006), with massive galaxies today generally being ellipticals having little

star formation or cold gas, while less massive galaxies tend to be blue spirals with cold gas. Despite being recognized in the earliest observations of galaxies, the origin of this bimodality remains poorly understood. The lack of galaxies in the region between the red sequence of ellipticals and blue cloud of spirals (often called the green valley) indicates that star formation must be quenched rapidly in order to transform blue galaxies into red ones (Bell et al., 2004b; Blanton, 2006). The preponderance of active galactic nuclei (AGN) in the green valley suggests that AGN are somehow connected to the process of quenching star formation (e.g. Schawinski et al., 2009). Several physical mechanisms have been proposed to effect this transformation, with two front-runners garnering much attention recently: feedback associated with galaxy mergers, and quenching due to virial shock heating of accreted gas. Both of these invoke AGN as a crucial energy source, namely quasars in the former case and radio jets in the latter.

Understanding the origin of massive, passive "red and dead" galaxies remains a problem for models of galaxy evolution. Hydrodynamic simulations of gas-rich galaxy mergers have been shown to induce starbursts and fuel powerful quasars (Hernquist, 1989; Barnes & Hernquist, 1992; Di Matteo et al., 2005). Observations lend support to the idea of a connection between mergers and powerful AGN (Hutchings et al., 1988; Sanders & Mirabel, 1996; Canalizo & Stockton, 2001; Bennert et al., 2008; Urrutia et al., 2008; but not all: e.g. Bahcall et al. 1997; McLure et al. 1999; Grogin et al. 2005; Gabor et al. 2009; Georgakakis et al. 2009). In merger simulations, the combination of feedback from star formation and black hole accretion unbinds the gas from the merger remnant, leaving a red elliptical galaxy devoid of fuel for star formation (Silk & Rees, 1998; Springel et al., 2005; Hopkins et al., 2008). This is now colloquially known as "quasar mode" feedback. Observations support various aspects of this picture, including high-

velocity outflows from post-starburst galaxies (Tremonti et al., 2007) and QSOs (Feruglio et al., 2010), and a peak in the fraction of AGN host galaxies with colors between the red sequence and blue cloud (e.g. Silverman et al. 2008; Schawinski et al. 2009, but see also Silverman et al. 2009; Xue et al. 2010). Recent work hints that secular processes may induce AGN (Cisternas et al., 2011), but it is not clear whether such AGN alone can quench star-formation in their host galaxies.

The presence of hot X-ray emitting gaseous halos around red and dead galaxies in groups and clusters suggests that these may also be associated with quenching. In this scenario, gas falling into the halo from the intergalactic medium (IGM) collides with stationary hot gas already in the halo. The resulting shock heats the gas to the virial temperature, converting the gravitational energy of infall to thermal energy (cf. Eggen et al., 1962; Silk, 1977; Rees & Ostriker, 1977; White & Rees, 1978). Several recent hydrodynamic simulations show that radiative cooling dominates over this shock heating in dark matter halos below a rough critical mass of $\sim 10^{12} M_{\odot}$, which is suggestively close to the mass at which the color bimodality divides galaxies. Above this critical mass, a stable shock forms and the halo develops a stable hot gas halo (Birnboim & Dekel, 2003; Kereš et al., 2005, 2009). This hot halo will shock heat newly accreting gas, thus stalling the ultimate fuel for star formation (Dekel & Birnboim, 2006; Birnboim et al., 2007). Dense filaments of gas may penetrate this hot halo, avoiding the virial heating and providing fuel for star formation, but this is predicted to be uncommon at redshifts less than 2 (Dekel & Birnboim, 2006; Ocvirk et al., 2008; Dekel et al., 2009a) because filaments are less dense at late times.

In massive galaxy cluster halos with peaked density distributions (roughly half of all clusters; Bauer et al., 2005), the hot gas appears to be cooling rapidly via X-ray emission (Fabian et al., 1984), yet UV, optical, and NIR observations

indicate only trace levels of star formation (Smith et al., 1997; Crawford et al., 1999; Hicks & Mushotzky, 2005; Quillen et al., 2008; Donahue et al., 2010) and little cold gas (e.g. Salomé et al., 2006). Hence some additional heating mechanism must counteract the X-ray cooling; this is the well-known cooling flow problem (Fabian, 1994). Observations of X-ray cavities thought to result from powerful radio jets have motivated a picture where a radio AGN in the central cluster galaxy provides this extra heating (McNamara et al., 2000; Fabian et al., 2000; McNamara et al., 2005). As gas cools from the hot halo, some of it accretes onto the massive central black hole, inducing an AGN (Ciotti & Ostriker, 1997). The kinetic power emerging via radio jets creates bubbles of typical size ~ 10 kpc (Bîrzan et al., 2004) in the central regions of the cluster. These bubbles then expand and degenerate into sound waves that effectively isotropize outflow energy and heat the hot intracluster gas on scales $>$30 kpc (Fabian et al., 2003; Voit & Donahue, 2005; Fabian et al., 2006; De Young, 2010). From gas cooling to gas heating by the AGN, this entire cycle may repeat itself on $\sim 10^{8-9}$ yr timescales (Ciotti & Ostriker, 2001). This is now referred to as "radio mode" feedback (Croton et al., 2006).

Mechanisms unrelated to supermassive black holes may provide the additional heating in hot X-ray halos. Thermal conduction in clusters provides central heating and inhibits cooling instabilities, although it is not sufficient to prevent cooling flows in all clusters (Zakamska & Narayan, 2003; Parrish et al., 2009; Ruszkowski et al., 2010). Infalling galaxies or stellar clumps may dynamically heat halos by transferring gravitational energy to the gas (Dekel & Birnboim, 2008; Khochfar & Ostriker, 2008; Johansson et al., 2009; Ruszkowski & Oh, 2010; Birnboim & Dekel, 2010). Whatever the mechanism, the key requirement is to heat up the cores enough to prevent substantial cooling and star formation, while allowing central cooling times less than the Hubble time (or even < 1 Gyr) to per-

sist in a substantial fraction of clusters and groups.

Debate persists about the effectiveness of these proposed quenching mechanisms on scales smaller than a kpc, within a single galaxy. Various simulations use different models for black hole accretion and feedback (Springel et al., 2005; Booth & Schaye, 2009; DeBuhr et al., 2009; Levine et al., 2010), and recent work raises doubts that even a powerful quasar could significantly affect star-forming gas throughout a galaxy (DeBuhr et al., 2009, 2010). In radio mode feedback, the observed AGN energy output is generally sufficient to counteract the radiative cooling in clusters or groups (McNamara et al., 2006; Best et al., 2006; Giodini et al., 2010). How this energy is efficiently distributed over space and time to prevent substantial cooling and star formation remains unclear, and cosmological models generally do not include realistic AGN radio jet physics. Hence while supermassive black holes are likely to be responsible for quenching, direct ab initio simulations of this process on a cosmological scale remain beyond current reach.

Semi-analytic models (SAMs), which marry analytic prescriptions for baryon physics to merger trees from cosmological simulations of dark matter, have successfully incorporated quenching mechanisms to create reasonable red sequence populations. Among analytic prescriptions for gas cooling and star formation, these models typically incorporate a starburst and bulge growth during galaxy mergers. These merger prescriptions are not enough to make massive galaxies red, so modelers include some suppression of cooling in hot, massive halos, usually via AGN feedback (Croton et al., 2006; Bower et al., 2006; Somerville et al., 2008). While most SAMs contain such prescriptions, the exact amount of quenching feedback required and the mechanisms by which they operate differ widely among models, possibly because these models must make many assumptions regarding the gas dynamics which can be quite uncertain (Lu et al., 2010; De Lucia

et al., 2010).

Hydrodynamic cosmological models follow the gas dynamics directly, but without some explicit quenching mechanisms they generally do not yield a realistic red sequence with appropriate luminosity or mass functions. These models greatly reduce the number of free parameters relative to SAMs by tracking the dynamics of gas inflows and outflows directly, at large computational cost. Although hydrodynamic models directly track the dynamics of galaxy mergers and yield hot gas in massive halos, they still produce only constantly growing, blue, star-forming galaxies at the massive end of the mass function. Recent work has begun to include black hole fueling and feedback. These works have focused on reproducing the black hole mass–bulge velocity dispersion ($M-\sigma$) relation, black hole properties, and AGN population properties, with significant successes (e.g. Sijacki et al., 2007; Degraf et al., 2010; Booth & Schaye, 2009, 2010). Typical models involve Bondi-Hoyle accretion of surrounding gas by the central black hole, with some assumed fraction of the accreted rest-mass converted to heat in the surrounding gas (Springel et al., 2005; Booth & Schaye, 2009). These prescriptions, while pioneering, are poorly constrained and may not properly model the dominant accretion mechanisms (Booth & Schaye, 2009; DeBuhr et al., 2009). They also do not focus on producing red sequence galaxies as observed, and have had only limited success doing so.

In this work we also employ hydrodynamic simulations, but we focus on reproducing the observed galaxy population rather than the observed black hole and AGN population. Our approach is therefore somewhat different, in a sense intermediate between fully hydrodynamical simulations and SAMs. Here we simply ask, how is quenching related to the evolutionary properties of galaxies and their halos? We apply heuristic models for quenching by adding energy

in various forms to galaxies and their surrounding gas during the evolution of the simulation, and ask which models are successful at producing red and dead galaxies as observed. We do not try to explicitly grow black holes and account for their feedback. In Gabor et al. (2010), we conducted a precursor study on *post-processed* star formation histories, and concluded that both radio mode and quasar mode feedback could in principle produce red galaxies if all future star formation was assumed to be suppressed, but several other attempted mechanisms such as shutting off hot mode accretion or recycled wind mode accretion could not. As such, we now focus particularly on the two popular mechanisms of radio mode and quasar mode, with the goal of determining which one drives the quenching of massive galaxies.

Here, as in Gabor et al. (2010), we compare our simulation results to observations of the galaxy population at redshift $z \approx 0$, and leave detailed evolutionary studies for the future. We consider the red sequence in color-magnitude diagrams, and the corresponding red galaxy luminosity function. Due to uncertainties in dust models, we use galaxy stellar mass functions to compare our simulated blue cloud population observations. Our main result is that superwinds induced by galaxy mergers cannot create a red sequence, because galaxies continue to accrete gas from the IGM even after a merger, while our quenching mechanism based on hot halo gas produces a successful match to the observed red galaxy luminosity function. This favors radio mode feedback as the primary driver for the formation of the massive red galaxy population.

We describe the physics of our simulations in §3.2, including our newly implemented quenching models in §3.2.1. In §3.3 we describe the observational data. We compare the results of these new models to observed color-magnitude diagrams (CMDs) and luminosity functions (LFs) for local galaxies in §3.4. We then

consider physical consequences of our models in §3.5, and discuss future directions in the discussion.

3.2 Simulations

Our simulations are run with an extended version of the N-body + smoothed particle hydrodynamics (SPH) cosmological simulation code GADGET-2 (Springel, 2005), as described in Oppenheimer & Davé (2008). Along with gas cooling and star-formation, our version includes galactic winds tied to the star formation and a chemodynamical model with sources including AGB stars and Type Ia supernovae. In the following subsections, we describe additional modifications to the code to implement quenching of star formation.

For star formation in cold, dense regions, we use the two-phase model of Springel & Hernquist (2003). This model, based on McKee & Ostriker (1977), assumes that any gas particle dense enough to be Jeans unstable contains a hot medium and cold clouds in pressure equilibrium. Stars form from the the cold clouds with a characteristic timescale, τ. This timescale effectively sets the efficiency of star formation, and Springel & Hernquist (2003) find that $\tau \approx 2$ Gyrs yields galaxy models that match the observed Kennicutt relation (Kennicutt, 1998). The three model components exchange mass, energy, and metals via condensation and feedback from supernovae.

Star-forming gas particles in the simulations spawn star particles with a probability based on the star-formation rate. The resulting collisionless star particle takes on a mass equal to half the original mass of a gas particle. The average gas particle spawns up to two star particles in this stochastic way.

Along with the feedback implicit in the star-formation model, our simulations include an explicit stochastic model of galactic winds (Oppenheimer & Davé,

2008). We eject star-forming gas particles from galaxies by giving them a velocity kick v_w (Springel & Hernquist, 2003). The probability that a gas particle will enter a wind in the first place is the mass-loading factor η (the ratio of mass entering winds to the mass of stars formed) times the probability for star formation. In our simulations v_w is proportional to, and η inversely proportional to, the galaxy circular velocity. These scalings, which arise in the momentum-driven wind model of Murray et al. (2005), are motivated by observations of winds in local galaxies (Martin, 2005; Rupke et al., 2005). Once a gas particle enters a wind, we decouple it hydrodynamically until it reaches a density 0.1 times the critical density for star formation (up to a maximum duration of 20 kpc/v_w). This decoupling is intended to represent chimneys through which material can escape easily but that cannot be reliably modeled by the spherically-averaging SPH algorithm.

In order to study the chemical enrichment of galaxies and the IGM, our code includes models for stellar mass loss and Type Ia supernovae, described in Oppenheimer & Davé (2008). As the stellar population represented by a star particle ages, mass loss from AGB stars injects metal-enriched mass to the nearest 3 gas particles based on the mass-loss rates from Bruzual & Charlot (2003). We estimate Type Ia supernova rates for each star particle using Scannapieco & Bildsten (2005), with a prompt and delayed component. Each supernova injects both energy and metal mass into the surrounding gas.

With this treatment of galactic winds, our simulations match broad observations of star-forming galaxies and the IGM, including the chemical enrichment of the IGM at $z > 2$ (Oppenheimer & Davé, 2006, 2008), the galaxy mass-metallicity relation (Davé et al., 2007; Finlator & Davé, 2008), and the luminosity functions of high-redshift galaxies (Davé et al., 2006; Finlator et al., 2007). These simulations do not, however, yield massive red and dead galaxies, and galaxies are far too

massive and bright at low redshifts. We require some additional mechanisms to halt star-formation in massive galaxies – the hydrodynamics and feedback models we have described above are insufficient.

3.2.1 Quenching Prescriptions

We incorporate two independent quenching models (which may be combined) into GADGET-2. We are deliberately agnostic about whether supermassive black holes or some other mechanisms provide the energy or momentum in these feedback prescriptions. For the first, we assume that major galaxy mergers ultimately drive the transformation of galaxies from blue to red. We identify mergers in the simulation, and add a kinetic kick to the gas in the merger remnant to expel star-forming gas. This burst of energy mimics the effects of a powerful quasar or starburst (e.g. Di Matteo et al., 2005).

In the second quenching model, we assume that the hot gas halos surrounding massive galaxies facilitate quenching. We identify these hot, massive halos in the simulation, then continually add thermal energy to the halo gas in order to cut off the fuel for star-formation. The addition of thermal energy mimics the added heat from radio AGN (e.g. McNamara et al., 2005), unresolved gravitational heating (e.g. Dekel & Birnboim, 2008), conduction (e.g. Jubelgas et al., 2004), or cosmic rays (e.g. Guo & Oh, 2008).

3.2.1.1 Quenching via galaxy mergers

Our first quenching prescription ties truncation of star formation to galaxy mergers. This requires identifying galaxy mergers within the simulations on the fly, then applying some quenching process to the particles in those mergers. We implement empirically-motived, high-velocity winds that eject cold gas from merger remnants.

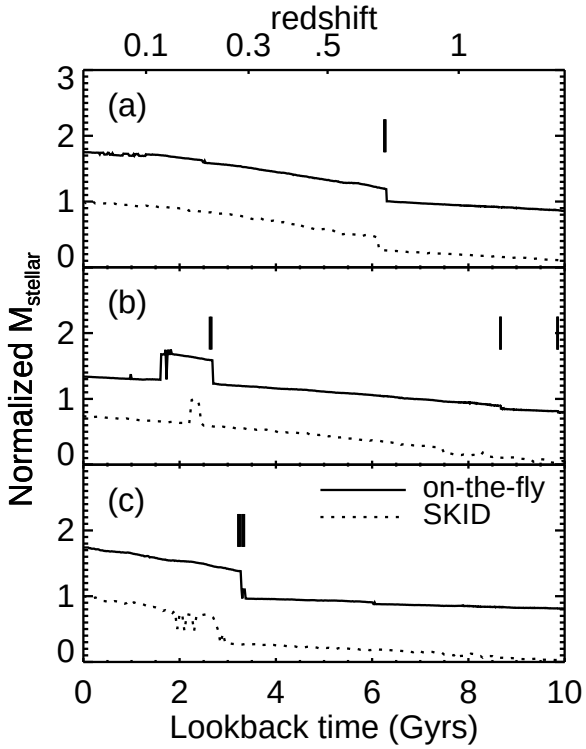

Figure 3.1 Comparison of stellar mass histories calculated using two different group-finders for three galaxies (one galaxy per panel). Dotted lines show normalized masses identified by SKID in post-processing, while solid lines show our faster on-the-fly FOF masses offset by 0.75. Vertical line segments indicate mergers identified on-the-fly. **(a)** A galaxy with an easily identified major merger. **(b)** A galaxy with a major fly-by, incorrectly identified as a merger. **(c)** A merger where the final coalescence is ~ 1 Gyr later with SKID than with our on-the-fly method. The latter two problems are sufficiently rare to have little impact on our results.

Merger identification is based on our on-the-fly galaxy finder, developed in Oppenheimer & Davé (2008). This algorithm uses a parallel friends-of-friends (FOF) algorithm to group together particles into galaxies. We set the linking length between particles to $0.06 r_s (H(z)/H_0)^{1/3}$, where r_s is the mean interparticle separation, H_0 is the hubble constant (70 km s^{-1}), and $H(z)$ is the hubble parameter as a function of redshift. Oppenheimer & Davé (2008) showed that stellar masses of groups found with this prescription successfully matched those obtained in post-processing with the slower but more physically-motivated Spline Kernel Interpolative Denmax (SKID) [1] algorithm (Kereš et al., 2005). To optimize for speed, we divide the simulation volume into grid cells and only calculate distances between particles in neighboring grid cells. We identify groups independently for each central processing unit, then merge groups split onto adjacent CPUs by checking whether groups separated by less than 30 linking lengths indeed have particles that should be linked together. The frequency with which we run the galaxy finder varies from a few Myr to a few 10's of Myr, depending on the adaptive time-step intervals.

We identify mergers on-the-fly by looking for persistent, rapid increases in stellar mass growth. This requires knowing the recent mass history of each galaxy. We track the 6 most recent galaxy catalogs constructed by the galaxy finder, then connect galaxies in the most recent catalog to their earlier most-massive progenitors. By tracking both the current and previous galaxy host of each particle, we can easily identify the progenitors of a given galaxy by searching through its constituent particles and noting their previous host galaxies.

For a given galaxy, we identify a merger by comparing its current stellar mass to that of its recent progenitor galaxy. In detail, we compare the median mass of

[1] http://www-hpcc.astro.washington.edu/tools/skid.html

the three most recent progenitors ($M_{\rm recent}$) to the median mass of the three older progenitors ($M_{\rm older}$). If $M_{\rm recent}/M_{\rm older} > (1 + 1/r)$ then we flag the galaxy as a merger. We use the median approach, rather than just comparing the most recent galaxy mass to the previous one, to avoid declaring mergers of brief encounters and fly-by's. Since the usual value of $r = 3$ yielded good matches to the galaxy luminosity function in Gabor et al. (2010), we use the same choice here (see §3.4.4 for further discussion).

This method of identifying mergers likely declares the merger before galaxies have fully merged. Since we use all particle types in the galaxy finder, two merging galaxies will appear as one once the central regions of their dark matter halos overlap. Similarly, when two galaxies closely pass by each other, our method will declare a merger whether the galaxies eventually coalesce or not. Based on the work of Maller et al. (2006), this appears to be a generic problem with merger identification in cosmological simulations. We mitigate this effect partially by taking the median masses over several time steps as described above – rapid fly-by's will not alter the median mass enough to cause a merger identification, although some longer, close fly-by's do (as we show below). In cases where the two galaxies do finally coalesce, the precise timing of the quenching does not matter much, since we effectively get rid of all cold gas in the remnant (see below). Early quenching could, however, stunt the star formation that might naturally occur during the merging process, leading to slightly smaller stellar masses and lower metallicities in merger remnants. In the end, our results are not expected to be sensitive to these effects.

To illustrate the successes and challenges of our merger identification method, in Figure 3.1 we compare the stellar mass histories of galaxies identified on-the-fly to the masses of the same galaxies identified with SKID in post-processing.

The mass growth histories from the on-the-fly FOF method broadly match those from SKID, and ∼60% of galaxies with $M_{\rm stellar} > 10^{10} M_{\odot}$ in this simulation undergo at least one merger in the last 10 Gyr. Panel (a) shows a well-matched single major merger. Panel (b) illustrates the difficulty with fly-by's that do not end up merging. Both FOF and SKID combine the two galaxies into a single galaxy at some point, and then separate them again as the two galaxies move apart. Among galaxies with at least one merger, our method mis-identifies fly-by's as major mergers in $< 10\%$ of the cases. Panel (c) shows a case where detailed structure in the mass history identified by SKID is missed by FOF. In the FOF case, it looks like a clean-cut major merger. With SKID, however, the stellar mass jumps, then after a few hundred Myrs begins to fluctuate up and down before settling in a more massive state. This suggests an initial fly-by, then a few more close passages, then a final coalescence just over 1 Gyr after the initial merger identification. Among galaxies with at least one merger, our method identifies one of those mergers too early by > 500Myr in $\sim 25\%$. In future work we may attempt to identify the final coalescence, and avoid mis-identifying fly-by's, by invoking a delay time of a few hundred Myr before actually declaring the merger. Given the broad nature of this study, such details of merger identification do not substantially affect our results.

Once we have identified a merger, we apply energetic ejective feedback to the star-forming gas within the merger remnant, mimicking a powerful wind. Observations of post-starburst galaxies and QSOs suggest that such winds with velocities ~ 1000 km s^{-1} or more may be responsible for quenching star formation (Tremonti et al., 2007; Feruglio et al., 2010). We pursue the extreme case where all the star-forming gas is ejected in a wind because this is probably necessary to produce a red galaxy remnant (cf. Gabor et al., 2010). Each gas particle in the

merger remnant galaxy is given a velocity kick of $v_{\rm kick}$ in the direction $\vec{v}\times\vec{a}$, where $\vec{v}$ is the pre-kick velocity vector, and $\vec{a}$ is the acceleration vector.

Tremonti et al. (2007) compared post-starburst galaxies with winds ∼1000 km s^{-1} to low-ionization broad absorption line quasars (Trump et al., 2006) with winds up to $\sim 10^4$ km s^{-1}. We choose $v_{\rm kick} = 1500$ km s^{-1} as a compromise for large-scale outflows that have likely exited the galaxy. Simulations with $v_{\rm kick} = 1000$ km s^{-1} showed little difference in the results, since this is still well above the escape velocity for most halos. As with our winds associated with star-formation, we decouple the wind particles from hydrodynamic processes to enable escape from the ISM, just as we do with star formation-driven winds.

As an addition to ejective feedback, we optionally implemented a thermal feedback mechanism associated with galaxy mergers. In this case, we heat all the star-forming gas particles to the virial temperature of the halo, as estimated below in §3.2.1.2. It turns out that in combination with the ejective feedback, it makes little difference to the results, since ejected gas almost never returns to the galaxy whether we heat it or not.

3.2.1.2 Quenching in hot halos

The presence of a hot gaseous halo around most massive red and dead ellipticals hints at some role in quenching. Hence for our second main quenching mechanism, we heat gas in the hot gaseous halos around galaxies. For each galaxy identified on-the-fly, we estimate the hot gas fraction in its halo. In halos dominated by hot gas, we add heat by raising the temperature of gas particles around the galaxy.

To obtain the hot gas fractions of galactic halos, we estimate the virial radius corresponding to each halo, find all the gas particles within that radius, then count up the mass on either side of a temperature threshold defining "hot." We

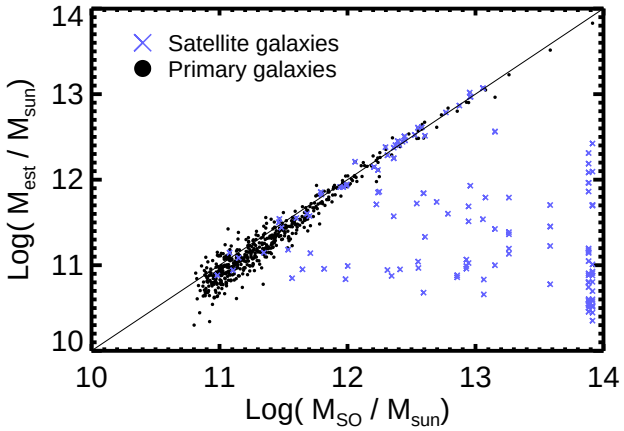

Figure 3.2 Comparison of halo mass estimates from our on-the-fly algorithm (y-axis) and a post-processing spherical overdensity algorithm (x-axis). The dotted line shows a perfect 1-to-1 correspondence. In the on-the-fly case, we multiply the baryonic (gas and stellar) mass found by our FOF galaxy finder by an empirical factor of 18 to get $M_{\rm est}$ with the best fit. This factor is larger than the expected cosmic factor (~ 6) because we tune the FOF linking length to match the stellar mass, not the total baryonic mass, of galaxies. Much of the baryonic mass remains in an extended halo not captured by the FOF method. The on-the-fly algorithm underestimates the halo masses of many satellite galaxies (blue crosses). This is because the spherical overdensity method associates satellite galaxies with their massive parent halo, whereas our FOF galaxy finder associates them with their smaller sub-halos.

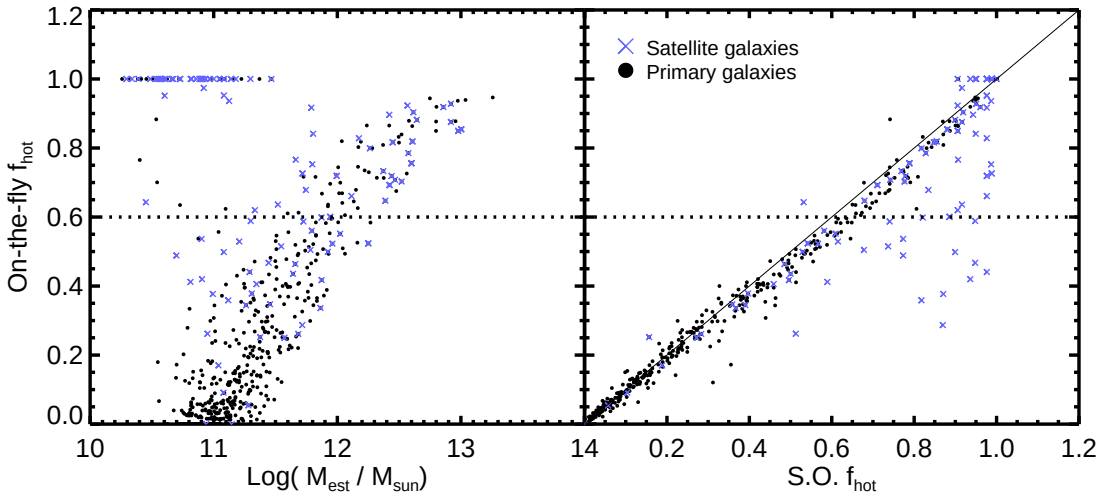

Figure 3.3 Hot gas fractions calculated on-the-fly vs. halo mass ($M_{\rm est}$) and spherical overdensity (SO) hot fraction for galaxies in a small volume simulation. Black dots show central galaxies and blue crosses satellite galaxies (as found using SO). Hot gas fractions are defined as the fraction of gas within the virial radius above 250,000 K. The left panel shows that low-mass halos have little hot gas in their surroundings, while increasingly larger halos have increasingly high hot fractions (cf. Kereš et al., 2005). The galaxies in low-mass halos with $f_{\rm hot} = 1$ are satellite galaxies embedded in massive, hot halos. The right panel compares our on-the-fly estimate to our post-processing, spherical overdensity estimate of $f_{\rm hot}$, and a thin solid line shows a perfect 1-to-1 correspondence. We can reliably estimate the hot fractions of galaxies on-the-fly in the simulation.

estimate the halo virial radius, $R_{\rm vir}$, using the equation $\rho_{\rm vir} = M_{\rm est}/(4/3\pi R_{\rm vir}^3)$. Here, $\rho_{\rm vir}$ is the virial density for collapsed structures at the appropriate epoch, and $M_{\rm est}$ is an estimated halo mass. We find $M_{\rm est}$ by scaling the baryonic mass of the galaxy from the group finder by a factor of 18. As shown in Figure 3.2, this empirical scale factor value best reproduces the total halo masses found using a more thorough spherical overdensity algorithm in post-processing. This departs significantly from the cosmic value of $\Omega_M/\Omega_{\rm baryon} \simeq 6$ because our on-the-fly group finder purposely does not capture the full radial extent of the halo. Our FOF linking length is chosen to match galaxy stellar masses, so it is too small to capture much of the outer halo. Nevertheless, the empirical factor of 18 nicely estimates the total halo mass.

We add the mass of each gas particle within the virial radius to a tally of the hot gas mass if the particle's temperature exceeds 250,000 K; otherwise, we consider it "cold" or warm for the purpose of identifying hot gas halos. We choose 250,000 (or $10^{5.4}$) K because this separates the main bulk of cooler IGM that eventually cools into galaxies from the hot tail of the IGM from which cooling and forming stars is rare (cf. Kereš et al., 2005, 2009; Gabor et al., 2010).

Once we have measured the hot and cold gas masses within the virial radius of each galaxy, we apply the quenching heat if $f_{\rm hot} \equiv m_{\rm hot}/(m_{\rm hot} + m_{\rm cold}) > 0.6$. A hot fraction of 0.6 corresponds roughly to halo masses of $10^{12} M_\odot$ (Kereš et al., 2005). In Gabor et al. (2010), we found that quenching star formation in halos with of $M > 10^{12} M_\odot$ or $f_{\rm hot} > 0.6$ led to luminosity functions that best reproduce those observed.

Figure 3.3 illustrates the effectiveness of our hot fraction estimate in a small simulation. Our on-the-fly hot fraction calculation accurately reproduces the trend noted by Kereš et al. (2005): halos above $\sim 10^{12} M_\odot$ have hot fractions above

~ 0.6 (left panel), and the transition between halos dominated by cold and hot gas is fairly abrupt. Outliers from the trend with low masses and $f_{\rm hot} = 1$ are small satellite galaxies embedded in the hot halo of a larger galaxy. In the right panel, we compare our on-the-fly hot fraction estimate to that from our post-processing, spherical overdensity method. With a high degree of reliability, we can determine whether the gaseous halo surrounding a galaxy is hot.

In FOF galaxies above the hot fraction threshold, we raise gas particles to the estimated virial temperature of the halo. In our base model, we only raise the temperatures of particles that are *not* star-forming, i.e. that are not within the existing cold ISM of galaxies within the halo. We also do not raise the temperature of particles already exceeding the virial temperature. We use equation 59 from Voit (2005) to estimate the virial temperature, using $M_{\rm est}$ for the halo virial mass:

$$k_B T = (8.2{\rm keV}) \left(\frac{{\rm M_{est}}}{10^{15}{\rm h^{-1}M_\odot}} \frac{{\rm H(z)}}{{\rm H_0}} \right)^{2/3} . \tag{3.1}$$

Here, k_B is Boltzmann's constant, $H(z)$ is the redshift-dependent Hubble parameter, and H_0 is the Hubble constant (at $z = 0$). In practice, we found that instantaneously heating particles to the virial temperature sometimes led to unphysically high hydrodynamic accelerations. To prevent adaptive time-steps from becoming too short, we instead double the entropy of the gas particle until it reaches the virial temperature. Through this heating mechanism, we prevent gas from ever cooling and forming stars.

A key aspect of our mechanism is that energy is continually added to keep particles hot. Gas within the hot halo that cools below $T_{\rm vir}$, or accreted gas that is below $T_{\rm vir}$, is heated as described above during every time step of the simulation. This is perhaps overkill; to suppress star formation, it may not be necessary to keep gas at or above the virial temperature, nor to do so at every timestep. Here, however, we will make this maximal heating assumption to ensure star formation

is suppressed, even though we will discuss later that the energetics of this are quite extreme. We will explore relaxing the heating assumption in future work.

Given the overall success of our hot gas quenching model, we explored many variants on our base model:

1. We heat *all* gas within halos to the virial temperature, including star-forming gas within the ISM of galaxies.

2. We use a criterion based directly on the halo mass (rather than hot gas fraction). While there is a close correlation between hot gas halos and massive dark matter halos (cf. Figure 3.3, Birnboim & Dekel 2003; Kereš et al. 2005), some models have had success quenching star formation above a particular halo mass, typically around $10^{12} M_{\odot}$ (e.g. Cattaneo et al., 2006; Gabor et al., 2010).

3. We restrict the heating to within a certain radius $r_{\rm heat}$ from the center of the halo. This is an attempt to mimic feedback from a central radio AGN. Voit & Donahue (2005) argue, based on observations of an entropy floor within the central 30 kpc in cooling flow clusters from Donahue et al. (2006), that an AGN outburst sufficient to counteract the cooling will create subsonic, buoyant bubbles at a typical radius of 30 kpc. The region outside this radius should be heated by the expanding bubbles. Following this, we use $r_{\rm heat} = 30$ kpc. A numerical difficulty with this is that we found that large galaxies in our simulations have star-forming regions at significantly larger radii. This result occurs for galaxies identified using both FOF and SKID methods. This may owe either to satellite galaxies at these radii being grouped into the central galaxy, or to the threshold density for star formation being too low. We note that the SF threshold is ≈ 0.1 cm^{-3}, which is

well below ISM densities where star formation occurs in reality. This is a historical numerical convenience motivated by the inability of our simulations to fully resolve ISM densities. In any case, this variant produces a red sequence, but has too many massive galaxies remain blue due to the ongoing star-formation. Apparently in our simulations, heating only the central regions of a halo does not heat the outer regions as suggested by observations of sound waves in clusters (Fabian et al., 2006). The failure of central heating to spread energy to large radii may suggest that we do not adequately resolve the hydrodynamics in our typical hot halos, or that raising the temperature to only $T_{\rm vir}$ may be insufficient, and we need to raise it further.

4. We do not heat gas below our 250000 K critical temperature. This is intended to allow for cold flows from IGM filaments to penetrate into hot halos, as has been argued by Dekel et al. (2009). We discuss this variant further in §3.4.3.

5. We do not heat gas within sub-halos. As indicated by Figure 3.2, many small satellite galaxies live in the hot gas halos of their larger hosts. AGN in these small galaxies may or may not contribute significantly to the overall heating of the hot gas halo. Since their importance in quenching massive galaxies is debatable, we implemented a method to identify these sub-halos and exclude them from the feedback prescription. When calculating hot gas fractions as described above, we estimate the virial radius of each FOF galaxy. If a galaxy's center falls within the virial radius of another, more massive, galaxy, then we consider it a sub-halo. Once we identify sub-halos, we do not apply the thermal feedback to gas within them. We discuss results of

this mechanism in §3.4.3.

3.2.2 Simulation parameters

Simulating massive galaxies presents a substantially larger computational challenge than simulating more common systems. One is pushed towards larger volumes ($\gtrsim 50$ Mpc/h) by the need to obtain a sufficient statistical sample of massive galaxies. Conversely, since massive galaxies begin forming stars first, this requires simulations that robustly resolve early star formation, requiring higher resolution (∼few kpc). Given computational resource limitations, we can only perform a few large runs. To explore all the variants listed above, we are forced to run smaller simulations. We choose to compromise on volume to ensure robust star formation histories.

Our primary simulations use a box size of $48h^{-1}$ Mpc and a gravitational softening length of $3.75h^{-1}$ kpc (equivalent Plummer), with 256^3 dark matter and 256^3 gas particles. This yields a gas particle mass of $1.2\times10^8 M_\odot$, and a dark matter particle mass $5.1\times$ larger. Our smaller simulations keep the same mass and spatial resolution, but reduce the box size to $24h^{-1}$ Mpc with 128^3 dark matter and 128^3 gas particles. All simulations and analyses use a *Wilkinson Microwave Anisotropy Probe* concordance cosmology (Komatsu et al., 2009) with $H_0 \equiv 100h = 70$km s^{-1} Mpc^{-1}, matter density $\Omega_m = 0.28$, baryon density $\Omega_b = 0.046$, a cosmological constant with $\Omega_\Lambda = 0.72$, root mean square mass fluctuation at separations of 8 Mpc $\sigma_8 = 0.82$, and a spectral index of $n = 0.96$. Our small runs are useful for testing some of the variations in the quenching physics, and also for tracking details of each on-the-fly galaxy and feedback event. The larger simulations do a much better job of sampling the massive end of the luminosity function, but take many weeks to run.

We focus primarily on three models which we refer to as *no quenching*, *merger*

quenching, and hot gas quenching. The no quenching model includes star formation and momentum-conserving winds, but no additional explicit feedback mechanism. It is effectively the same model as the "vzw" model of Oppenheimer & Davé (2008). The merger quenching model incorporates 1500 km s^{-1} winds from merger remnants to quench star formation. For the hot gas quenching, we focus on a model where we heat only the non-star-forming gas particles in FOF galaxies with $f_{\rm hot} > 0.6$. In §3.4 we will also explore some simulations with slight variations of the quenching models.

3.2.3 Simulation outputs and analysis tools

We output snapshots of each simulation at 108 redshifts, starting at $z = 30$ and ending at $z = 0$. The snapshots contain information for every simulation particle, including position, velocity, mass, metallicity, gas density, gas temperature, star-formation rate, and time of formation (for star particles). In addition to these outputs, we save the galaxy catalog from each instance of the on-the-fly galaxy finder for later analysis.

Our suite of analysis tools allows us to compare our simulation results directly with observations. SKID provides a list of member particles (star and star-forming gas) for each simulated galaxy. The sum of star particle masses is then the galaxy stellar mass, and the star formation rates of the gas particles are summed to give the star formation rate of the galaxy.

We then calculate galaxy spectra using the models of Bruzual & Charlot (2003). We treat each star particle as a single stellar population with an age and metallicity determined directly in the simulation. By adding up the spectra of all star particles within a galaxy, we obtain the spectrum of that galaxy. Then we convolve galaxy spectra with observational filter curves to obtain broad-band colors and magnitudes.

3.3 Observational Constraints

To characterize the effectiveness of our quenching models, we compare the results of our simulated galaxy populations to galaxy observations in the low-redshift ($z < 0.1$) universe. Our goal is to create a realistic red sequence, so we focus on color-magnitude diagrams (CMDs) and red-galaxy luminosity functions (LFs).

We follow Gabor et al. (2010) in using the low-redshift version of the Value-Added Galaxy Catalog (VAGC, Blanton et al., 2005) of the SDSS (Adelman-McCarthy et al., 2008; Padmanabhan et al., 2008). This catalog includes $ugriz + JHK$ absolute magnitudes for ~ 170000 galaxies with $z \lesssim 0.05$. After converting absolute magnitudes to our preferred cosmology (with $h = 0.70$), we can straightforwardly plot CMDs. We will plot $g - r$ vs r because the r-band light is a good tracer of stellar mass. For the luminosity functions, we use r-band luminosities and the $1/V_{\rm max}$ method (Schmidt, 1968) with the $V_{\rm max}$ values in the VAGC. We compare these observational results with simulation snapshots at $z = 0.025$, which we will refer to as low redshift or $z = 0$.

As discussed in Gabor et al. (2010) and §3.4.2, uncertainties in dust obscuration motivate us to compare mass functions (MFs) of blue galaxies rather than luminosity functions. For this we use publicly available stellar masses derived for SDSS galaxies by fitting observed galaxy spectra to templates (Kauffmann et al., 2003). We cross correlate this sample with the VAGC to obtain ~ 40000 galaxies with stellar masses and broad-band colors for the MFs.

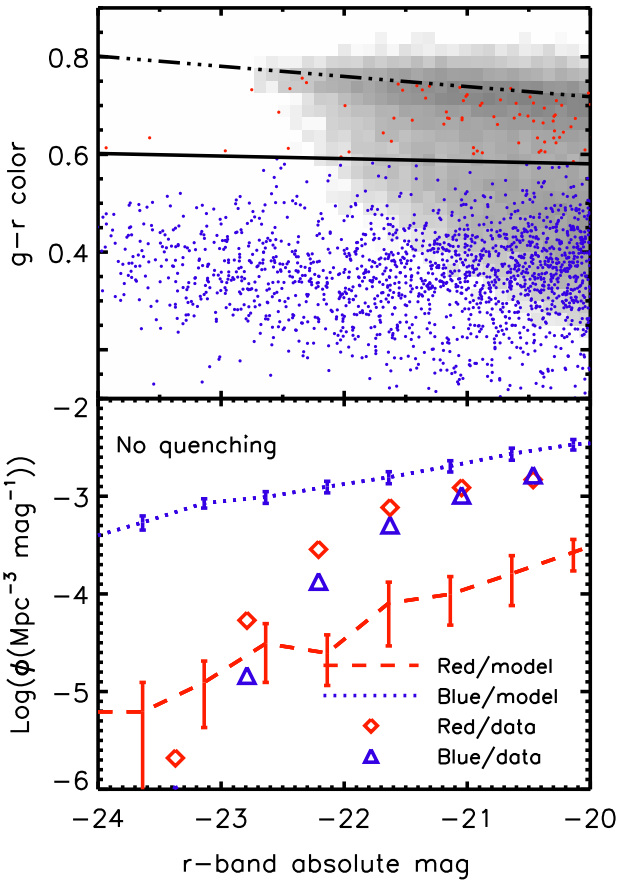

Figure 3.4 CMD (top panel) and LF (bottom) for a simulation with no quenching. In the CMD, grayscale represents the density of SDSS galaxies, points are simulated galaxies, the dot-dashed line is a fit to the observed red sequence, and the solid line separates the simulated red sequence and blue cloud. Without quenching, our simulations do not produce red galaxies. In the LF, symbols represent the observed luminosity functions for red and blue galaxies, and lines are for simulated galaxies. The red galaxy luminosity function is too low by roughly an order of magnitude. Simulated blue galaxy luminosities are computed without a correction for dust to distinguish the intrinsic red sequence more easily.

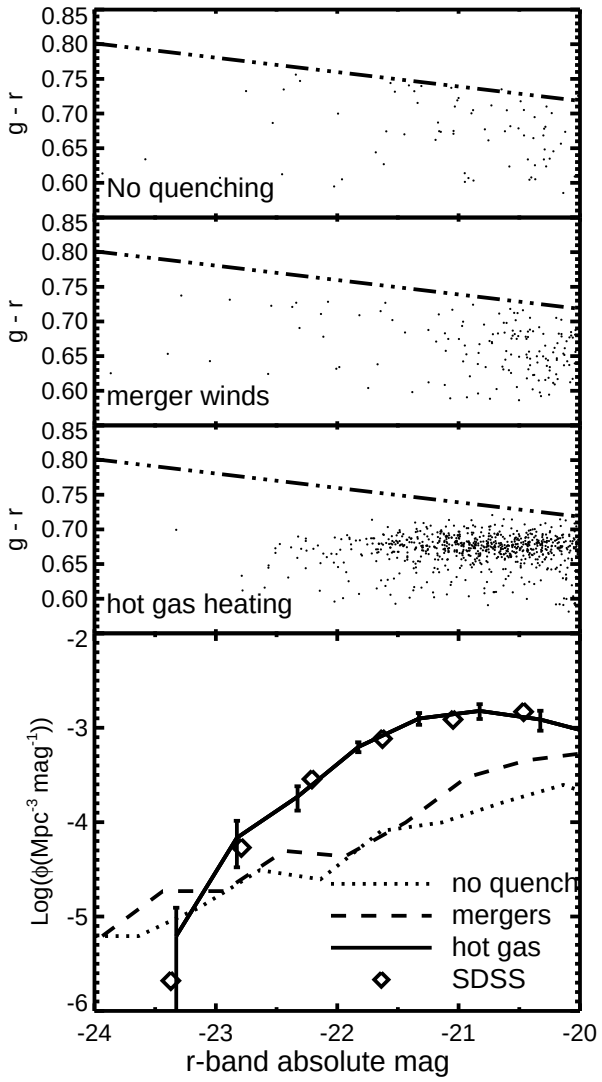

Figure 3.5 CMDs zoomed in on the red sequence (top 3 panels) and LFs (bottom panel) for simulations with no quenching, merger quenching, and hot gas quenching. This shows the main result of this work: merger quenching fails to produce a substantial red sequence, whereas hot gas quenching succeeds.

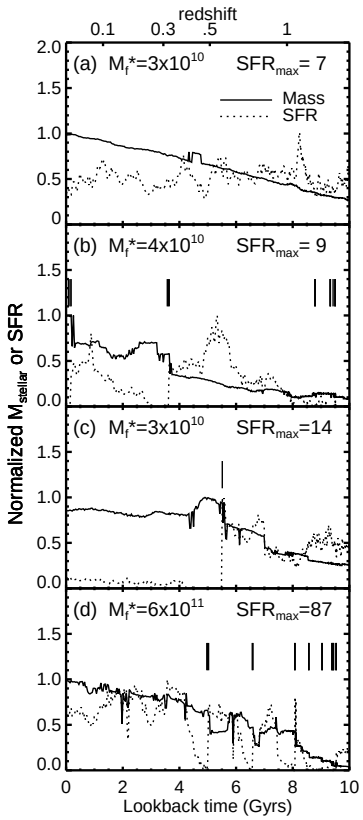

Figure 3.6 Cosmic histories of mass (solid lines) and instantaneous star-formation rate (dotted lines) for 4 galaxies from a simulation with merger quenching. These illustrate the variety of outcomes following major mergers. We show the $z = 0$ stellar mass (M_f^* in $M_\odot$) and maximum star-formation rate (in $M_\odot \mathrm{yr}^{-1}$) for each. (a) A galaxy with moderate, fairly constant star-formation rate. (b) A galaxy with some major mergers. By design, the star-formation rate drops to zero immediately following a merger. The star-formation rate recovers within about 2 Gyrs due to gas accretion and possible minor mergers. (c) A galaxy whose major merger quenches almost all subsequent star formation until $z = 0$. (d) The complex mass history of the central galaxy in one of the two most massive groups in the simulation. This galaxy undergoes several major mergers, after each of which the SFR recovers within 1 Gyr due to fresh inflows of gaseous fuel.

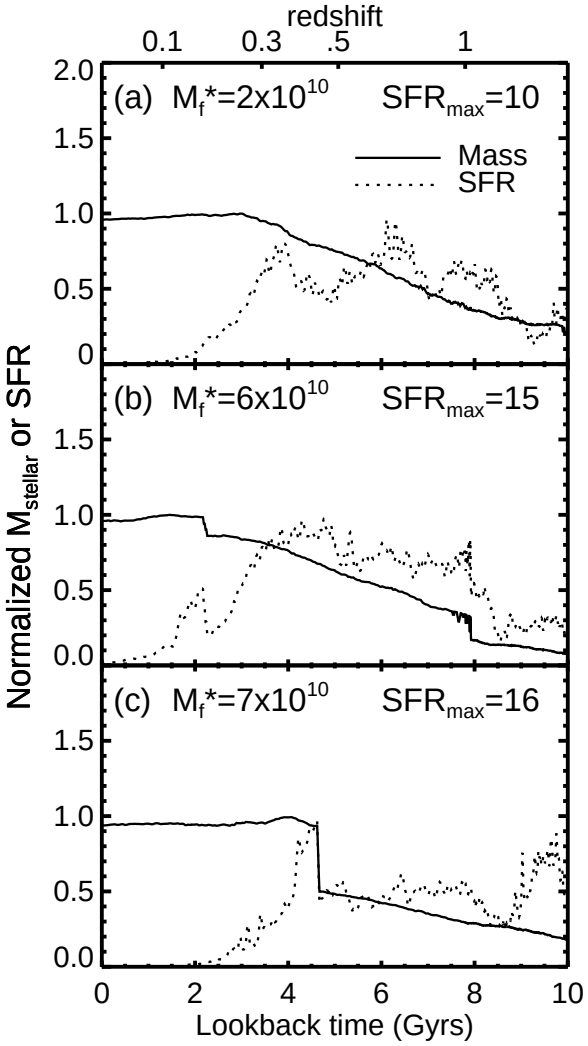

Figure 3.7 Star formation histories (dotted lines) and stellar masses (solid lines) for three galaxies in our hot gas quenching model (cf. Figure 3.6). (a) A galaxy with fairly quiescent star-formation and steady mass growth. At $z \approx 0.3$, this galaxy's halo becomes dominated by hot gas, after which we begin heating the gas to prevent cooling. Starved of new fuel, star-formation declines to zero over ~ 2 Gyr. (b) A minor merger (lookback time ≈ 2 Gyr) delivers fuel to a galaxy which had begun quenching about 2 Gyr earlier. (c) A major merger increases a galaxy's halo mass to the point where it can support a hot halo, after which it is quenched.

3.4 Constraining Quenching Models

3.4.1 Basic models: Red Galaxies

Since our goal is to reproduce a realistic red sequence, we compare the red galaxy CMDs and LFs produced by our various models to determine the best match. We first illustrate the problem with simulations that do not have additional quenching mechanisms. Figure 3.4 shows the full CMD and LF for a simulation with no quenching feedback, compared to observations. Following Gabor et al. (2010), we separate red simulated galaxies from blue in the CMD using the solid line. This line is bluer and shallower than that used for observed galaxies because it better captures the bimodality in our most successful models. As we discuss below (and in Gabor et al., 2010), our model red sequence is generally too blue and has little or no slope. We estimate LF uncertainties based on a jackknife re-sampling of the simulation volume (Finlator et al., 2006) (typical observational uncertainties are smaller than the symbols except for the brightest bins).

Almost all galaxies in this no-quenching simulation constantly accrete gas from the IGM, and this gas supplies the fuel for ongoing star formation. As a result, the simulation produces few red galaxies and many very massive, very bright blue galaxies. The LF reflects this effect. The red galaxy LF is too low (relative to that observed) by an order of magnitude for $r \approx -21.5$, and the blue LF is too high. Furthermore, this model does not produce the observed sharp turnover in the luminosity function at high masses (Oppenheimer et al., 2010).

We show the simulated blue galaxies without accounting for obscuration from dust to illustrate the intrinsic galaxy luminosities. Dust obscuration will push the blue galaxies up and to the right (redder and fainter) in the CMD, possibly contaminating the red sequence. The observed universe does not contain star-forming galaxies as massive as those shown here, so estimating the extinction in

these simulated galaxies would require large extrapolations that are unlikely to be robust. We discuss dust extinction and blue galaxies further in §3.4.2.

Focusing just on the red sequence, we compare results for models with no quenching, merger quenching, and hot gas quenching in Figure 3.5. Like the no quenching simulation, the merger quenching model leaves a very sparse red sequence. Our hot gas quenching model, however, produces a red sequence of galaxies well-separated from the blue cloud.

The luminosity function panel in Figure 3.5 represents one of the central results of this paper. It emphasizes that our hot gas quenching model nicely produces a sharp truncation in the red galaxy LF, while our merger quenching model does not. Because it produces so few red galaxies, merger quenching does not significantly improve the red galaxy luminosity function of our simulations without quenching. The hot gas quenching model fares well, matching the observed red sequence luminosity function at all magnitudes we resolve.

For the very brightest galaxies, the relatively small volume of our simulations hampers the comparison with data – we do not effectively sample the highest peaks in the density distribution that lead to the most massive galaxies. This is reflected in our errorbars.

Examining the halo quenching red sequence further, we see that it is too blue by about 0.1 magnitudes in $g - r$, and has a nearly flat slope that fails to match the observed trend that brighter red galaxies are redder. We examined this issue at length in Gabor et al. (2010), and the same underlying causes are likely here. The overall "blueness problem" may result from either metallicities that are too low or ages that are too young. Our red galaxies have metallicities lower than those inferred for the observed red sequence in the VAGC, and lower metallicities lead to bluer stars. Mean stellar ages of our galaxies are at least as old as those

inferred from the observations, so incorrect ages cannot cause the red sequence to be too blue. Since we match the stellar masses, the metallicity deficit is unlikely to owe to an under-production of stars. It could be that our outflow model ejects too many metals from these systems, or else we might have adopted supernova metal yields that are too low. The red sequence slope poses a subtler problem, perhaps suggesting that simulated massive galaxies merge with too many, too massive, or too young satellite galaxies with lower metallicities. In §3.4.2, we describe a metallicity re-calibration that matches our simulated red galaxy colors to those observed.

Why does merger quenching fail? In Gabor et al. (2010) we showed that if star formation is completely quenched in the remnants of major mergers, then our models can produce a reasonable match to the red sequence. Merger quenching therefore does not fail because there are too few major mergers. Rather, merger quenching fails because star formation resumes even after a merger remnant loses all its star-forming gas.

We illustrate the resumption of star formation after merging in Figure 3.6. Each panel corresponds to an individual galaxy taken from a small test simulation with merger quenching. For each galaxy we show the normalized star-formation history (dotted lines) and stellar mass history (solid lines) over cosmic time, with vertical tick marks indicating major mergers. Galaxies with no major mergers (panel a) have fairly constant star formation histories (since $z \sim 2$), with peaks and valleys depending on the details of accretion from the IGM and outflows powered by stars. Galaxies that undergo major mergers (panels b–d) generically stop forming stars when a merger occurs because we instantaneously eject all the cold gas. However, in every case the merger remnant resumes star formation as new fuel is accreted from the IGM. The timing and intensity of the

resumption of star-formation varies, probably depending on environment. A very massive galaxy living at the center of a large potential well (panel d) will accrete new gas and return to high star-formation rates in ~ 1 Gyr. Some smaller galaxies (e.g. panel c) never return to SFRs near their pre-merger levels, though they do resume some star-formation within ~ 2 Gyrs.

As a comparison, we show star-formation histories for quenched galaxies in our hot gas quenching model in Figure 3.7. The galaxy in panel (a) grows steadily in stellar mass until its halo becomes dominated by hot gas (at $z \approx 0.3$). At this point our hot gas heating cuts off additional fuel for star-formation, and the galaxy gradually uses up its pre-existing reservoir of gas. Star formation peters out after ~ 2 Gyrs. Even after the starvation process begins, merging galaxies can momentarily supply new fuel, as reflected by a jump in SFR in panel (b) at a lookback time of ~ 2 Gyrs. In panel (c) we show a galaxy whose major merger raises its halo mass enough that a hot gas halo becomes stable. These star-formation histories all show a slow decline in star-formation rate over ~ 2 Gyr timescales, similar to the star-formation timescale in our sub-grid star-formation model (Springel & Hernquist, 2003). After star formation stops, the galaxy stellar mass declines slowly owing to stellar evolution.

In summary, a simple model where all star formation is quenched in galaxies with a hot halo fraction above 60% produces a red galaxy luminosity function in very good agreement with observations. It also produces a reasonable red sequence, although it is still too blue and too shallow as we saw previously in Gabor et al. (2010), likely reflecting issues with enrichment. In contrast, assuming that all major mergers are associated with 1500 km s^{-1} outflows as suggested by observations (Tremonti et al., 2007) does not significantly populate the red sequence.

3.4.2 Basic models: blue galaxies

We have shown that additional heating in hot gas halos can produce a red sequence whose luminosity function matches that observed in the local universe. We now examine galaxy colors more closely. Since these are sensitive to uncertain dust corrections and problems with metallicities, we will use galaxy stellar mass functions later in this section.

Figure 3.8 shows a complete CMD and corresponding LFs for our hot gas quenching model. Here, we apply an ad hoc metallicity correction to force the simulated red sequence to match the observed colors. This assumes that our predicted stellar ages are correct, but that our simulations under-predict stellar metallicities in massive red galaxies. We add a metallicity of $Z_{\rm add}$ to each single stellar population (i.e. star particle) when calculating galaxy colors using stellar population synthesis models. By trial and error, we find a good fit using the relation

$$Z_{\rm add} = 0.003 + (6 \times 10^{-14} M_{\rm stellar}/M_{\odot}). \tag{3.2}$$

These are absolute metal mass fractions, and solar metallicity here is ≈ 0.012 (Asplund et al., 2005). This correction gives an indication of how far off our metallicities must be. For a $10^{11} M_{\odot}$ galaxy (with typical absolute magnitude $r \sim -22$), $Z_{add} = 0.009$, representing an increase of $\sim 50\%$ over typical simulated metallicities for such galaxies.

We show blue galaxies in the CMD with a correction for dust extinction of optical light in the g and r bands. In our dust prescription, the $E(B-V)$ extinction scales with star-formation rate based on empirical relations with UV luminosity of local galaxies (Wang & Heckman, 1996; Somerville et al., 2001; Finlator et al., 2006). We assume a Calzetti et al. (2000) reddening law. This dust prescription yields a blue cloud in fairly good agreement with data, especially in the qualita-

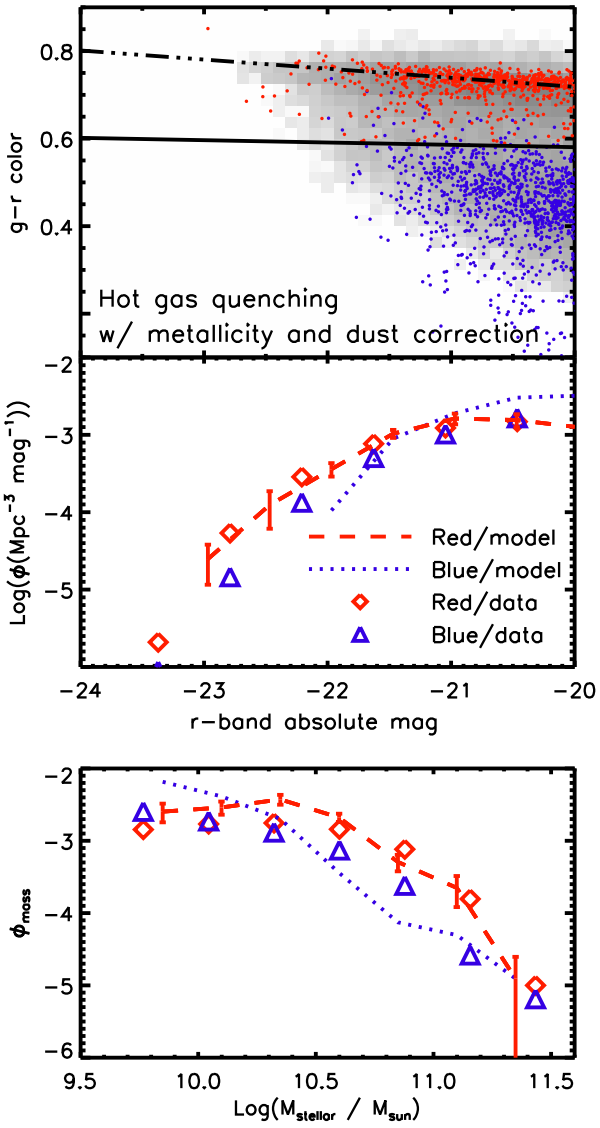

Figure 3.8 Full CMD (top panel), LFs (middle panel), and stellar mass functions (lower panel) for our hot gas quenching model. The simulated CMD includes a metallicity re-scaling to best reproduce the observed red sequence colors, as well as dust reddening and extinction for the blue galaxies. Due to uncertainties in the dust prescription, we prefer to use stellar mass functions (lower panel) to compare simulated and observed blue galaxies. Our hot gas quenching model yields too few massive blue galaxies.

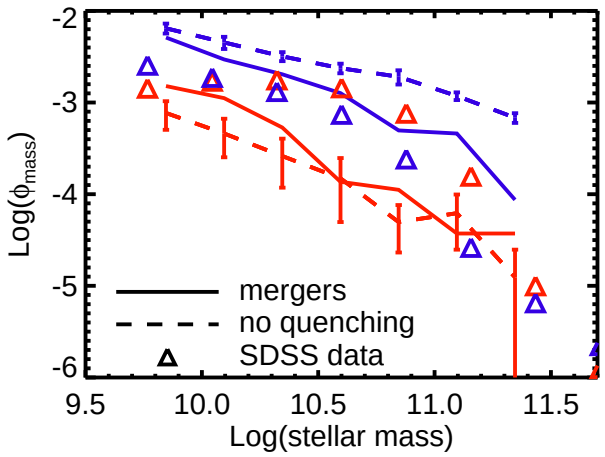

Figure 3.9 Stellar mass functions split into blue and red galaxies (colors) for a simulation with no quenching (dashed lines), a simulation with merger quenching (solid lines), and SDSS data (triangles). Inducing powerful outflows after galaxy mergers does suppress the growth of massive blue galaxies, but it does little to increase the number of red sequence galaxies above that produced in the no-quenching simulation.

tive shape. It also shifts a small number of intrinsically blue galaxies onto the red sequence, but we count these galaxies as blue for the purposes of calculating the luminosity and mass functions.

In Gabor et al. (2010), we discussed the difficulties in modeling extinction. Given a model galaxy with a specified star-formation and gas accretion history, we need to know the level of dust extinction and reddening to compare colors with observed galaxies. Several dust extinction prescriptions keyed to physical properties of galaxies, such as metallicity or star-formation rate, have been proposed (Finlator et al., 2006). Different dust prescriptions yield substantially different colors and magnitudes for our star-forming model galaxies, suggesting large uncertainties. This is especially true for large, bright blue galaxies since these are not well represented in the real Universe. For red galaxies this is not a problem because they have very little extinction (Lauer et al., 2005).

One way to mitigate the large uncertainties in dust obscuration is by examining stellar mass functions for the blue galaxies, rather than luminosity functions. We use stellar mass estimates from Kauffmann et al. (2003) based on SDSS spectra, which account for extinction self-consistently within the SED fitting procedure for each galaxy. We cross-correlate these stellar mass measurements with galaxies from the VAGC, allowing us to use broad-band colors and generate mass functions using the $1/V_{\rm max}$ method. Using the broad-band colors, we separate the galaxies into the red sequence and blue cloud as before.

We show the resulting stellar mass functions for our hot gas quenching model in the bottom panel of Figure 3.8. As expected from the luminosity function results, and given the tight correspondence between luminosity and mass for old stellar populations, the red galaxy mass function matches the observations well. The blue galaxy stellar mass function is overall a good match to data as well, al-

though it shows a slight under-production of star-forming galaxies just above the knee of the LF. The small number of galaxies (< 10) populating the bright end show only trace levels of star-formation. Our hot fraction criterion ($f_{\rm hot} > 60\%$) for feedback results in a fairly sharp critical halo mass of $\sim 10^{12} M_{\odot}$ (Figure 3.3), and therefore stellar mass of $\sim 10^{10.5} M_{\odot}$, above which fueling of star-formation is turned off. Nevertheless, later infall of blue systems can turn a massive galaxy somewhat bluer temporarily. Hence this model produces massive blue galaxies, although the details of that are quite sensitive to our quenching prescription and should be taken with some caution.

This quenching model minimally impacts small galaxies, basically only when they are satellites within larger halos. Davé et al. (2011) show that the fraction of satellite galaxies at these masses is about one-third, which explains why any impact on satellites results in only minor changes to the mass function. At the faint end, our model somewhat over-produces the faint star-forming galaxy population, which is a result also seen in the total mass function examined in Oppenheimer et al. (2010). Thus, while our hot gas quenching model successfully matches the observed number densities of red sequence galaxies, it fails to match all the details of the blue galaxy population.

For comparison, we show the galaxy stellar mass functions for our no-quenching and merger outflows simulations in Figure 3.9. Solid lines correspond to our no-quenching model, and dashed lines to merger quenching. By ejecting the gas from galaxy merger remnants, we substantially reduce the number density of very massive star-forming galaxies. As indicated by the luminosity function analysis above, merger quenching does not substantially increase the number of red galaxies. In both models, both red and blue mass functions look roughly like power laws, lacking the exponential cutoff observed in SDSS. This shows that

merger quenching helps with only one of the two problems in the simulated LFs, namely that it reduces the number of blue galaxies, but it does not increase the number of red galaxies.

In summary, quenching by halo hot fraction successfully reproduces the SDSS red galaxy LF, and broadly reproduces the SDSS red sequence. An empirical augmentation to galaxy metallicities given in equation 3.2, which increases metal content by typically 50% (with a range of 10–100%), results in an excellent match to the red sequence. The predicted red galaxy mass function is likewise an excellent fit to data, and the blue galaxy mass function broadly matches as well although there is a hint of too few bright galaxies and too many faint ones. The agreement using hot halo quenching is far superior to that using merger quenching, as the latter does not increase the red sequence over a no-quenching model although it does significantly suppress blue galaxies. These simulations therefore suggest that halo gas quenching, by itself, drives the formation of the red sequence.

3.4.3 Model variations

We now consider physically-motivated variations on our basic models. Here we present three variations that all include hot gas heating. In the first we combine our merger winds quenching model with our hot gas heating model. Both of these mechanisms are well-motivated by observations, hence both processes may occur in the real universe. We refer to this as the "combined" model.

In a second variation, we add an exception to the hot gas heating model. Several authors have argued that cold flows of gas along filaments can penetrate hot gas halos at high redshift, since filaments are denser at earlier epochs. In principle our simulations should capture this behavior with their hydrodynamic treatment. Our basic hot gas heating model, however, bypasses the hydrodynamics to

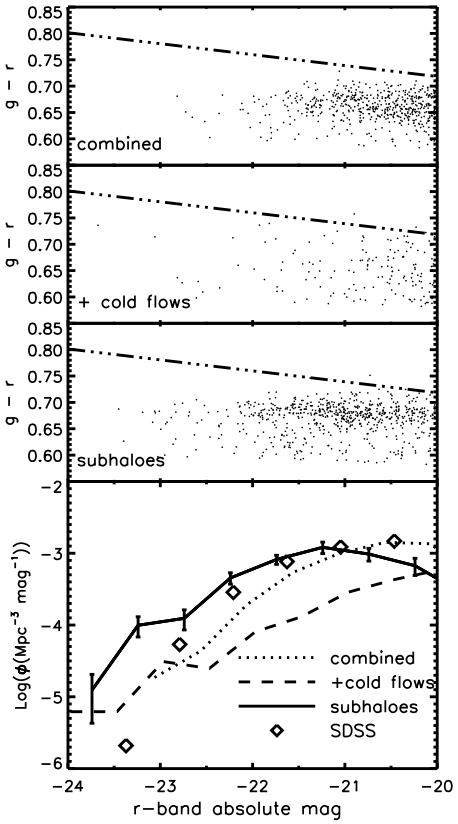

Figure 3.10 CMDs (top 3 panels) and LFs (bottom panel) for three alternative quenching models: combined hot gas heating + merger winds (top CMD, dotted line in LF), the same combined model except *without* heating any gas below 250000 K (middle CMD, dashed line in LF), and a model with hot gas quenching *without* heating gas around sub-halos (bottom CMD, solid line in LF). The combined model performs well, with slightly lower LFs than the hot gas quenching-only model. Allowing cold flows fails due to wind recycling, and allowing gas fueling in sub-halos leads to discrepancies at both low and high luminosities in this range.

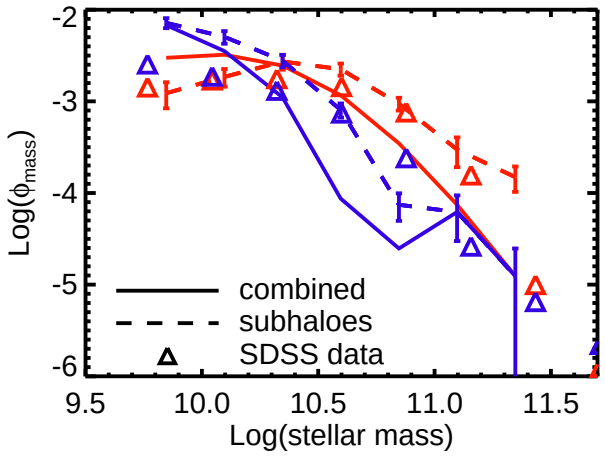

Figure 3.11 Blue and red galaxy mass functions (color-coded) for our combined quenching model (solid lines) and our model without heating gas around subhalos (dashed lines). The combined model shows a larger deficit of massive blue galaxies, and the subhalos model shows a similar deficit to that in our basic hot gas heating model.

heat all (non-star-forming) gas around a galaxy. In order to prevent artificial heating of these cold flows, allowing them to penetrate hot halos, we implemented a model where we only heat gas that is already above our hot gas cutoff of 250000 K. We present this variation with the combined mergers + hot gas model, but we note that the results are similar when we apply this variation to our basic hot gas heating model. We refer to this as the "cold flows" model.

In a third variation, we tested a model where we do not heat the hot gas in the vicinity of sub-halos. In our simulations, some sub-halos are embedded in their parent's hot gas halo, even if the sub-halo is too small to support its own hot gas. Our basic quenching model heats the gas in these sub-halos just the same as in the massive, parent halos. Heating from AGN feedback is typically observed in the centers of groups and clusters, and it is not clear whether heating from AGN in small satellite galaxies actually occurs in the real Universe. In our simulations, many satellites particularly at low masses are stripped of gas owing to ram pressure or starvation (Davé et al., 2011), but larger satellites are typically star-forming. X-ray observations do suggest that most satellites in clusters have mini cooling cores analogous to those seen in brightest cluster galaxies, and that heating by supernovae or AGN may be necessary to quench them (Sun et al., 2007). Some satellite elliptical galaxies show evidence for AGN outbursts (Jones et al., 2002; Machacek et al., 2006).

To distinguish sub-halos (or satellite galaxies) from their parent halos, we use the virial radii estimated when calculating hot gas fractions. If we consider two halos A and B, then halo A is a subhalo of halo B if and only if (1) the center of halo A falls within halo B's virial radius and (2) halo B is more massive than halo A. We flag sub-halos in our group catalog, and we do not add heat to their gas. Note that in this "subhalos" variant, we do not induce outflows in galaxy merger

remnants.

We show results from these three model variations in Figures 3.10 and 3.11. Figure 3.10, analogous to Figure 3.5, shows CMDs and LFs for just the red sequence in our three variant quenching models. Combined quenching has only a small overall effect on the red sequence when compared to our basic hot gas quenching: at all masses, the number density of red galaxies is slightly below that observed. In short, merger quenching has little overall effect on the galaxy population.

Our "cold flows" model fails to produce a red sequence. This is *not* due primarily to pristine infall along filaments, but rather due to recycling of material expelled by star formation-driven winds (Oppenheimer et al., 2010). Wind recycling dominates infall in galaxies since $z \sim 1$, and is stronger in more massive systems that have short recycling times. Although particles in these systems are ejected at speeds of up to ~ 1000 km/s, their cooling times times are short owing to the high level of enrichment, and so many never heat above the shock threshold. We discuss this issue further in §3.6.

Our variation that excludes heating in sub-halos (the "subhalos" model) increases the number of bright red galaxies and decreases the number of faint ($r \lesssim -20$) red ones. The deficit of faint red galaxies is straightforward – turning off quenching in satellites allows those satellites to accrete gas and remain blue. The excess of bright red galaxies arises because the massive galaxies that make up the bright end grow significant mass via mergers with their satellites, even after the central galaxies have been quenched (Gabor et al., 2010). Without quenching, these merging satellites form more stars before they are subsumed than they do with quenching. These mergers then result in more massive central galaxies, and a corresponding increase in the bright-end luminosity function.

To study the blue galaxies in these variant models, we again look at stellar mass functions. Figure 3.11 shows mass functions for the combined quenching model (solid) and the hot gas quenching model without sub-halo heating. In comparison to our basic hot gas heating model, the combined model results in a sharper cut-off in the blue galaxy mass function above $M_{\rm stellar} \sim 10^{10.5} M_{\odot}$, leading to a larger deficit of massive blue galaxies. The model without sub-halo quenching yields a similar blue galaxy mass function to our basic hot gas heating model.

Overall, the variant models we tested do not solve the underlying problems with our basic models, while introducing new problems. Our combined model exacerbates the deficit of blue galaxies at masses $\gtrsim 10^{10.5} M_{\odot}$. Our model with cold flows fails to produce a red sequence. Our model without heating of sub-halos creates discrepancies in the bright and faint end red galaxy LF.

The combined model leads to similar results as the basic model, but with fewer red sequence galaxies. In Gabor et al. (2010) we showed that the halo mass cutoff, or correspondingly the hot fraction cutoff, above which we quench star-formation largely determines where the exponential cutoff begins in the LF. We therefore expect that raising $f_{\rm hot}^{\rm crit}$ from 0.6 to, say, 0.7 might bring the combined quenching model into better agreement with observations. We cannot therefore easily distinguish between the basic hot gas quenching and the combined quenching models.

In summary, by testing many variants on our basic quenching models, we find that hot gas quenching is required to get a red sequence, while merger quenching has minimal impact. Variations based on not quenching gas in cold flows or subhalos have a noticeable but not large effect on the LF and CMD. None of these variants impact the slope or blueness of the red sequence, which continue to be

a difficulty. Hence while all these quenching model variants are physically motivated, in the end a model with simple hot gas quenching matches the ensemble data as well as or better than any of the others.

3.4.4 The dependence of merger quenching on the critical mass ratio

Studies typically define major mergers as those with a 3:1 mass ratio or smaller. We have adopted this critical mass ratio ($r = 3$) here for merger quenching, assuming that mergers with larger mass ratios have no effect. In this appendix, we show that allowing larger mass ratio mergers to trigger quenching does not lead to a red sequence in better agreement with observations. Although using $r > 3$ leads, in a general sense, to more quenching, it does not lead to a bimodality in galaxy colors nor a significant number of red galaxies.

Figure 3.12 compares color-magnitude diagrams and luminosity functions for four different simulations: one with our preferred hot gas quenching model, and our merger quenching model with three values of the critical mass ratio, $r = 3, 5,$ and 10. These simulations are run with the same resolution as our main simulations, but with a volume $8\times$ smaller. While this volume does not sample massive galaxies well, it does illustrate the main trends. In particular, we show the hot gas model because it exhibits a well-populated red sequence distinct from the blue cloud. We show marginally resolved galaxies with $r-$band > -20 to help clarify the underlying behavior of the simulations.

As described in the text, the merger quenching model under-produces red galaxies while suppressing overall galaxy growth (compared to a model without quenching). This is true for any value of the critical mass ratio. Furthermore, the sparsely populated region of red galaxies is poorly separated from the blue cloud, representing the tail of a unimodal distribution rather than one peak of a bimodal distribution. As we move to higher values of the mass ratio, over-

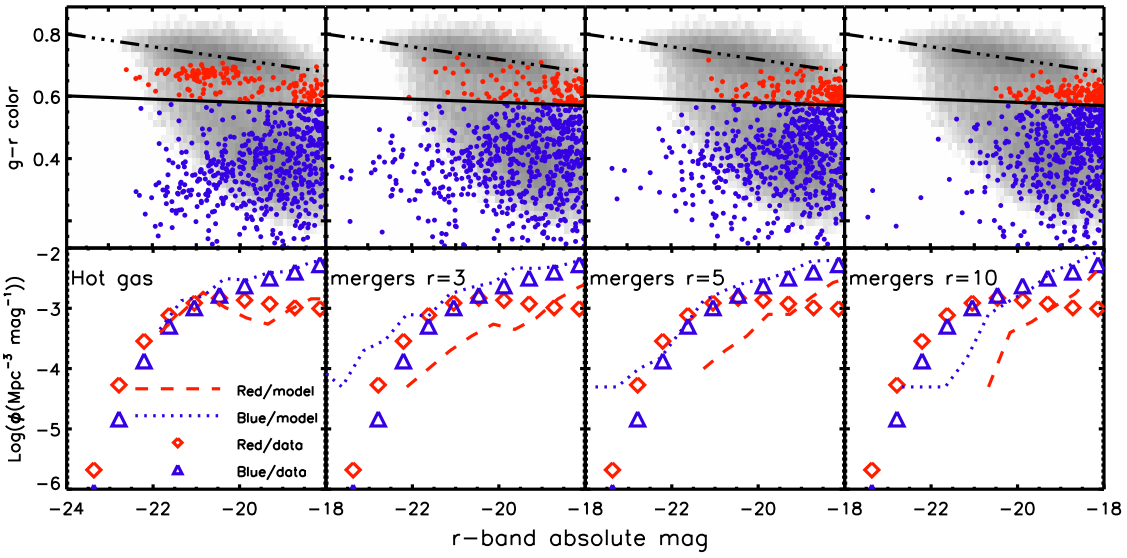

Figure 3.12 Using a critical mass ratio $r > 3$ to define major mergers does not yield a red sequence, as indicated by color-magnitude diagrams (top row) and luminosity functions (bottom row) for hot gas quenching (left column) and merger quenching with $r = 3, 5,$ and 10. These simulations were run in boxes of side length $24h^{-1}$ Mpc. Even at this smaller volume, hot gas quenching results in an obvious red sequence with number densities close to those observed. Merger quenching with values of $r > 3$ leads to a stronger suppression of galaxy growth (fewer bright galaxies, e.g. right column), but does not yield a distinct red sequence with substantial number densities.

all galaxy growth is suppressed more and more, but only a few galaxies at any given time are red. Even with frequent quenching events due to minor mergers, galaxies continuously accrete new material from the IGM to fuel star-formation.

3.5 Physical Impact of Quenching

Our quenching models have many physical and observable implications for galaxies and the IGM. Winds from merger quenching could impact the diffuse IGM. Our hot halo quenching has a major impact because it changes star formation histories. Since outflows associated with star formation enrich the IGM and often end up returning to galaxies, changes in the star-formation rates can lead to changes in IGM and galaxy properties in complicated ways. Exploring all these changes is beyond the scope of this work, but here we explore two physical consequences of quenching – feedback energetics, and the overall build-up of the red sequence.

3.5.1 Quenching energetics

In our simple implementations of quenching mechanisms, we have made no effort to limit the energy available to, e.g., that accreted onto a supermassive black hole. We simply eject or heat up the prescribed gas particles. Here we investigate whether the energy added via quenching is reasonable and in line with expectations.

We track the energy associated with our quenching implementations on galaxy-by-galaxy and event-by-event bases. For hot halo quenching event, we add up the change in energy for each gas particle affected, or quenched, by the event. With hot gas heating, each heated gas particle changes in energy by $\Delta E = 3/2 N k_B \Delta T = 3/2 (M_{\rm particle}/(\mu m_p)) k_B \Delta T$, where $M_{\rm particle}$ is the total mass of the particle, $\mu = 0.6$ is a typical mean molecular weight for gas in clusters (Rosati et al., 2002), m_p is

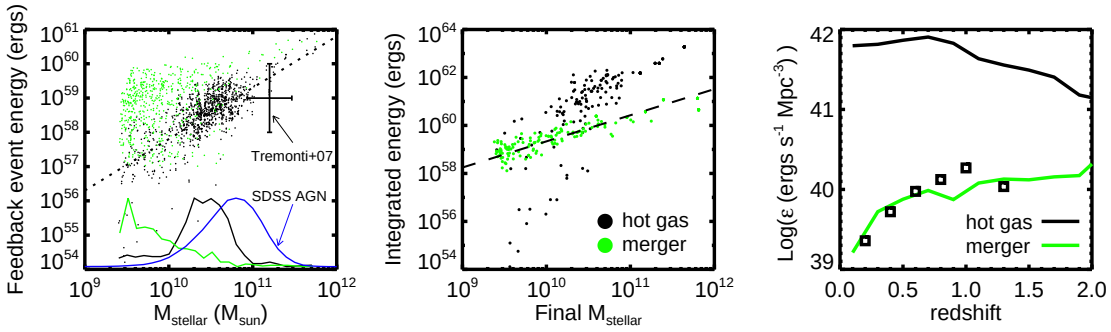

Figure 3.13 Relations between quenching energetics and galaxies, for both merger winds (green) and hot gas heating (black). **Left:** Energy associated with each quenching event vs. the stellar mass of the galaxy hosting that event. Since hot gas heating is actually continuous, each "event" is ambiguous, but corresponds to $\sim 10^7$ yrs. Errorbars show an estimate of the energy output in winds from post-starburst galaxies based on Tremonti et al. (2007). Corresponding color-coded histograms of stellar mass are shown at the bottom, with blue for optically-selected SDSS AGN. The dotted line shows a scaling $E \propto M^{2/3}$ motivated by the hydrostatic temperature scaling with halo mass. **Middle:** Time-integrated energy from quenching feedback as a function of $z = 0$ galaxy stellar mass. This is the total energy of feedback processes over each galaxy's lifetime, but excludes feedback events that occur in small galaxies that merge with the main progenitor. The dashed line shows the slope of the $M_{\rm BH} - M_{\rm stellar}$ relation for galactic bulges from Bennert et al. (2010). **Right:** Total energy density production rate of feedback processes vs. redshift. Squares show a scaled estimate of the total luminosity density of AGN from Barger et al. (2005).

the proton mass, k_B is Boltzmann's constant, and ΔT is the temperature change of the gas particle. Since each heated particle is associated with a galaxy from the group finder, we attribute its change in energy to the feedback energy tally for that galaxy.

In our merger quenching model, we estimate the feedback energy for each particle as the final kinetic energy: $E = 0.5 M_p v_{\rm kick}^2$. Here $v_{\rm kick}$ is the kick velocity of gas ejected in winds associated with mergers. The total feedback energy from a single merger is then summed over all particles that experienced the feedback in a galaxy. Thus, for our basic model, the total energy in a merger is effectively $E_{\rm merger} = 0.5 M_{\rm coldgas} (1500 {\rm kms}^{-1})^2$, where $M_{\rm coldgas}$ is the total cold gas mass in the merger remnant at the time of expulsion.

In Figure 3.13, we compare our quenching energy calculations to observations associated with feedback processes. In the left panel, we show the energy of each feedback event as a function of its host galaxy's stellar mass. Since hot gas quenching is actually continuous, there are too many points to plot clearly, so we randomly choose 1000 events. The event energy rises steeply with stellar mass since more massive halos have more gas that requires heating to a higher virial temperature. Since hydrostatic halos follow the scaling $M \propto T^{3/2}$, we overplot a dotted line with $E \propto M_{\rm stellar}^{2/3}$ (with arbitrary normalization). The hot gas quenching events follow this trend, although with some scatter, suggesting that the virial temperature is the most important factor in determining how much energy is injected in this model.

Merger quenching shows more scatter and less steep dependence on stellar mass, both of which are driven by gas fraction trends. The event energy for mergers is solely determined by the cold gas mass (since $v_{\rm kick}$ is the same for all galaxies), so the scatter in the relation owes to variations in the cold gas mass at any

fixed stellar mass. In our simulations, more massive galaxies tend to have smaller gas fractions, which counteracts the overall increase in mass in these systems, leading to a sub-linear relation between merger event energy and host galaxy stellar mass.

For comparison with the merger quenching energetics, we estimate the energy output associated with the massive outflows observed in post-starburst galaxies. Tremonti et al. (2007) measured outflow velocities ~ 1000 km s^{-1}, and estimated outflow masses at $M_{\rm wind} \sim 10^{9-11} M_{\odot}$. From this we estimate the kinetic energy as $0.5 M_{\rm wind} v_{\rm wind}^2$, using the full range of mass estimates to get the errorbars, but neglecting (substantial) variations in wind velocity. Tremonti et al. (2007) also measured stellar masses for their sample of post-starburst galaxies, and we plot errorbars based on the standard deviation of the logarithm of those masses. Our merger outflow energies fall at the high end of this observational estimate, entirely consistent given that we used $v_{\rm wind} = 1500$ km s^{-1} in the simulation.

We also show histograms of the stellar mass distribution of feedback events along the x-axis. As indicated by the black histogram, most hot gas quenching events are associated with galaxy stellar masses between 10^{10} and $10^{11} M_{\odot}$. Because of the steep cutoff in the galaxy stellar mass function, there are few galaxies above this mass, and galaxies at lower masses do not have hot halos. In contrast, the distribution of stellar masses of merger events (green line) is skewed toward the low mass end, reflecting the greater frequency of mergers of low-mass galaxies when averaged over cosmic time. For comparison we show in blue the distribution of stellar masses of AGN host galaxies for AGN selected from SDSS using the Baldwin-Phillips-Terlevich (Baldwin et al., 1981) diagnostic with SDSS optical spectra (Kauffmann et al., 2003a). The general trend is similar though the predicted histogram is shifted to somewhat lower masses. This indirectly sug-

gests that AGN activity is indicative of ongoing hot halo quenching.

In the middle panel of Figure 3.13, we show the time-integrated feedback energy as a function of host galaxy $z = 0$ stellar mass. If the feedback energy originated from black hole accretion, this enables comparison with final black hole masses, modulo corrections for the efficiency at which accreted mass is converted to output energy, and the coupling of that energy to the gas. As with individual event energies, the integrated energy rises more steeply with stellar mass for hot gas heating than for merger winds. A dashed line shows the slope of the $M_{\rm BH} - M_{\rm stellar}$ relation for local galactic bulges from Bennert et al. (2010), assuming that the integrated feedback energy is $\propto M_{\rm BH}$. The amplitude is arbitrarily normalized to coincide with the mean energy for merger winds at the low-mass end. The slope for merger winds, though slightly shallower than the $M_{\rm BH} - M_{\rm stellar}$ relation, is a good match to the observations. The slope for hot gas quenching is also in good agreement at the high mass end, but drops away quickly to low masses where little energy input has occurred. Note that the observed $M_{\rm BH} - M_{\rm stellar}$ relation uses the *bulge* stellar mass, whereas the simulated galaxies show the total stellar mass. Hence the dropoff to low masses in the hot gas quenching case may partly be reconciled by lower bulge-to-disk ratios in sub-$L^\star$ galaxies.

Finally, the right plot shows the energy density production rate of quenching as a function of redshift. This is analogous to the plot of Madau et al. (1998) of galaxy luminosity density evolution, and directly comparable to the plot of Barger et al. (2005) of AGN luminosity density evolution (see also Cowie & Barger, 2004). We take data from Figure 25 of Barger et al. for spectroscopically identified sources with $L_{2-10\rm keV} \gtrsim 10^{42}$ ergs s^{-1} and multiply by their suggested bolometric correction of 35 to get the total luminosity. Then we multiply by a coupling effi-

ciency which determines what fraction of an AGN's total luminosity couples to the surrounding gas. We choose a somewhat high value of 0.1 (0.05 is typical Di Matteo et al., 2005) to match the normalization of the energy density production rate for the merger quenching model, and show the result as squares in the figure. Outflows from galaxy mergers in our simulations match the shape of measured energetics of luminous AGNs. The total energy requirements for hot gas heating appear much higher. This may indicate that hot gas quenching in the real universe (1) is tied to lower-luminosity AGN, (2) does not heat gas up to the virial temperature, and/or (3) is intermittent with a small duty cycle.

Overall, our results are broadly consistent with the idea that AGN are responsible for providing the energy for quenching feedback. Various authors have already shown that merger-driven feedback can lead to galaxies that are consistent with the $M - \sigma$ relation; our simulations likewise appear to do so. However, our simulations also show that merger quenching is, in itself, unlikely to be responsible for producing red and dead galaxies. The energetic requirements of hot gas quenching are quite severe in our current model implementation. For instance, such energy injection will excessively heat intragroup gas, likely leading to a mismatch with observed temperature and entropy profiles; we plan to explore this in future work. We speculate that intermittent heating, perhaps triggered by an accumulation of cold gas in the halo center, might work just as well to quench star formation with a significantly lower energy budget. Hence while forcing gas in hot halos to remain at the virial temperature produces a reasonable red galaxy population, further work is required to construct a fully viable physical model.

3.5.2 Red sequence build-up over cosmic time

The build up of the red sequence over time can place strong constraints on quenching physics. Here we investigate two simple parameterizations: the galaxy num-

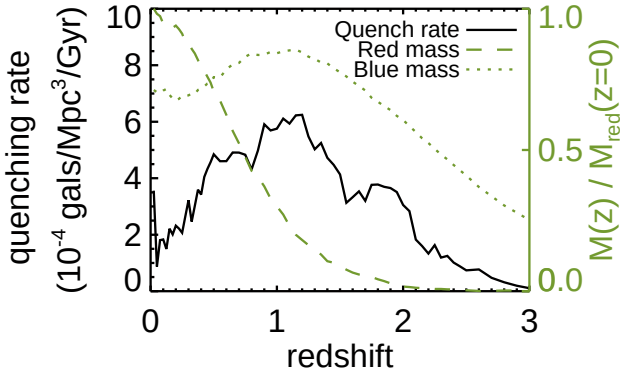

Figure 3.14 Quenching rate (black, left axis) and mass growth history normalized to $z = 0$ (green, right axis) of red sequence galaxies with $M_{\rm stellar} > 10^{9.5} M_{\odot}$ in the hot gas quenching model. In this model, quenching peaks at $z \approx 1$, declining at late times. About 2/3 of the mass of the red sequence builds up at $z < 1$, while the mass in the blue cloud declines during the same period.

ber quenching rate and the mass growth histories of the red sequence. For both quantities, we restrict ourselves to red galaxies with stellar masses above $10^{9.5} M_{\odot}$.

We calculate the quenching rate by comparing each consecutive pair of snapshot outputs from our basic hot gas quenching simulation. The quenching rate, $dN_{\rm quenched}/dt$ is estimated as $\Delta N_{\rm lowssfr}/\Delta t_{\rm snap}$. Here, $\Delta N_{\rm lowssfr}$ is the difference in the number of galaxies with specific star formation rates (SSFRs) below 10^{-12} yr^{-1} between the two snapshots, and $\Delta t_{\rm snap}$ is the time between snapshots. The red sequence mass growth is the total stellar mass in such low-SSFR galaxies, $M_{\rm red}(z)$, normalized to the total stellar mass at in these galaxies $z = 0$, $M_{\rm red}(z = 0)$. We also calculate the mass growth of galaxies with SSFRs above this cutoff, $M_{\rm blue}(z)$, normalizing to the mass in red galaxies $M_{\rm red}(z = 0)$ to track relative changes in the blue and red populations.

Figure 3.14 shows the results. The quenching rate is small at $z > 2$, after

which it rapidly increases. The rate peaks at $z \approx 1$, declining at low redshift. Observations tend to indicate that the mean formation time of stellar populations in massive ellipticals is at $z \gtrsim 2$ (e.g. Graves et al., 2009). In our model, while massive galaxies tend to have old stellar populations, they do not quench their star formation until typically $z \sim 1$. This may be related to why the color-density relation disappears or inverts at $z \gtrsim 1$: At low-z, typical central massive galaxies are red, leading to the familiar positive color-density correlation, while prior to $z \sim 1$ central galaxies have typically not quenched and are blue, leading to an inverted relation.

The total mass on the red sequence at $z = 1$ is about 1/3 the final value at $z = 0$; half the mass on the present-day red sequence is in place at $z = 0.8$. This significant late build-up is slightly more than the factor of 2 in stellar mass (Bell et al., 2004b) and galaxy number (Faber et al., 2007) suggested by observations, although such estimates are presented as lower limits. The mass on the blue cloud rises at early times, declining at $z < 1$ as many star-forming galaxies become quenched. This reflects a decrease in the number density of blue galaxies by $\sim 20\%$, substantially different from the empirical analysis of Blanton (2006), which found no evolution in number density of the observed blue cloud to within 10%. By $z = 0$, the total stellar mass in blue galaxies (above our resolution limit of $\sim 3 \times 10^9 M_\odot$) is $\sim 70\%$ that in red galaxies.

3.6 Discussion

3.6.1 Red galaxy morphologies

In this work we have focused on the transformation of galaxy colors, but of course color and morphology are closely correlated in the local universe. Our simulations' resolution is poorly suited to study morphologies (see e.g. Brook et al.,

2011, for a fuller discussion of why). In our favored hot gas model, starvation by the hot halo only stops star-formation without changing the morphology. Once star-formation stops, a galaxy must undergo (possibly minor) mergers to disrupt the remaining disk and form an elliptical. Such dry (gas-poor) mergers may have difficulty reproducing the observed phase-space densities of stellar orbits in the centers of some elliptical galaxies (Hopkins et al., 2009), but some fraction of the bulge may have built up via dissipational mergers before the galaxy starved (e.g. Bournaud et al., 2007).

One key argument in favor of gas-rich major mergers as a transformative process is that they might turn a star-forming disk into a quiescent elliptical all at once. However, recent observations of quenched late-type galaxies disfavor the merger-only scenario, and suggest that a substantial fraction of passive galaxies must have gone through a "passive disk" phase (Bundy et al., 2010; van der Wel et al., 2010). Our results reinforce the theoretical difficulty seen in earlier models: after halting star-formation at any given time in a galaxy's evolution, something must prevent future gas accretion to keep that galaxy red and dead (Hopkins et al., 2008; Croton et al., 2006; Bower et al., 2006).

Finally, we note that our hot gas quenching model does not produce passive field galaxies in low-mass halos (which are not dominated by hot gas), and this may violate observational constraints on the relationship between stellar-mass and the fraction of passive galaxies (Hopkins et al., 2008). Ultimately, morphologies provide an interesting constraint on quenching models, but higher-resolution simulations or sub-resolution morphological models are required to properly apply them. Insofar as galaxy structure influences star-formation histories (Martig et al., 2009), such models may be necessary to understand red galaxy formation.

3.6.2 The importance of hot halo gas

Our favored model relies on the hot gas surrounding massive galaxies. This hot corona is a robust prediction of years of theoretical work, yet its existence has not been universally established at mass scales below groups. X-ray observations have revealed diffuse hot gas around only some of the most massive field galaxies (Mulchaey & Jeltema, 2010), but recent simulations predict that the halo gas around $L^*_{\rm optical}$ galaxies should have X-ray luminosities too faint for current observatories (Crain et al., 2010a). The gas may be there, we just cannot see it.

Why should the hot gas be implicated in shutting down star formation? The hot gas may be crucial to triggering the *type* of feedback that best couples with surrounding gas (i.e. radio jets Di Matteo et al., 2000), or it may simply be a more effective "net" than cold IGM to "catch" the energetic output of an AGN. It seems an unlikely coincidence that the mass scale where a stable hot halo can form just happens to be around the turnover in the stellar mass function, but observations do not unambiguously favor a direct connection. Among field galaxies with diffuse X-ray gas detections, both star-forming and passive galaxies are well-represented (Crain et al., 2010b). This result is not entirely inconsistent with our model – after new accretion is quenched, a galaxy will remain star-forming for ~ 2 Gyrs while surrounded by a substantial hot gaseous halo. Nevertheless, the under-abundance of massive star-forming galaxies in our favored model suggests a less direct relationship between hot gas and quenching than our simple prescription. Perhaps quenching depends jointly on hot gas and the mass of the central black hole, which itself is the product of a complicated history that may involve galaxy mergers and secular growth.

3.6.3 Comparison to other models

Our on-the-fly quenching models build on the post-processing models of Gabor et al. (2010), and the results show some similarities. The color of the red sequence is too blue and roughly constant with mass, which we attribute to difficulties with supernova metal yields, the redistribution of metals by star-formation-driven winds, and/or a poor treatment of merger-induced starbursts in our simulations. We also observe a similar sharp cutoff in the blue galaxy mass function in our best model. A major difference, however, is that re-fueling of merger remnants prevents our merger quenching model from yielding a red sequence, whereas in Gabor et al. (2010) we assumed that all future star-formation was quenched after a merger.

With many successes at matching observations, SAMs also serve as a useful benchmark for our models. Unlike our simulations, typical SAMs already resulted in a substantial red sequence even before invoking quenching feedback models (Croton et al., 2006; Bower et al., 2006). The red galaxies arise due to rapid gas consumption in a starburst associated with a merger or disk instability, or due to gas stripping as a satellite galaxy falls into a larger halo. Our simulations do produce quenched satellites (Davé et al., 2011), but probably do not track secular disk evolution properly. Nevertheless, our merger quenching model shares the generic feature with modern SAMs that further ongoing quenching is required to ensure that the most massive galaxies remain red and dead. Different models incorporate different mechanisms for this added quenching, from various radio mode feedback prescriptions to a simple halo mass cutoff (Croton et al., 2006; Bower et al., 2006; Cattaneo et al., 2006; Somerville et al., 2008). It is worth recognizing that our late-time re-accretion of gas is dominated by recycled winds, something that is not dynamically followed in the SAMs.

Cosmological hydrodynamic simulations akin to ours have included various feedback processes, but (to our knowledge) none has previously produced a realistic red sequence and mass/luminosity function. Simulations with neither stellar nor black hole feedback produce massive galaxies with low star-formation rates, but their stellar masses are much too large (Kereš et al., 2009a). Our simulations with only stellar feedback can bring the low-mass end of the galactic stellar mass function into agreement with observations, but massive galaxies form stars at excessive rates (Oppenheimer et al., 2010). By coupling sub-grid Bondi-Hoyle-Lyttleton black hole accretion with models for the associated energy output, other simulations show promise for matching black hole growth and suppressing star-formation in massive galaxies (Sijacki et al., 2007; Di Matteo et al., 2008; Booth & Schaye, 2009, 2010; Degraf et al., 2010; McCarthy et al., 2010), but it is unclear whether they produce a red sequence as observed. Understanding the differences between these models and ours will provide complementary insights into the physical processes behind quenching.

3.6.4 Star-formation driven winds and quenching

Oppenheimer et al. (2010) highlighted the importance of wind recycling accretion in our simulations (without quenching), showing that star-formation in galaxies with $M_{\rm stellar} \gtrsim 10^{10} M_{\odot}$ is fueled mainly by gas that was earlier ejected in winds. Because this wind recycling dominates the fuel for star-formation in massive galaxies, it is the main fueling mode we are trying to quench in this work.

Our treatment of star-formation driven winds may not be physically accurate. Once launched, we decouple the winds from hydrodynamic interactions with surrounding gas to allow them to escape the galaxy in a resolution-converged way (Springel & Hernquist, 2003; Schaye et al., 2010). Even after re-activation of the hydrodynamics, the wind particles may not merge seamlessly with sur-

rounding gas. Upon escape from galaxies, wind particles are cold, dense, and metal-rich. While they decrease in density as they move away from the galaxy, they remain enriched since we don't include diffusion of metals among gas particles. Metal-line cooling makes them cool faster than surrounding gas, so they stay cold and dense, and more likely to return to galaxies. It is unclear how realistic the assumed complete lack of mixing is, but we note that this wind model has resulted in agreement with observations of IGM metal absorbers (Oppenheimer & Davé, 2006, 2008; Oppenheimer et al., 2009).

Wind recycling, and the possibility of over-recycling, has implications for all our quenching models. As shown in Oppenheimer et al. (2010) and Gabor et al. (2010), simply stopping wind recycling is unlikely to produce a realistic red sequence – doing so suppresses star formation too much to create enough $\sim L^*$ galaxies, while small amounts of cold and hot accretion keep too many galaxies forming stars. In our merger quenching model, we have emphasized the refueling of merger remnants after ~ 2 Gyr. Based on the origin of star-forming gas explored in Oppenheimer et al. (2010), most of the accreted fuel comes from wind recycling, although a significant sub-dominant component comes from cold and hot accretion. Therefore in our hot gas quenching model, where we expressly heat all non-star-forming gas, most of the gas we must quench had been expelled in winds. Hence we caution that the hydrodynamics of winds may play a critical role in quantitatively assessing the amount and location of quenching feedback needed to produce a red sequence.

3.6.5 Guidelines for future models

Given the wide range of physical scales important in galaxy evolution, developers of cosmological simulations have little choice but to resort to sub-resolution quenching models for the foreseeable future. Here we discuss ways of improving

these models. Any model quenching mechanism requires 3 steps:

1. Criteria to start (and stop) the feedback process.

2. An estimate of the energy budget or luminosity available.

3. A method to couple feedback energy to surrounding gas.

The first two steps may be linked in models where the feedback energy varies over time: e.g. the black hole accretion rate varies by several orders of magnitude between states where the feedback is important and negligible. In our current hot gas quenching model, (i) is the existence of a hot gas-dominated halo, (ii) is effectively unlimited, and for (iii) we heat all the non-star-forming gas in the FOF group. We have seen that this successfully creates a red sequence of galaxies, but that it leads to a dearth of star-forming galaxies with $M_{\rm stellar} \gtrsim 10^{10.5} M_{\odot}$ and requires too much energy input. Below we discuss each of these steps in the context of radio mode AGN feedback.

3.6.5.1 (i) Triggering mechanisms

Triggering radio mode feedback requires accretion onto a supermassive black hole. In massive (cluster) halos, the black hole may accrete directly from the hot halo in a Bondi process (Quataert & Narayan, 2000), or a black hole may be fueled by cold clouds that condense from the hot medium (Soker, 2006; McNamara et al., 2010). Bondi accretion of hot gas may be more conducive to the formation of a powerful radio jet than rapid, radiatively efficient accretion (Di Matteo et al., 2000). The formation of a jet may additionally require significant black hole spin (Narayan & Quataert, 2005). Based on the present work, the presence of hot gas seems to be crucial for triggering radio mode feedback.

Models have used a variety of triggers for AGN feedback. SAMs typically assume that feedback operates in hot, massive halos. Hydrodynamic models usually adopt a Bondi-Hoyle prescription, or a simple scaling with gas mass in the black hole vicinity (Vernaleo & Reynolds, 2006; Brüggen & Scannapieco, 2009), to control black hole accretion and thus triggering.

Observationally, most X-ray bright clusters, groups, and elliptical galaxies host some level of central radio AGN, with AGN more likely in systems with shorter central cooling times, and more luminous in more massive systems (Burns, 1990; Mittal et al., 2009; Sun, 2009; Dunn et al., 2010). Outbursts that induce X-ray cavities typically occur every 10^{7-8} years with energies $\sim 10^{55-60}$ ergs (Voit & Donahue, 2005; David et al., 2010; Randall et al., 2010). These observations suggest a triggering mechanism linked to gas cooling in the central regions of a hot halo, which may be a resolvable triggering mechanism in cosmological simulations. This may provide a more observationally-calibratable method for triggering AGN feedback than Bondi-Hoyle accretion.

3.6.5.2 (ii) Available energy for feedback

The energy of feedback mainly depends on the black hole accretion rate. Most models assume some fraction of the accretion rest-mass-energy acts on surrounding gas. The accretion rate is typically determined through simple scalings with black hole and halo mass in SAMs and through Bondi-Hoyle models in simulations.

Observations suggest kinetic power output from central bursts of $\sim 10^{45}$ erg s^{-1} over $\sim 10^{8}$ years in some clusters, consistent with total energy in inflated bubbles ($\sim 10^{60}$ ergs). As mentioned above, radio emission scales with cluster size, but it is not clear to what extent the burst energies depend on halo properties. The fact that few very massive galaxies have enough star-formation to give

them blue colors suggests that there is enough heating power to offset cooling. This may imply a self-regulating cycle (cf. Ciotti & Ostriker, 1997, 2001; Churazov et al., 2005). Hydrodynamic models that directly track black hole accretion or use some estimate based on the mass within the central regions of the halo can achieve this self-regulation (e.g. Brüggen & Scannapieco, 2009).

In our hot gas quenching model, the required energy budget is large, although it is not clear that significantly less energy input could be equally effective. It is also difficult to exceed the theoretical maximum energy output of black holes; models typically assume efficiency of mass-energy coupling to surrounding gas of less than 1%. So the energy budget remains an interesting constraint, but the most attractive scenario is that black holes emit just enough energy to remove or starve their cold gas reservoir, at which point they become quiescent again.

3.6.5.3 (iii) Coupling of feedback to gas

How AGN energy couples with the surrounding medium is another matter of debate. Supersonic jets induce bow shocks in the surrounding gas (Voit & Donahue, 2005; Randall et al., 2010), and subsonic jets entrain material and thermalize their energy via turbulent mixing (De Young, 2010). The outflows can apparently evacuate ~ 10 kpc-scale "bubbles" in hot intragroup gas (Bîrzan et al., 2004), and the bubbles then share their energy at scales $\sim 10 - 100$ kpc via buoyant uplift, mixing, and sound waves (Churazov et al., 2001; Voit & Donahue, 2005; Nulsen et al., 2007; Scannapieco & Brüggen, 2008; Brüggen & Scannapieco, 2009; Fabian et al., 2003; Sanders & Fabian, 2007, 2008).

While idealized hydrodynamic models have directly examined the interaction of jets and bubbles with the ICM (e.g. Ruszkowski et al., 2004; Brüggen et al., 2005; Heinz et al., 2006; Scannapieco & Brüggen, 2008; Brüggen et al., 2009; Morsony et al., 2010; Mendygral et al., 2011), SAMs typically assume that feedback

directly offsets the cooling for simplicity. Cosmological hydrodynamic simulations usually inject the feedback energy into one or a few resolution elements near the black hole, relying on the hydrodynamic calculations to distribute the energy to large scales in the halo (e.g. Booth & Schaye, 2009; Teyssier et al., 2011). In our models, suppressing star-formation in accordance with observations requires heating gas throughout the circum-galactic region, on scales of > 10 kpc, to prevent the formation of cold clumps.

In summary, a path for modeling quenching feedback would be as follows: 1) Trigger feedback when the central cooling time drops below e.g. 1 Gyr, or some fraction of the hubble time; 2) Calculate energy for feedback as some fraction of the rest-mass energy of cold or cooling gas in the central regions; 3) Increase the entropy of the gas with some radial dependence in a manner consistent with higher-resolution simulations. We will explore models based on these principles in future work.

3.7 Summary and Conclusion

With the goal of building a realistic red sequence of galaxies in cosmological hydrodynamic simulations, we have implemented novel mechanisms for quenching star-formation in the simulation code GADGET-2. By identifying mergers and halos on-the-fly within simulations, we implement and test various models for quenching feedback related to these processes. While our work is motivated by feedback resulting from AGN, we explicitly avoid examining black hole growth in order to concentrate on constraints from the massive galaxy population.

Motivated by observations of massive outflows from post-starburst galaxies attributed to quasar feedback, we implement 1500 km s^{-1} superwinds in the rem-

nants of galaxy mergers that expels all the cold gas. To do so, we first use an FOF group finder to identify galaxy mergers on-the-fly, and then give a velocity kick to all the star-forming gas. We have shown that this quenching mechanism alone does not produce a red sequence in our simulations. Even after all the gas is expelled from a merger remnant, new supplies of gas accrete from the IGM to re-fuel star-formation, typically within ~ 2 Gyr.

Motivated by observations of radio AGN and X-ray cavities in the hot gas of galaxy groups, we add thermal heating to hot gas in massive dark matter halos. We calculate the hot gas fraction $f_{\rm hot}$ in the halo, and if $f_{\rm hot} > 0.6$ (roughly corresponding to halo masses $\gtrsim 10^{12} M_{\odot}$), then we heat all its gas outside of the ISM to the halo virial temperature. By keeping the surrounding gas hot, we starve galaxies embedded in hot halos of new fuel for star-formation. We have shown that this hot gas quenching model yields a red sequence whose luminosity function provides an excellent match with observations of local galaxies (Figure 3.5).

Our main results are:

- Galactic-scale outflows triggered by mergers (i.e. quasar mode feedback) do not produce a substantial red sequence on their own because gas accretion from the IGM re-fuels star-formation within $\sim 1 - 2$ Gyr.

- Adding thermal energy to hot X-ray gas around massive galaxies (analogous to radio mode AGN feedback) successfully produces a red sequence whose luminosity function matches observations.

- This heating must occur around satellite galaxies embedded in the hot gas of their parent halos to match the faint-end red galaxy luminosity function.

- A combination of hot gas heating with merger-triggered outflows may be empirically motivated and perform as well as the heating-only model, but

hot gas heating is the crucial required component.

- Our simple hot gas heating model produces somewhat too few massive blue galaxies, possibly owing to the sharp truncation in gas accretion onto galaxies as soon as their halos are dominated by hot gas.

- As in Gabor et al. (2010), our baseline model produces a red sequence that is too blue and too shallow, likely owing to issues related to enrichment. We empirically recalibrate the metallicities to obtain agreement, which requires a metallicity increase up to $\times 2$ in the most massive systems.

The overall success of reproducing the observed red sequence and associated luminosity function is a first for cosmological hydrodynamic simulations. Doing so has already elucidated stringent constraints on how quenching must operate under the scenarios explored. While hot halo quenching appears to be necessary and sufficient to reproduce observations of red galaxies as well as any model at $z = 0$, our current simplistic implementation requires more energy than is thought to be available and likely overheats surrounding gas. We have yet to explore details of redshift evolution, clustering, or the impact of quenching on the surrounding intergalactic gas; these may motivate variants on this simple scenario. The beauty of implementing quenching models self-consistently within large-scale hydrodynamics simulations of galaxy formation is that such models open up a host of new avenues to constrain quenching physics.

In future work, we aim to develop more physically consistent models for quenching star-formation. To do so, we advocate connecting well-resolved structures and processes in the simulations to feedback processes that operate below the resolution scale. Such sub-resolution models will require guidance from observations and higher-resolution simulations of individual galaxies or clusters.

We outline a particular path forward for this based on current intuition that we will explore in future work. By combining insights from advancing theoretical work on all scales and advancing observations across cosmic time, we hope to continue refining our models to better understand how massive red and dead galaxies come to be.

CHAPTER 4

THE GROWTH OF RED SEQUENCE GALAXIES IN A COSMOLOGICAL HYDRODYNAMIC SIMULATION

We examine the evolution of the red sequence in a cosmological hydrodynamic simulation that includes a simple prescription for quenching star formation that yields realistic number densities of red galaxies at redshift zero. In this model (from Gabor et al. 2011), the circum-galactic medium in hot gaseous halos is heated to prevent it from fueling new star-formation in galaxies. Since hot coronae only form in halos above $\sim 10^{12} M_{\odot}$, galaxies with stellar masses $\sim 10^{10.5} M_{\odot}$ are the first to be quenched and move onto the red sequence at $z > 2$. Until $z \sim 0$ the number density of red galaxies with stellar masses $\sim 10^{10} M_{\odot}$ is lower than that of higher mass galaxies, reflected by a dip in the red galaxy stellar mass function that agrees qualitatively with observations. At late times many of these low mass galaxies in high-density environments move onto the red sequence under the influence of their more massive neighbors' hot coronae. Stellar mass growth (along with size growth) continues for galaxies even after joining the red sequence, primarily through minor mergers with a typical mass ratio $\sim 20\%$, but this mass growth appears to exceed that allowable by observational constraints.

4.1 Introduction

Although they host most of the stellar mass in the local universe (Hogg et al., 2002), red sequence galaxies are not fully understood. Debate continues about what mechanisms quench star-formation to create these gas-poor galaxies dominated by old stars (e.g. Hopkins et al., 2008). Further questions have emerged about how red galaxies evolve over cosmic time: when did they first become

red? How do they change in mass and size over time?

Much of our knowledge stems from "archaeology" of local red sequence galaxies – studying their stellar light in enough detail to learn about their histories. Most present day red-sequence galaxies have old stellar populations, with perhaps a "frosting" of star formation contributing little to the stellar mass at later times (Bower et al., 1998; Trager et al., 1998, 2008). They have mostly elliptical morphologies, especially at the massive end, though passive disks make up a large proportion at the low-mass end (Bundy et al., 2010; van der Wel et al., 2010).

Recent and upcoming observations, however, enable more direct observations of red galaxy populations over cosmic time. Wide field surveys have already placed constraints on the bright red galaxies at $z \sim 1$ and even > 2 (e.g. Bell et al., 2004b; Faber et al., 2007; Brown et al., 2007; Cool et al., 2008; Kriek et al., 2008; Stutz et al., 2008; Taylor et al., 2009; Brammer et al., 2009; Marchesini et al., 2010; Whitaker et al., 2010), and upcoming deep surveys will probe red galaxies with stellar masses down to $\sim 10^9 M_\odot$ (e.g. CANDELS; Grogin et al., 2011). Current data indicates the bright end of the red galaxy luminosity function has changed little (after correction for the aging of stars) since $z \sim 1$, suggesting these galaxies were "in place" 7 Gyrs ago. At the same time, high-resolution imaging has revealed that red galaxies are typically much smaller at $z > 1$, by factors ~ 5 compared to their present-day descendents (Daddi et al., 2005; van Dokkum et al., 2008, 2010).

Numerous physical processes are thought to contribute to the formation and evolution of red galaxies, and many potential effects have proven difficult to rule out. Gas-rich galaxy mergers, complete with starburst and quasar, may drive the initial quenching of massive red galaxies (Springel et al., 2005; Hopkins et al., 2006, 2008). Alternatively, hot gaseous coronae that form in halos above

$\sim 10^{12} M_{\odot}$, supplemented by additional heating from an AGN or another source, may starve galaxies of fuel for star-formation (Birnboim & Dekel, 2003; Kereš et al., 2005; Dekel & Birnboim, 2006; Croton et al., 2006; Cattaneo et al., 2006). Among satellite galaxies additional possibilities may drive quenching: perhaps starvation by hot intra-group or intra-cluster gas plays a role, but ram-pressure stripping and glancing interactions with other galaxies have also been implicated (Gunn & Gott, 1972; Abadi et al., 1999; Quilis et al., 2000; Larson et al., 1980; Bekki et al., 2002; Richstone, 1976; Moore et al., 1998). All these processes may act in combination to form the red galaxies observed.

Once red and "dead," the evolution of these galaxies may be deceptively complex. Although there is likely little or no new star formation, the aging stellar population sheds much ($\sim 1/2$) of its mass via stellar winds (Jungwiert et al., 2001; Bruzual & Charlot, 2003). Furthermore, red galaxies are subject to mergers and accretion of small satellite galaxies, which alter the stellar populations and add mass. Mergers also alter the galaxy structure (e.g. from disky ordered rotation to spheroidal random orbits) (Barnes, 1990), change the characteristic size of the galaxy (Cox et al., 2006a), possibly strip stars (into, e.g., the intracluster medium, Gallagher & Ostriker, 1972; Murante et al., 2004), and possibly add cold gas. Such processes may all contribute to the observed evolution of the red sequence, and hypotheses addressing the observed *lack* of evolution must explain why these processes did not act.

Complete, cosmological theories of galaxy evolution, combined with myriad existing and impending observational constraints, provide a convenient method to test some of the mechanisms that drive red galaxy formation. Relationships between physical processes and statistically robust observables are often indirect, but models that include many processes enable unearthing of the connections.

In this work, we study red galaxy growth with cosmological hydrodynamic simulations. As described in citetgabor11, we incorporate quenching mechanisms that yield a $z = 0$ population of red galaxies whose stellar mass and luminosity functions match observations. Specifically, we include a prescription where we ensure that halos dominated by hot gas are continuously heated to keep circum-galactic gas hot. This simple and extreme prescription, approximating the effects of a heat source such as an AGN radio jet, successfully cuts off the fuel supply for star-formation in massive halos. We found in Gabor et al. (2011) that a quenching prescription based on mergers fails to produce significant numbers of red galaxies. Although significant challenges remain for our favored model, it provides a general qualitative guide for models where hot massive halos are the main drivers of red galaxy formation.

After describing our simulations in more detail in §4.2, we discuss various aspects of the evolution of simulated red galaxy populations in §4.3. These include galaxy number density evolution, where we find that red galaxies with $M_{\rm stellar} < 10^{10.5} M_{\odot}$ emerge much later than more massive red galaxies; and galaxy mass growth, where we find that the most massive red galaxies grow in mass by factors of several after quenching, mostly via minor mergers. Finally, we conclude with brief summary.

4.2 Simulations

We analyze cosmological hydrodynamic simulations described in Gabor et al. (2011). For clarity, we summarize the simulations here. They were run with an extended version of the N-body + smoothed particle hydrodynamics code GADGET-2 (Springel, 2005). In addition to the basic N-body and hydrodynamics calculations, our version of the code includes sub-resolution modeling of gas

cooling, star-formation, a model for chemical enrichment via AGB stars and both Type Ia and core-collapse supernovae, galactic winds associated with star-formation, and simple prescriptions for quenching star-formation.

Cooling is implemented via a look-up table in gas temperature and metallicity. That is, a gas particle with given temperature and metallicity will have a cooling rate based on tables from Sutherland & Dopita (1993). Owing to metagalactic UV radiation, gas particles less than about 10^4 Kelvin will undergo heating rather than cooling. For a full description of the cooling implementation, see Oppenheimer & Davé (2006, 2008).

For star-formation we use the two-phase model of Springel & Hernquist (2003) based on the analytic description of McKee & Ostriker (1977). Gas particles above a density threshold and below a temperature threshold are modeled as cold, star-forming clouds embedded in a hot diffuse medium. The masses in the cold and hot phases are determined by the balance between heating by core-collapse supernovae and cooling via radiation. The star-formation rate is then determined by the timescale over which cold clouds collapse into stars, and the model parameters are set so that the resulting star-formation rates are consistent with the observed relation to surface gas density (Kennicutt, 1998). Star-forming gas particles are converted into collisionless star particles stochastically, with a probability derived from the star-formation rate. Gas particles may spawn up to two such star particles.

As a gas particle is undergoing star-formation, it self-enriches with metals from core-collapse supernovae. Furthermore, star particles share energy, mass, and metals with neighboring gas particles as a result of stellar mass loss from AGB stars and Type Ia supernovae. Stellar mass loss is calculated by assuming an IMF (Chabrier, 2003) and applying the stellar population models of Bruzual

& Charlot (2003, , BC03), which account the mass lost by a stellar population at discrete times after the initial star-formation event. We use Type Ia supernova rates from Scannapieco et al. (2006), and each supernova results in the production of metals (mainly iron) that are shared with neighboring gas particles.

Along with the feedback implicit in the star-formation model and the explicit feedback from AGB stars and Type Ia supernovae, our code includes feedback in the form of galactic winds driven by star-formation (Oppenheimer & Davé, 2006, 2008). Just as a star-forming gas particle has some probability of being converted into a star particle, it has a probability of being kicked in a wind. A wind particle is expelled from its host galaxy at a velocity typically a few hundred km s^{-1}, and it is briefly decoupled from normal hydrodynamic interactions to approximate chimneys of escaping gas (Springel & Hernquist, 2003). The velocity kick and mass-loading factor are chosen to match observations of local galaxies (Martin, 2005; Rupke et al., 2005), and naturally arise from momentum-driven wind models (Murray et al., 2005). With these winds, our simulations match a broad array observational constraints on star-forming galaxies and the IGM (Oppenheimer & Davé, 2006, 2008; Davé et al., 2006, 2007; Finlator et al., 2007; Finlator & Davé, 2008).

Despite their success, winds driven by star-formation generally do not result in the formation of red and dead galaxies. We incorporate a heuristic quenching model specifically to solve this problem (Gabor et al., 2011). For this model, we run a spherical overdensity algorithm on-the-fly to separate gas above and below 250,000 Kelvin in each galaxy's halo. In halos with $> 60\%$ of all gas above this temperature cutoff, we apply constant heating (at every time-step) to all circumgalactic gas to keep it at the halo virial temperature. Such heating could plausibly result from an AGN radio jet, but our model in fact uses more energy than

thought to be available from observed AGN sources. We exclude star-forming gas particles from this heating since a radio jet is unlikely to disrupt dense star-forming clouds on galactic scales. The heating we apply to circum-galactic gas is sufficient to prevent it from condensing onto the galaxy, thus starving the galaxy of new fuel for star-formation. This model results in a bimodal color distribution of galaxies, and red galaxy luminosity and mass functions that match observations of the local universe. Although the model has some difficulties (like the required energy mentioned above), it should be a good representation of models where galaxies are quenched due to starvation enabled by their surrounding hot coronae.

For the analysis in this work, we use a simulation of a $48h^{-1}$ comoving Mpc cube with 256^3 dark and 256^3 gas particles that incorporates all the above models. We use a *Wilkinson Microwave Anisotropy Probe* concordance cosmology (Komatsu et al., 2009) with $H_0 \equiv 100h = 70$km s^{-1} Mpc^{-1}, matter density $\Omega_m = 0.28$, baryon density $\Omega_b = 0.046$, a cosmological constant with $\Omega_\Lambda = 0.72$, root mean square mass fluctuation at separations of 8 Mpc $\sigma_8 = 0.82$, and a spectral index of $n = 0.96$. Our simulation uses a gravitational softening length of $3.75h^{-1}$ kpc. The initial gas particle mass is $1.2 \times 10^8 M_\odot$, the typical star particle mass is half that, and our simulation results in ~ 3000 resolved galaxies at $z = 0$.

4.2.1 Simulation outputs and analysis tools

We configured GADGET-2 to save snapshots of the simulation at 108 redshifts, starting at $z = 30$ and ending at $z = 0$. The time between snapshots ranges from a few tens of Myrs at high redshift to ~ 300 Myr at low redshift. The snapshots contain information for simulation particles, such as position, velocity, mass, metallicity, gas density, gas temperature, and star-formation rate. From these particle data, we determine galaxy properties to compare with observables.

We use SKID [1] to identify galaxies (cf. Gelb & Bertschinger, 1994; Kereš et al., 2005). SKID provides a list of member particles (star and star-forming gas) for each simulated galaxy. The sum of member star particle masses is then the galaxy stellar mass, and the star formation rates of the gas particles are summed to give the star formation rate of the galaxy.

We then calculate galaxy spectra using the models of Bruzual & Charlot (2003), as in Finlator et al. (2006). We treat each star particle as a single stellar population with an age and metallicity determined directly in the simulation. By adding up the spectra of all star particles within a galaxy, we obtain the spectrum of that galaxy, from which we can measure galaxy colors and magnitudes in various bands.

Beyond knowing galaxy properties at a given redshift, we wish to study the histories of individual galaxies as they evolve. For this we must connect each galaxy at $z = 0$ to its progenitor galaxies at earlier redshifts: build a merger tree. We do so by determining, for every star particle in a given galaxy, which galaxy from an earlier snapshot that star particle lived in. If the star formed recently it wouldn't have lived in any previous galaxy. By tracing star particles in this way, we determine the immediately preceding progenitors of each galaxy. Galaxies with multiple progenitors must have undergone a merger (or at least some galaxy interaction, such as stellar stripping).

Unfortunately, SKID (along with other galaxy finders) does not self-consistently identify galaxies in all timesteps. If two galaxies fly by each other in a close encounter, SKID will often identify them as a single galaxy during one or a few timesteps, but then again as separate galaxies at later times. More rarely, a group of stars that make up a galaxy at one timestep may be assigned to no galaxy at

[1] http://www-hpcc.astro.washington.edu/tools/skid.html

all in a subsequent timestep, giving the appearance that a galaxy disappeared. This can happen with quite large galaxies (> 1000 particles). These and related complications make merger-tree building difficult.

To surmount these difficulties, we follow strategies described in Maller et al. (2006), who dealt with the same problems. We distinguish SKID groups from galaxies, the latter being defined in terms of our merger trees. For each star particle in a SKID group at $z = 0$, we trace the history of its host SKID groups over all timesteps. If the star particle does not appear in any SKID group during some timestep, then we assign it to a virtual group where it is the only member (except when the star particle was not yet formed).

We then assign each group (real and virtual) to a galaxy. At the highest-redshift timestep of interest, each SKID group is defined as a separate galaxy. In the subsequent timesteps, each group is assigned to the same galaxy as its most massive progenitor from the immediately preceding timestep. Thus if two separate SKID groups share the same progenitor, then they are both assigned to the same galaxy. This helps correct for cases where two merging galaxies undergo a close passage, then separate before the final merger. It may get the precise timing of mergers off by ~ 1 Gyr, but our results do not rely on this timing aspect. Likewise, virtual groups that were not part of any SKID groups are assigned to galaxies that they once inhabited. Once all groups are assigned to galaxies, their constituent particles can also be assigned to those galaxies.

Some fly-by interactions will not in fact lead to mergers. To account for this, we identify galaxies at $z = 0$ that are composed of multiple SKID groups and separate those groups into distinct galaxies. We find the earliest timestep when both groups' stars are assigned to the same galaxy, and from then on assign a new galaxy ID to those stars in the smaller of the two groups. With every star particle

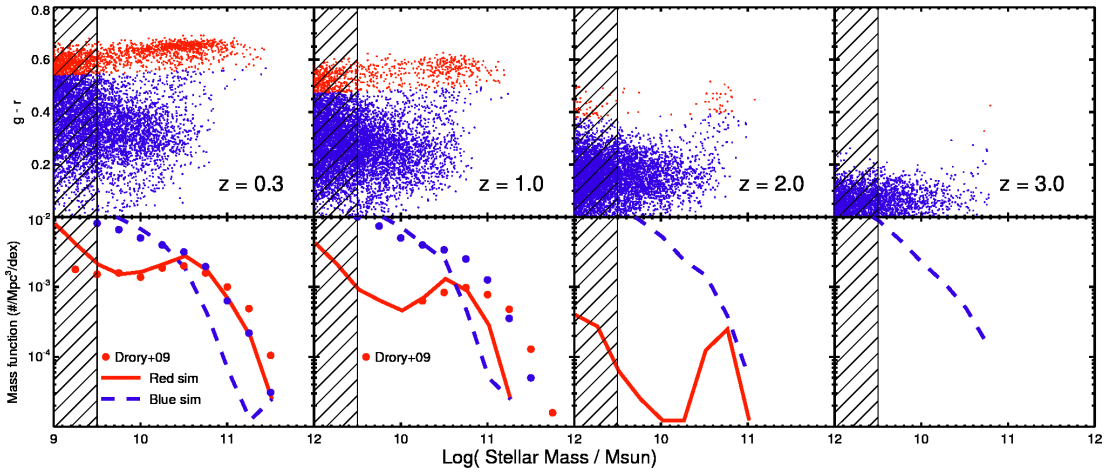

Figure 4.1 Redshift evolution of color-mass diagrams (top row) and galaxy stellar mass functions (bottom row). Redshift increases from left to right, as labeled. Red and blue galaxies are separated using a redshift-dependent cut, as illustrated by the red and blue color-coding in the CMD. In the mass function panels, solid lines denote the simulated red sequence, dashed lines the simulated blue cloud, and observed data points are taken from the literature. The hatched region indicates poorly resolved galaxies. Massive red galaxies emerge at $z > 2$, but there is an obvious dearth of less massive galaxies ($\sim 10^{10} M_{\odot}$) that is more pronounced at higher redshift.

assigned to a galaxy at every timestep, we then identify all progenitor galaxies to each galaxy.

4.3 The Growth of the Red Sequence

4.3.1 Evolution in color and number density

New instruments and surveys enable two simple but powerful constraints on the emergence and evolution of red galaxies: galaxy colors and their number densities. In this section we examine how these colors and number densities (via the

galaxy stellar mass function) evolve with redshift in our simulations. Since our simulations have difficulty in some quantitative comparisons with observations noted in Gabor et al. (2011), we focus here on qualitative trends. We highlight two main features of our model: (1) the first red galaxies emerging at $z > 2$ are at the massive end of galaxy stellar mass function, followed by small satellites then finally the middle region of $10^{10} M_{\odot}$ galaxies. (2) The most massive red galaxies in our model grow substantially at late times, apparently in conflict with observations.

Figure 4.1 shows color-mass diagrams and galaxy stellar mass functions for simulated galaxies at redshifts 0, 1, 2, and 3. The $g - r$ colors are rest-frame SDSS filter bands, and do not include any correction for obscuration due to dust – these are intrinsic colors. We divide the galaxy population into blue and red using a straight line in $g - r$ color versus r magnitude space in the same way as in Gabor et al. (2011). This translates to a similar separation in color-mass space, as indicated by the sharp demarcation between blue and red points in the top left panel. We evolve the normalization (but not the slope) of our color separation in a simple linear way that accounts for passive evolution: $y_{\rm sep}(z) = y_{\rm sep}(z = 0) - 0.1 * z$. Here $y_{\rm sep}$ is the y-intercept of the line of separation, and z is the redshift. The resulting separation indicated by the color-coding of blue and red galaxies in the top panels of Figure 4.1 suggests this is a reasonable choice. The hatched region of the figure indicates simulated galaxies that are poorly resolved.

The color evolution of the galaxy population is clear from the figure, and it appears to be dominated by passive evolution. That is, the colors of blue galaxies, which evolve in color due both to changes in star-formation as well as aging of their stellar populations, do not evolve much more rapidly than those of red galaxies, which only change via stellar aging. The emergence and growth of the

red sequence is also apparent in the figure.

The lower set of panels of Figure 4.1 shows galaxy stellar mass functions separated into blue (dashed line) and red (solid line) populations. We also plot mass function points at $z = 0.3$ and 1.0 taken from citetdrory09, who also split galaxies into star-forming and quiescent populations (red vs. blue points). While the simulated blue galaxy stellar mass function evolves only weakly with redshift, the red galaxy mass function obviously undergoes drastic changes from $z = 3$ to 0.

4.3.1.1 Massive galaxies are the first to be quenched

The development of the red sequence in the color-mass diagrams shows that the first red galaxies form at the massive end between $z \approx 3$ and $z = 2$. Then small satellites of the first quenched galaxies become red as well, and finally the middle range of galaxies with $M_{\rm stellar} \approx 10^{10} M_{\odot}$. There remains until $z \lesssim 1$ a distinct gap between the massive and low-mass ends of the red sequence. This gap is reflected in the mass functions.

The mass functions show that the number density of red galaxies builds substantially over time. Reflecting quenching of star-forming galaxies due to starvation in our model (see Gabor et al. (2011)), the red sequence grows from nonexistent at $z \sim 3$ to dominating the galaxy population at $z \sim 0$. The mass functions clearly show that the most massive galaxies are the first to become red, followed by low-mass galaxies that are satellites to the massive ones. This directly results from the fact that the most massive galaxies in our simulations are the first to form a corona of hot gas. Massive galaxies tend to live in massive dark matter halos, and massive dark matter halos have low enough densities that virial shock heating outpaces radiative cooling, allowing a hot gaseous halo to develop.

Fewer galaxies in the mass range $10^{10} - 10^{10.5} M_{\odot}$ move to the red sequence at $z > 1$, but this region fills in over time. Galaxies in this mass range typically are

neither massive enough to support their own hot coronae, nor close enough to larger halos to live in the hot gas environment of a group or cluster. By redshift zero, however, many galaxies within this mass range live in halos dominated by hot gas due to the presence of very massive neighbors. While they may not occupy the same virialized halo, they live in a nascent super-group with pervasive hot gas. We discuss the physical effects of environment further in §4.3.3.

The dearth of red galaxies in the middle of our mass range at higher redshifts causes a dip in the red galaxy mass function. This behavior is consistent with existing observational constraints. Stutz et al. (2008) found six massive ($> 10^{10.4} M_{\odot}$) but zero low-mass galaxies with old stellar populations at $z \sim 3$ in the HUDF (Beckwith et al., 2006), despite being sensitive to stellar masses $< 10^{10} M_{\odot}$ (see also Toft et al., 2005). Rudnick et al. (2009) noted that in clusters, the low mass end of the mass function must build up more rapidly than the massive end from $z \sim 0.8$ to $z = 0$ in order to "catch up" in number density. In the field, Drory et al. (2009) traced the evolution of the red galaxy stellar mass function for $z < 1$, finding a dip at medium masses that is more prominent at higher redshift. Some of these data are plotted in Figure 4.1. Our simple model, where hot gas dictates the formation of the red sequence, provides a compelling physical picture behind this trend.

Figure 4.2 illustrates the evolutionary trends in red galaxy number density more explicitly. We consider three bins in stellar mass, and show how the number density of galaxies in each bin changes with redshift. Red galaxies with masses between $10^{10.5}$ and $10^{11.0} M_{\odot}$ are the most numerous at all epochs. Less massive galaxies with $M_{\rm stellar} \sim 10^{10} M_{\odot}$ emerge after a delay of ~ 1 Gyr compared to the more massive bin. They increase in number more rapidly, nearly converging with the more massive bin by $z \sim 0$. Finally, red sequence galaxies more massive than

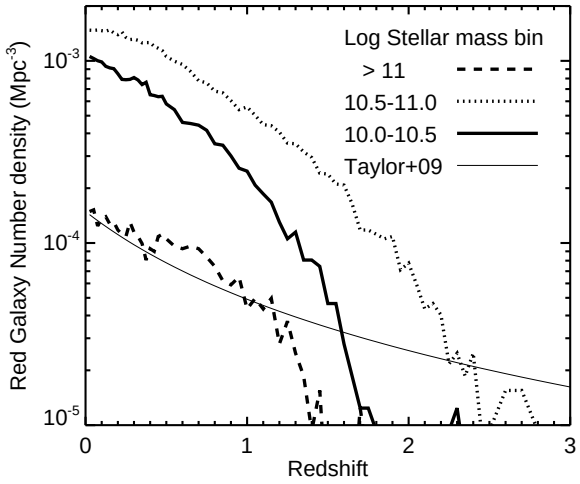

Figure 4.2 Evolution in the number density of red sequence galaxies within three mass bins (different line styles, as labeled). Galaxies with a characteristic mass of $\sim 5 \times 10^{10} M_{\odot}$ are the first to become red, followed by lower mass galaxies. The very massive end ($> 10^{11} M_{\odot}$) of the red sequence follows last, as red galaxies gain mass via mergers. For comparison with the most massive bin, we show an observational trend (thin solid line), normalized to match the $z = 0$ simulation results, from citettaylor09.

$10^{11} M_{\odot}$ appear as red galaxies migrate from the lower-mass bins by acquiring mass through mergers.

4.3.1.2 Simulated massive red galaxies undergo strong evolution

Comparison between simulated and observed red galaxy mass functions in Figure 4.1 shows that our model under-predicts the numbers of massive ($> 10^{11} M_{\odot}$) red galaxies, especially at high redshifts. At low redshift the number density of red galaxies is in reasonably good agreement with observations. Long after massive galaxies are quenched in our model, they continue to grow via the accretion of stars from merging galaxies. This leads to strong evolution in the mass function. In the observed universe, significant populations of massive red galaxies exist at $z \gtrsim 2$, and they grow little in number or mass at redshifts $z < 1$ (Cool et al., 2008; Taylor et al., 2009). The $z = 1$ data plotted from Drory et al. (2009) in Figure 4.1 reflect this discrepancy.

Figure 4.2 shows the strong number density evolution of these massive galaxies (dashed line), compared with an observational trend from Taylor et al. (2009, thin solid line). This trend is a best-fit power law based on observations up to $z \sim 2$. Since the simulated number density of the most massive galaxies does not match the $z \sim 0$ observed data, we have normalized the observed trend to match the simulated $z = 0$ point. Even with this re-normalization, our simulations sharply diverge from the observed trend at $z > 1$, in the sense that we simulate too few red galaxies at high redshift. The observed number density of massive red galaxies evolves more slowly than our simulations.

In order to correct the disagreement with observations, our model would have to form massive red galaxies at an earlier stage, and then prevent growth at late times. It is unclear what combination of mechanisms might accomplish this task. Both the red mass function at high redshifts and the blue mass function at all

redshifts suggest that our model should allow galaxies to grow more massive before they become quenched. Increasing the critical hot gas fraction threshold for quenching would, for example, permit higher numbers of massive blue galaxies, as pointed out in Gabor et al. (2011). It would also increase the characteristic mass of the first galaxies to become red. Then stronger quenching of satellite galaxies might be needed to prevent the first red galaxies from gaining too much mass via mergers.

On the other hand, observational biases may help explain the discrepancy with our model. Dust reddening may place intrinsically blue star-forming galaxies on the red sequence, adding to their numbers at higher redshifts. Observers have mitigated this problem by using near-IR data, which is less prone to dust obscuration, to help derive stellar masses. Furthermore, mid-IR observations can help identify dusty galaxies and separate them from quiescent ones. Another potential bias arises from uncertainty in estimated stellar masses. Since the mass function is very steep at high masses, small mass errors can lead to relatively large errors in number density.

In summary, our model predicts that galaxies with $M_{\rm stellar} \sim 5 \times 10^{10} M_{\odot}$ are the first to become red, but it under-predicts the numbers of galaxies with $M_{\rm stellar} > 10^{11} M_{\odot}$ at high redshifts. The key feature driving these trends is that our quenching mechanism, tied to the hot gas coronae that form in halos $\sim 10^{12} M_{\odot}$, selects a characteristic mass for red galaxies. That is, once a star-forming galaxy achieves a mass $\gtrsim 10^{10.5} M_{\odot}$, it will become quenched and move to the red sequence. Less massive galaxies are only quenched as satellites of more massive parent halos. More massive galaxies are not allowed to form stars in-situ since they are starved of fuel by their hot halos. While quantitative details may vary with parameter choices, these are generic outcomes for quenching models

keyed to a critical halo mass.

4.3.2 Paths to the red sequence

Having addressed above the evolution of the colors and number densities of the galaxy population as a whole, we now turn to individual galaxies. Given a red galaxy at $z \sim 0$, what path did it take to get there? Massive galaxies in our models follow paths much like those in the schematic diagram of Faber et al. (2007): they move onto the red sequence at masses near the turnover in the mass function, then grow further through mergers and accretion of satellite galaxies.

In Figure 4.3 we show the paths of three typical galaxies (lines with circles marking different redshifts) in the color-mass diagram. We plot a background of simulated galaxies at $z = 0$ (points), and we correct for passive evolution of colors for the galaxy paths in the same way that we evolved our line separating blue and red galaxies §4.3.1. We also include a simple prescription for dust that is tied to the star-formation rate of each galaxy (Somerville et al., 2001; Wang & Heckman, 1996; Gabor et al., 2010).

All three of these galaxies build stellar mass via star-formation for several Gyrs before moving onto the red sequence. Once quenched, they stop building stellar mass and cross vertically over the green valley to the red sequence in $\sim 2Gyrs$ (see also star-formation histories in Gabor et al., 2011). The two less massive galaxies make this transition at late times ($z < 0.2$), and do not change in mass or color after reaching the red sequence. The most massive galaxy, however, becomes red when it has a mass a few $\times 10^{10} M_{\odot}$, and then continues to grow in mass. Growing via mergers and accretion of smaller satellites, it eventually obtains a mass $\sim 10^{11} M_{\odot}$. These paths are fairly representative for galaxies in their respective mass ranges. Low-mass galaxies tend to move onto the red sequence at late times, and grow little after doing so. The most massive red galaxies form

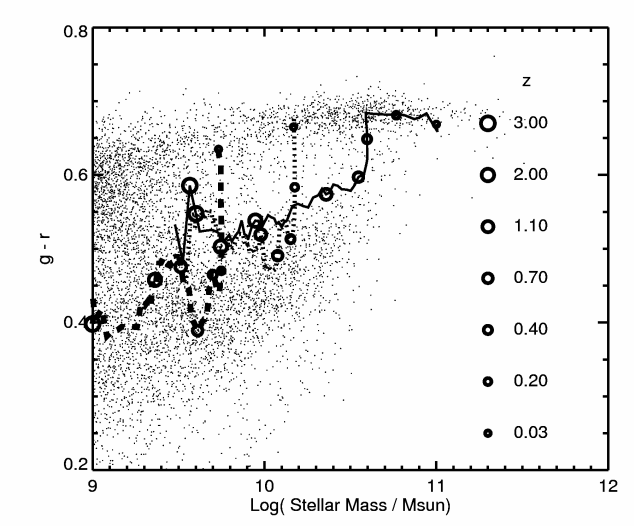

Figure 4.3 Example evolutionary paths in the color-mass diagram. We show the paths of three galaxies (lines) as they evolve through the color-mass diagram, as represented by $z = 0$ galaxies (small points) in the background. This is analogous to the schematic diagram of Faber et al. (2007). Both background galaxies and paths include a prescription for dust obscuration, and paths are corrected for passive color evolution. Open circles indicate redshifts (at ~ 2 Gyr intervals) along the evolutionary paths. Galaxies grow in stellar mass along the blue sequence, then move vertically to the red after quenching. Once on the red sequence, galaxies grow only via mergers and accretion of satellites. Such growth can be substantial, as for the path of the most massive galaxy shown (solid line).

via mass growth of smaller red galaxies.

All three of the galaxies whose paths are shown are identified as central galaxies by the spherical overdensity algorithm. They do not live within the virial radii of larger neighbors. This is surprising for the two smaller galaxies because their halos are not massive enough to support a stable virial shock, which drives quenching in our model. This suggests an important role for large-scale galaxy environment, as we explore in the next section.

4.3.3 Environmental Factors

As shown above, the massive end of the red sequence grows first in our model. Not until $z \lesssim 0.3$ do galaxies in the $10^{10} M_{\odot}$ mass range appear as numerous on the red sequence as more massive galaxies. In this section, we examine how environmental factors drive this behavior.

The initial emergence of the massive red sequence is fairly simple to understand. Our model requires that a galaxy's halo be dominated by hot gas for quenching to begin. Early analytic, spherically symmetric theories of galaxy evolution assumed that gas in the halo of a forming galaxy should be virialized (Rees & Ostriker, 1977; Silk, 1977; White & Rees, 1978). Theorists soon realized, however, that gas in low-mass halos will have short cooling times, so that it never reaches the virial temperature of the halo. Several recent hydrodynamic studies have shown that a hot circum-galactic corona only forms, via the virial shock, in halos above a few $\times 10^{11}$ or $10^{12} M_{\odot}$ (Birnboim & Dekel, 2003; Kereš et al., 2005). The key assumption in our model is that in such massive halos, gas is very inefficiently deposited onto the galaxy, likely with the contribution of some heating process like an AGN (cf. Croton et al., 2006). These massive halos are very rare at $z > 3$ in a CDM universe. Since galaxy masses are well-correlated with halo masses below the cutoff for quenching, only the galaxies with the highest stellar

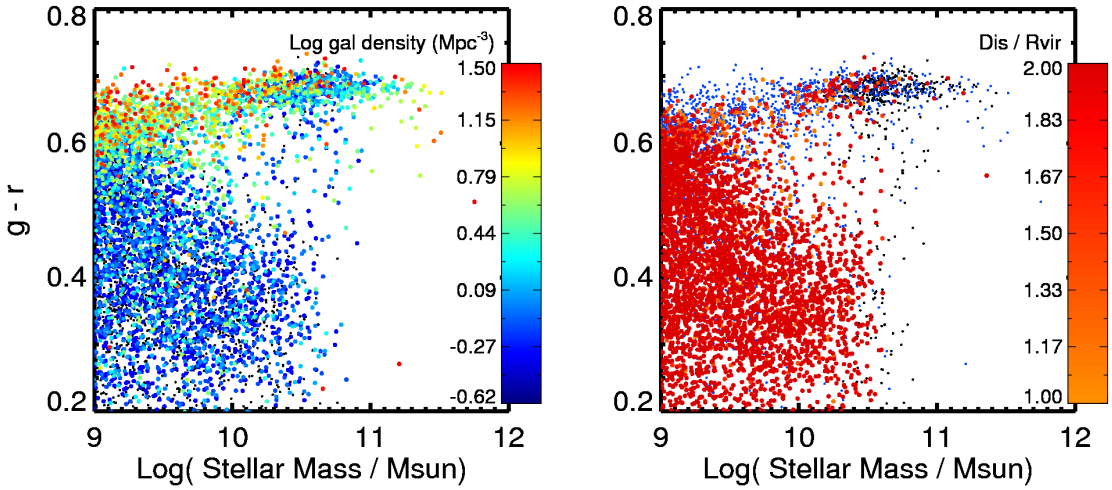

Figure 4.4 CMDs with galaxies color-coded by the local galaxy density (left) and the distance to the closest massive halo (right). Local galaxy density is computed by counting the number of galaxies within a radius of 1 Mpc. "Massive" halos are defined by a mass of $10^{12} M_{\odot}$, as found using a spherical overdensity algorithm. This is roughly the mass at which a halo is dominated by hot gas ($> 250,000$ K). Black points are galaxies at the centers of their (massive) halos, blue points are within the virial radius of a massive halo, and red points are outside the virial radius of the nearest massive halo. Massive red sequence galaxies tend to live in less dense environments than low-mass ones. Low-mass galaxies only become red when in the presence of a larger halo that can support a virial shock.

masses will live in hot halos at early times.

As the universe evolves, additional galaxies and halos newly grow large enough to support hot halos. Massive galaxies continue to move onto the red sequence. Our hot gas fraction cutoff of 60% corresponds to a stellar mass of about $10^{10.5} M_{\odot}$. Once galaxies exceed this stellar mass, they will tend to migrate toward the red sequence.

At the same time, satellite galaxies will enter the halos of more massive quenched galaxies. These satellites, embedded in the hot gas of their larger parent halo, undergo quenching as well. As massive group and cluster halos continue to accrete mass, they will add satellite galaxies that become quenched by the hot intragroup medium.

We illustrate these environmental effects in Figure 4.4. On the left we show a color-mass diagram where the galaxies are color-coded by their local galaxy density. We calculate the density measure simply by counting the number of simulated galaxies within 1 Mpc of the galaxy of interest. The resulting trend is clear: massive red sequence galaxies live in less dense environments than their less massive analogs. This is because massive galaxies in the field, once massive enough, can get to the red sequence "on their own" by forming their own hot halos. Less massive galaxies, in order to be quenched, have no alternative to living in the hot environment of more massive neighbors.

In the right panel of Figure 4.4 we color-code galaxies by the distance to the nearest halo with a mass $> 10^{12} M_{\odot}$. This is roughly the halo mass where hot halos will form independently in our simulations. Black points are for galaxies within $10h^{-1}$ Mpc of the centers of massive halos, blue points are for galaxies within the virial radius of such halos, and red points are for galaxies outside those halos' virial radii. For each galaxy, we calculate $d_i/R_{\mathrm{vir},i}$, the ratio of its distance

from the center of each halo i to that halo's virial radius, and we use the minimum value over all i. The color-coded distance is $(d/R_{\rm vir})_{\rm min}$ for those galaxies where that quantity is > 1. Massive red galaxies are typically within such halos. A substantial number of lower-mass galaxies, however, lie outside the virial radius of the nearest massive hot halo, yet they've managed to become red galaxies. Combined with the density plot on the left, this suggests a larger environmental effect – these galaxies are part of super-group structures. Although these large structures have not fully virialized, the effects of hot intergalactic gas can be felt beyond the virial radius of member galaxies. This result suggests more generally that environmental factors beyond the halo play a significant role in galaxy evolution. Observations have suggested a role for environment in some galaxy properties (Cooper et al., 2008a,b, 2010), and our simulations indicate that environment may be important for the quenching of star-formation.

4.3.4 Mergers and growth along the red sequence

As demonstrated above, a galaxy does not stop evolving once it reaches the red sequence. Its existing stellar population ages, that population sheds mass via stellar winds, and it obtains new stars (and gas) via mergers. Here we show that massive galaxies, which are quenched at early times ($z > 1$), often grow by factors of a few between quenching and the present day. In contrast, low-mass galaxies tend to lose mass through stellar mass loss without undergoing significant mass growth via mergers.

The top panel of Figure 4.5 shows, as a function of the $z = 0$ stellar mass, the fractional mass growth of red sequence galaxies between the redshift of quenching and the present day, $M_{\rm stellar}(z = 0)/M_{\rm stellar}(z = z_{\rm quenched})$. Since much of the red sequence growth occurs at late times, most galaxies have not changed much in stellar mass since being quenched (indicated by the dark shading along the

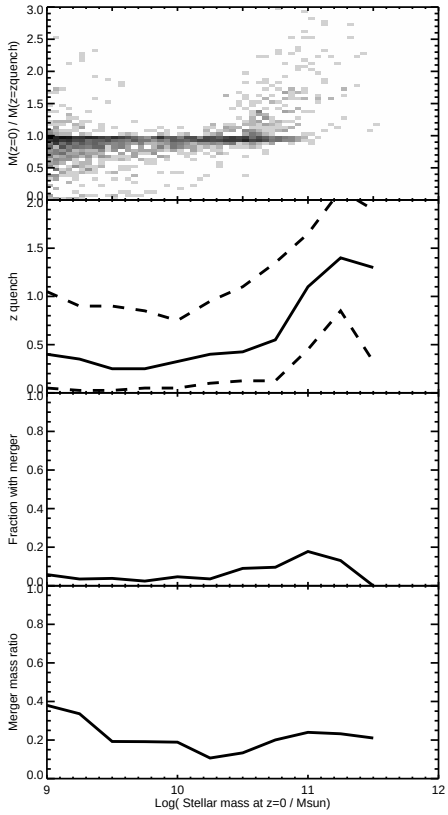

Figure 4.5 Growth of galaxies along the red sequence. **Top Panel:** fractional mass growth of red sequence galaxies since the redshift at which they were quenched, as a function of stellar mass at $z = 0$. **Second Panel** (from the top): median (solid line) and 90th percentiles of the redshift at which galaxies were quenched in different mass bins. **Third Panel** (from the top): the fraction of galaxies per bin that have undergone at least one major merger since being quenched. **Bottom Panel**: among galaxies that became red before $z = 0.5$, the mass-weighted average merger mass ratio. In our model, the most massive galaxies typically grew by factors of a few since being quenched at $z \sim 1$, and that mass growth is dominated by minor mergers.

$y = 1$ line). A significant proportion of galaxies with $M > 10^{10.5} M_{\odot}$, however, have grown substantially, by factors ~ 3. As shown in the second panel of Figure 4.5 these massive galaxies have been red for longer, typically since $z \sim 1$. With this ~ 7 Gyr baseline for growth, combined with the fact that these massive galaxies reside at the centers of groups, they have more opportunities to acquire mass through mergers than smaller red galaxies.

To further explore the nature of post-quenching mass growth in our model, we separate major mergers (those with a mass ratio smaller than 3:1) and minor mergers (any merger with a larger mass ratio). We include in the minor merger component accretion of existing stars that do not live in well-resolved galaxies, but changing this has little impact on the results. The third panel of Figure 4.5 shows the fraction of $z = 0$ red sequence galaxies that have undergone at least one major merger since being quenched. Post-quenching major mergers are very rare for galaxies at masses $< 10^{10} M_{\odot}$, but become more common for masses $> 10^{11} M_{\odot}$. This is a natural consequence of the typical time since quenching. Even at the peak around $10^{11} M_{\odot}$, though, only $\sim 20\%$ of galaxies have undergone at least one major merger since being quenched. Given that many of these galaxies have grown by factors > 2 in mass (and undergone stellar mass loss), this result immediately suggests that minor mergers play a crucial role in the growth of massive red galaxies.

The bottom panel of Figure 4.5 shows the mean mass-weighted merger mass ratio as a function of $z = 0$ stellar mass. Here we only include galaxies that became red at $z > 0.5$ to obtain a substantial time baseline over which to assess the relative contribution of major versus minor mergers. Using a cutoff at $z = 1$ does little to change the results. The typical merger mass ratio in our simulations is ~ 0.2, below the typical $1/3$ cutoff for major mergers. Our simulated value

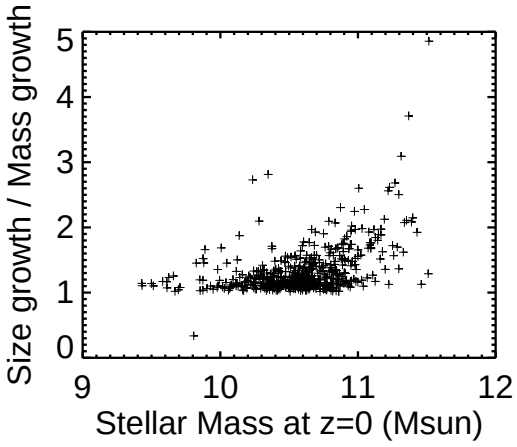

Figure 4.6 The ratio of size growth to mass growth for red sequence galaxies as a function of their stellar mass at $z = 0$. We show only galaxies that have undergone mergers, major or minor, since being quenched. In some rare cases the galaxy size may evolve several times (~ 3) more than the mass. This is roughly in line with observations, where the ratio is typically ~ 2 for evolution since $z \sim 2$.

agrees with the higher-resolution simulations of Oser et al. (2011). At all stellar masses, red galaxy mass growth is dominated by minor mergers.

In summary, massive red galaxies in our simulation grow by factors of several in mass between the time they are quenched (typically $z \sim 1$) and redshift 0. This mass growth is dominated by minor mergers, although major mergers contribute significantly to the growth.

4.3.5 Size evolution of passive galaxies

Observations indicate that massive red galaxies are more compact at $z > 1 - 2$ than at $z \sim 0$ by typical factors of 6 or more (Toft et al., 2007; van der Wel et al., 2008; van Dokkum et al., 2008). While observational biases presented an initial concern, recent work suggests that much of the evolution must be physi-

cal, and probably arises from a combination of several physical processes. These processes include adiabatic expansion associated with mass loss of stars, major mergers, minor mergers, and evolution in mass-to-light ratios (Naab et al., 2009; Hopkins et al., 2010).

The resolution of our simulations is not well-suited to study the structure of individual galaxies. Instead, we can use simple analytic estimates to approximate the size growth simulated galaxies might undergo. We construct a simple model for the effects of mergers based on the energy considerations of Naab et al. (2009) based on the virial theorem, and we ignore other processes that contribute to size evolution. Given a stellar accretion event (i.e. a merger) of mass M_a onto a galaxy of mass M_g, the ratio of final to initial size of the galaxy is given by:

$$\frac{r_f}{r_i} = \frac{(1+\eta)^2}{1+\eta\epsilon}. \tag{4.1}$$

Here, $\eta = M_a/M_g$ is the fractional mass increase, and $\epsilon =< v_a^2 > / < v_g^2 >$ is the ratio of the two galaxies' stellar populations' mean square speeds. This relation stems from a simple application of the virial theorem and an assumption that total energy is conserved.

To use this model, we must estimate the mass ratio and the velocity dispersion ratio between the satellite (i.e. less massive) and central (more massive) galaxies. We know the ratio of stellar masses directly from the simulations, and we use an observational relation between stellar mass and velocity dispersion for elliptical galaxies from Gallazzi et al. (2006): $\log\sigma = -0.895 + 0.286\log M_{\rm stellar}$. With this relation, $\epsilon = (\sigma_a/\sigma_g)^2 = (M_a/M_g)^{0.57}$. Thus, for each merger event, we can calculate the fractional size growth of the remnant galaxy. Taking each $z = 0$ red galaxy, we consider its entire merger history since being quenched. We account for the size growth of each of its merger events and multiply them to find the galaxy's total fractional mass growth.

We show the results of this exercise in Figure 4.6. Instead of the actual size growth, r_f/r_i, we plot this quantity as a ratio of the stellar mass growth, M_f/M_i. We have already shown that massive red galaxies in our simulations grow by too large a factor between quenching and $z = 0$, and that growth is driven by mergers. This "extra" merging would naturally cause our size growth estimates to be too high, so we account for this difficulty by comparing the size growth relative to the mass growth of galaxies.

Based on this simple modeling, minor mergers appear to be numerous enough to drive the factors of several in size growth of passive galaxies over time. Galaxies with stellar masses $> 10^{11} M_{\odot}$ show typical size growth a factor of 2 greater than their mass growth, indicating that a series of minor mergers tends puff up these galaxies. Lower mass galaxies, typically recently quenched, have not changed as much since moving onto the red sequence. These results, using a simple analytic model, are broadly consistent with the idea that minor mergers dominate the size growth of massive red galaxies.

4.4 Summary and Conclusion

We have analyzed a cosmological hydrodynamic simulation to explore the evolution of the red sequence. A key feature of our simulation is a simple quenching prescription tied to the presence of hot gas. Galaxies whose halos are dominated by hot gas are starved of star-forming fuel by heating the circum-galactic medium. This simple model yields number densities of red sequence galaxies that agree with observations (Gabor et al., 2011), and provides a tool for studying the emergence and growth of the red sequence over cosmic time. While some details of our model may disagree with observations, it serves as a representative of a general class of quenching models where quenching is driven by hot coronae

or tied to halo mass.

We found that the first galaxies to turn red at $z \gtrsim 2$ are among the most massive in the universe (at that epoch), $M_{\rm stellar} \sim 10^{10.5-11} M_{\odot}$. While massive red galaxies grow in number, less massive $\sim 10^{10} M_{\odot}$ ones lag behind, leaving an apparent dip in the red galaxy mass function at high redshift. This dearth of low-mass red galaxies is consistent with a observations at moderate ($\lesssim 1$) and high redshift ($z \gtrsim 2-3$). At later times, the number of moderate-mass red galaxies catches up to the number of more massive ones, so that the dip in the red galaxy mass function is less pronounced by $z = 0$.

Essentially all simulated red galaxies with stellar mass $> 10^{11} M_{\odot}$ form from smaller red galaxies that grow mass via mergers once on the red sequence. This massive end of the red sequence does not emerge until $z \sim 1.5$, and it grows in number by factors of several at late times. This rapid evolution of the massive end of the mass function appears to conflict with observations indicating that massive red galaxies are in place at $z > 1$.

Most of the mass growth of individual red galaxies is due to minor mergers, with major mergers being rare and a sub-dominant component of mass growth. Based on a simple analytic model, these numerous minor mergers can lead to size growth that is a factor of 2 or more times that of a galaxy's corresponding mass growth. This suggests that minor mergers dominate the dramatic size evolution of massive galaxies, in accordance with earlier work (Naab et al., 2009; Hopkins et al., 2010).

CHAPTER 5

CONCLUSION

The results of our quenching models are highly suggestive that hot gaseous coronae play a crucial role in quenching star-formation. Simply by cutting off the fuel supply for galaxies embedded in hot halos, we were able to match the observed red galaxy luminosity and mass functions at $z = 0$. Despite the fact that there are enough mergers to explain the numbers of red sequence galaxies in a merger quenching scenario, our simulations indicate that gas from the IGM will re-fuel merger remnant galaxies. Mergers thus play a secondary role in forming the red sequence.

As we have seen, though, critical problems remain in our favored quenching model. The energy required to offset cooling is extreme. The formation of massive blue galaxies is stifled by the sharp cutoff in hot gas fraction. Massive red galaxies are not numerous enough at high redshifts, and they grow too much over cosmic time. These problems may be addressed by future models that incorporate new observational and theoretical constraints.

5.1 What next?

A realistic model for quenching star-formation in cosmological simulations remains elusive. Since the presence of hot coronae is critical, the next major step is to develop a successful model for the heating of these coronae. We have implemented a series of preliminary heating models associated with AGN feedback, but even reproducing the successes of Chapter 2 has proved difficult.

In an attempt to simplify matters, we trigger feedback at semi-regular intervals in all galaxies, and determine the AGN feedback luminosity using a simple

scaling law. We add a burst of feedback energy every time we run the galaxy finder algorithm, roughly every 10^7 years. For the feedback energy, we use the successful SAM of Croton et al. (2006) as a guide: the AGN luminosity scales with the mass of hot gas in the halo and the mass of the black hole. Since we do not track black hole growth, we assume that the local $M_{\rm BH} - M_{\rm bulge}$ (Bennert et al., 2010) relation holds for all galaxies, and we use a simple relation between halo mass and bulge fraction from De Lucia et al. (2010). Thus we determine the AGN luminosity from a galaxy's stellar mass and the mass of hot gas in its halo, combined with a free-parameter normalization.

From this starting point we tried a variety of methods for distributing the feedback energy. The simplest is to deposit the energy equally into all gas particles within some radius, typically a few resolution elements. This seems inappropriate for feedback from a radio AGN, however, which is unlikely to drastically affect cold dense gas in a galaxy and more effective at heating diffuse intracluster gas. So we developed other models that distribute the thermal energy over tens of kpc. In the end, these energy distribution models perform differently from one another, but none performs satisfactorily. In some cases a distinct red sequence does not form. The best cases, in which a reasonable red sequence forms, require two orders of magnitude more energy than the values used by Croton et al. (2006) (which are in line with observational estimates of radio AGN luminosity functions).

One potentially big problem with our simulations is the inhomogeneity of the hot circum-galactic medium. This effect arises in all our models, even without quenching. Our cooling and star-formation feedback prescriptions generate halos where thermal energy and metals are highly clumped – within the diffuse hot halo there are many small, isolated, cold, metal-rich clumps. These clumps

frequently form at the resolution limit of our simulations. Their metal-richness increases their cooling rates, and since they are already cold (typically $\sim 1-2$ orders of magnitude colder than the hot intra-group medium) they quickly reach the cooling floor at $\sim 10^4$ K. Being cold, they easily fall onto the central galaxy and fuel star-formation. In massive galaxies with hot halos, such cold clumps fuel much, if not most, of the star-formation.

Where do these cold clumps come from? Most of the cold clumps ultimately result from galactic-scale winds driven by star-formation. Our wind prescription launches individual gas particles from star-forming regions. Star-forming regions are highly metal enriched (relative to the "pristine" IGM), so the ejected gas carries metals into the IGM. Since an individual ejected gas particle retains its metals, it cools more quickly than metal-poor IGM and eventually returns to fuel star-formation in the galaxy. Some of the cold clumps have another origin, dubbed "cold drizzle" in Kereš et al. (2009) but not fully understood. These come from the $\sim 10^4$ K filaments in the IGM that feed the halos. We typically expect the hot halo gas to shock-heat such infalling filamentary gas, but the code does not always do so. This may be because the shocks are poorly resolved in the simulations and the SPH shock algorithm is not robust on these scales. Or it may relate to the fact that most gas processes are smoothed over many particles, but cooling is performed on a particle-by-particle basis. In any case, cold clumps are difficult to heat up through most feedback mechanisms. Shocks induced by an AGN jet, for example, are more effective at heating diffuse gas and sustaining hot gas at high temperature, rather than heating gas clumps by two orders of magnitude (Voit & Donahue, 2005).

Are the cold clumps physically realistic? One immediate clue that they are not realistic is that they form at the resolution scale, i.e. from a single gas particle. On

the other hand, the cooling instability may give rise to similar clumps in nature. In this scenario a slightly overdense perturbation in an otherwise uniform halo will cool faster than its surroundings since cooling increases with density. Cooling decreases the clump's internal pressure, so it contracts, getting denser and thus cooling even faster in a runaway cycle. This cooling instability can be suppressed if hotter surrounding gas can efficiently share thermal energy with any given clump, via conduction or turbulent mixing. Observational characterization of the clumpiness of the intra-group and intra-cluster medium is rare, but may be a worthy pursuit to constrain hydrodynamic models like ours.

The realization that turbulence may suppress clump formation, and by extension star-formation, has led to another pursuit: sub-resolution mixing. We have implemented a simple analytic mixing scheme inspired by the Kelvin-Helmholtz instability. Early tests show that the scheme does help disrupt clumps. A determination of whether this treatment is realistic, and whether it substantially influences galaxy properties, awaits future tests.

References

Abadi M. G., Moore B., Bower R. G., 1999, MNRAS, 308, 947

Adelman-McCarthy J. K., Agüeros M. A., Allam S. S. et al., 2008, ApJS, 175, 297

Agertz O., Moore B., Stadel J. et al., 2007, MNRAS, 380, 963

Arrigoni M., Trager S. C., Somerville R. S., Gibson B. K., 2009, MNRAS, 1814

Asplund M., Grevesse N., Sauval A. J., 2005, in Astronomical Society of the Pacific Conference Series, Vol. 336, Cosmic Abundances as Records of Stellar Evolution and Nucleosynthesis, T. G. Barnes III & F. N. Bash, ed., pp. 25–+

Bahcall J. N., Kirhakos S., Saxe D. H., Schneider D. P., 1997, ApJ, 479, 642

Baldry I. K., Glazebrook K., Brinkmann J., Ivezić Ž., Lupton R. H., Nichol R. C., Szalay A. S., 2004, ApJ, 600, 681

Baldry I. K., Balogh M. L., Bower R. G., Glazebrook K., Nichol R. C., Budavari T., 2006, MNRAS, 373, 469

Baldry I. K., Glazebrook K., Driver S. P., 2008, MNRAS, 388, 945

Baldwin J. A., Phillips M. M., Terlevich R., 1981, PASP, 93, 5

Balogh M. L., Navarro J. F., Morris S. L., 2000, ApJ, 540, 113

Balogh M. L., Baldry I. K., Nichol R., Miller C., Bower R., Glazebrook K., 2004, ApJ, 615, L101

Balogh M. L., Miller C., Nichol R., Zabludoff A., Goto T., 2005, MNRAS, 360, 587

Banerji M., Ferreras I., Abdalla F. B., Hewett P., Lahav O., 2009, ArXiv e-prints

Barger A. J., Cowie L. L., Mushotzky R. F., Yang Y., Wang W., Steffen A. T., Capak P., 2005, AJ, 129, 578

Barnes J. E., 1988, ApJ, 331, 699

—, 1989, Nature, 338, 123

—, 1990, Nature, 344, 379

Barnes J. E., Hernquist L., 1992, ARA&A, 30, 705

Bauer F. E., Fabian A. C., Sanders J. S., Allen S. W., Johnstone R. M., 2005, MNRAS, 359, 1481

Baugh C. M., Lacey C. G., Frenk C. S., Granato G. L., Silva L., Bressan A., Cole S., 2005, MNRAS, 356, 1191

Beckwith S. V. W. et al., 2006, AJ, 132, 1729

Bekki K., Couch W. J., Shioya Y., 2002, ApJ, 577, 651

Bell E. F., McIntosh D. H., Barden M. et al., 2004a, ApJ, 600, L11

Bell E. F., Wolf C., Meisenheimer K. et al., 2004b, ApJ, 608, 752

Bennert N., Canalizo G., Jungwiert B., Stockton A., Schweizer F., Peng C. Y., Lacy M., 2008, ApJ, 677, 846

Bennert V. N., Auger M. W., Treu T., Woo J., Malkan M. A., 2010, ArXiv e-prints

Benson A. J., Lacey C. G., Baugh C. M., Cole S., Frenk C. S., 2002, MNRAS, 333, 156

Best P. N., Kaiser C. R., Heckman T. M., Kauffmann G., 2006, MNRAS, 368, L67

Binney J., 1977, ApJ, 215, 483

Binney J., Tabor G., 1995, MNRAS, 276, 663

Birnboim Y., Dekel A., 2003, MNRAS, 345, 349

Birnboim Y., Dekel A., Neistein E., 2007, MNRAS, 380, 339

—, 2010, ArXiv e-prints

Blake C., Pracy M. B., Couch W. J. et al., 2004, MNRAS, 355, 713

Blanton M. R. et al., 2003, ApJ, 594, 186

Blanton M. R., Schlegel D. J., Strauss M. A. et al., 2005, AJ, 129, 2562

Blanton M. R., 2006, ApJ, 648, 268

Blanton M. R., Roweis S., 2007, AJ, 133, 734

Blumenthal G. R., Faber S. M., Primack J. R., Rees M. J., 1984, Nature, 311, 517

Booth C. M., Schaye J., 2009, MNRAS, 398, 53

—, 2010, MNRAS, 405, L1

Bournaud F., Combes F., Jog C. J., 2004, A&A, 418, L27

Bournaud F., Jog C. J., Combes F., 2007, A&A, 476, 1179

Bower R. G., Kodama T., Terlevich A., 1998, MNRAS, 299, 1193

Bower R. G., Benson A. J., Malbon R., Helly J. C., Frenk C. S., Baugh C. M., Cole S., Lacey C. G., 2006, MNRAS, 370, 645

Brammer G. B. et al., 2009, ApJ, 706, L173

Brooks A. M., Governato F., Quinn T., Brook C. B., Wadsley J., 2009, ApJ, 694, 396

Brook C. B. et al., 2011, MNRAS, 595

Brown M. J. I., Dey A., Jannuzi B. T., Brand K., Benson A. J., Brodwin M., Croton D. J., Eisenhardt P. R., 2007, ApJ, 654, 858

Brown M. J. I., Zheng Z., White M. et al., 2008, ApJ, 682, 937

Bruzual G., Charlot S., 2003, MNRAS, 344, 1000

Brüggen M., Ruszkowski M., Hallman E., 2005, ApJ, 630, 740

Brüggen M., Scannapieco E., 2009, MNRAS, 398, 548

Brüggen M., Scannapieco E., Heinz S., 2009, MNRAS, 395, 2210

Bundy K. et al., 2010, ApJ, 719, 1969

Burns J. O., 1990, AJ, 99, 14

Bîrzan L., Rafferty D. A., McNamara B. R., Wise M. W., Nulsen P. E. J., 2004, ApJ, 607, 800

Calzetti D., Armus L., Bohlin R. C., Kinney A. L., Koornneef J., 2000, ApJ, 533, 682

Canalizo G., Stockton A., 2001, ApJ, 555, 719

Carlberg R. G., 1984, ApJ, 286, 403

Cattaneo A., Dekel A., Devriendt J., Guiderdoni B., Blaizot J., 2006, MNRAS, 370, 1651

Chabrier G., 2003, ApJ, 586, L133

Charlot S., Worthey G., Bressan A., 1996, ApJ, 457, 625

Chieffi A., Limongi M., 2004, ApJ, 608, 405

Churazov E., Brüggen M., Kaiser C. R., Böhringer H., Forman W., 2001, ApJ, 554, 261

Churazov E., Sazonov S., Sunyaev R., Forman W., Jones C., Böhringer H., 2005, MNRAS, 363, L91

Ciotti L., Ostriker J. P., 1997, ApJ, 487, L105+

—, 2001, ApJ, 551, 131

Cisternas M. et al., 2011, ApJ, 726, 57

Coil A. L., Newman J. A., Croton D. et al., 2008, ApJ, 672, 153

Colberg J. M., Di Matteo T., 2008, MNRAS, 387, 1163

Cole S., 1991, ApJ, 367, 45

Cole S., Aragon-Salamanca A., Frenk C. S., Navarro J. F., Zepf S. E., 1994, MNRAS, 271, 781

Cole S., Lacey C. G., Baugh C. M., Frenk C. S., 2000, MNRAS, 319, 168

Conroy C., Ho S., White M., 2007, MNRAS, 379, 1491

Conroy C., Gunn J. E., White M., 2009, ApJ, 699, 486

Cool R. J., Eisenstein D. J., Johnston D., Scranton R., Brinkmann J., Zehavi I., 2006, AJ, 131, 736

Cool R. J., Eisenstein D. J., Fan X. et al., 2008, ApJ, 682, 919

Cooper M. C., Newman J. A., Croton D. J. et al., 2006, MNRAS, 370, 198

Cooper M. C., Newman J. A., Coil A. L. et al., 2007, MNRAS, 376, 1445

Cooper M. C., Newman J. A., Weiner B. J., Yan R., Willmer C. N. A., Bundy K., Coil A. L., Conselice C. J., Davis M., Faber S. M., Gerke B. F., Guhathakurta P., Koo D. C., Noeske K. G., 2008a, MNRAS, 383, 1058

Cooper M. C., Tremonti C. A., Newman J. A., Zabludoff A. I., 2008b, MNRAS, 390, 245

Cooper M. C., Gallazzi A., Newman J. A., Yan R., 2009, ArXiv e-prints

Cooper M. C. et al., 2010, MNRAS, 409, 337

Cowie L. L., Songaila A., Hu E. M., Cohen J. G., 1996, AJ, 112, 839

Cowie L. L., Barger A. J., 2004, in Astrophysics and Space Science Library, Vol. 308, Supermassive Black Holes in the Distant Universe, A. J. Barger, ed., pp. 273–+

Cox T. J., Primack J., Jonsson P., Somerville R. S., 2004, ApJ, 607, L87

Cox T. J., Dutta S. N., Di Matteo T., Hernquist L., Hopkins P. F., Robertson B., Springel V., 2006a, ApJ, 650, 791

Cox T. J., Jonsson P., Primack J. R., Somerville R. S., 2006b, MNRAS, 373, 1013

Crain R. A., McCarthy I. G., Frenk C. S., Theuns T., Schaye J., 2010a, MNRAS, 407, 1403

Crain R. A., McCarthy I. G., Schaye J., Frenk C. S., Theuns T., 2010b, ArXiv e-prints

Crawford C. S., Allen S. W., Ebeling H., Edge A. C., Fabian A. C., 1999, MNRAS, 306, 857

Croft R. A. C., Di Matteo T., Springel V., Hernquist L., 2009, MNRAS, 1486

Croton D. J. et al., 2006, MNRAS, 365, 11

Daddi E. et al., 2005, ApJ, 626, 680

Dasyra K. M., Tacconi L. J., Davies R. I. et al., 2006, ApJ, 638, 745

David L. P. et al., 2010, ArXiv e-prints

Davis M., Geller M. J., 1976, ApJ, 208, 13

Davis M., Efstathiou G., Frenk C. S., White S. D. M., 1985, ApJ, 292, 371

Davé R., Finlator K., Oppenheimer B. D., 2006, MNRAS, 370, 273

—, 2007, in EAS Publications Series, Vol. 24, EAS Publications Series, E. Emsellem, H. Wozniak, G. Massacrier, J.-F. Gonzalez, J. Devriendt, & N. Champavert, ed., pp. 183–189

Davé R., Oppenheimer B. D., Finlator K., 2011, ArXiv e-prints

De Lucia G., Kauffmann G., White S. D. M., 2004, MNRAS, 349, 1101

De Lucia G., Boylan-Kolchin M., Benson A. J., Fontanot F., Monaco P., 2010, MNRAS, 406, 1533

De Young D. S., 2010, ApJ, 710, 743

DeBuhr J., Quataert E., Ma C., Hopkins P., 2009, ArXiv e-prints

DeBuhr J., Quataert E., Ma C., 2010, ArXiv e-prints

Degraf C., Di Matteo T., Springel V., 2010, MNRAS, 402, 1927

Dekel A., Birnboim Y., 2006, MNRAS, 368, 2

—, 2008, MNRAS, 383, 119

Dekel A., Sari R., Ceverino D., 2009, ApJ, 703, 785

Dekel A., Birnboim Y., Engel G., Freundlich J., Goerdt T., Mumcuoglu M., Neistein E., Pichon C., Teyssier R., Zinger E., 2009a, Nature, 457, 451

Di Matteo T., Quataert E., Allen S. W., Narayan R., Fabian A. C., 2000, MNRAS, 311, 507

Di Matteo T., Springel V., Hernquist L., 2005, Nature, 433, 604

Di Matteo T., Colberg J., Springel V., Hernquist L., Sijacki D., 2008, ApJ, 676, 33

Donahue M., Horner D. J., Cavagnolo K. W., Voit G. M., 2006, ApJ, 643, 730

Donahue M. et al., 2010, ApJ, 715, 881

Dressler A., 1980, ApJ, 236, 351

Drory N., Bender R., Feulner G., Hopp U., Maraston C., Snigula J., Hill G. J., 2003, ApJ, 595, 698

Drory N. et al., 2009, ApJ, 707, 1595

Dunn R. J. H., Allen S. W., Taylor G. B., Shurkin K. F., Gentile G., Fabian A. C., Reynolds C. S., 2010, MNRAS, 404, 180

Eggen O. J., Lynden-Bell D., Sandage A. R., 1962, ApJ, 136, 748

Ellison S. L., Patton D. R., Simard L., McConnachie A. W., 2008, ApJ, 672, L107

Erb D. K., Shapley A. E., Pettini M., Steidel C. C., Reddy N. A., 2006, ApJ, 644, 813

Faber S. M. et al., 2007, ApJ, 665, 265

Fabian A. C., Nulsen P. E. J., Canizares C. R., 1984, Nature, 310, 733

Fabian A. C., 1994, ARA&A, 32, 277

Fabian A. C. et al., 2000, MNRAS, 318, L65

Fabian A. C., Sanders J. S., Allen S. W., Crawford C. S., Iwasawa K., Johnstone R. M., Schmidt R. W., Taylor G. B., 2003, MNRAS, 344, L43

Fabian A. C., Sanders J. S., Taylor G. B., Allen S. W., Crawford C. S., Johnstone R. M., Iwasawa K., 2006, MNRAS, 366, 417

Fardal M. A., Katz N., Gardner J. P., Hernquist L., Weinberg D. H., Davé R., 2001, ApJ, 562, 605

Ferrarese L., Merritt D., 2000, ApJ, 539, L9

Feruglio C., Maiolino R., Piconcelli E., Menci N., Aussel H., Lamastra A., Fiore F., 2010, ArXiv e-prints

Finlator K., Davé R., Papovich C., Hernquist L., 2006, ApJ, 639, 672

Finlator K., Davé R., Oppenheimer B. D., 2007, MNRAS, 376, 1861

Finlator K., Davé R., 2008, MNRAS, 385, 2181

Gabor J. M. et al., 2009, ApJ, 691, 705

Gabor J. M., Davé R., Finlator K., Oppenheimer B. D., 2010, MNRAS, 407, 749

—, 2011, MNRAS, in press

Gallagher III J. S., Ostriker J. P., 1972, AJ, 77, 288

Gallazzi A., Charlot S., Brinchmann J., White S. D. M., 2006, MNRAS, 370, 1106

Gebhardt K., Bender R., Bower G. et al., 2000, ApJ, 539, L13

Gelb J. M., Bertschinger E., 1994, ApJ, 436, 467

Georgakakis A. et al., 2009, MNRAS, 397, 623

Giodini S. et al., 2010, ApJ, 714, 218

Governato F., Willman B., Mayer L., Brooks A., Stinson G., Valenzuela O., Quinn T., 2007, MNRAS, 374, 1479

Governato F., Brook C. B., Brooks A. M. et al., 2009, MNRAS, 398, 312

Graves G. J., Faber S. M., Schiavon R. P., Yan R., 2007, ApJ, 671, 243

Graves G. J., Faber S. M., Schiavon R. P., 2009, ApJ, 693, 486

Grogin N. A., Conselice C. J., Chatzichristou E. et al., 2005, ApJ, 627, L97

Grogin N. A. et al., 2011, ArXiv e-prints

Gunn J. E., Gott J. R. I., 1972, ApJ, 176, 1

Guo F., Oh S. P., 2008, MNRAS, 384, 251

Heavens A., Panter B., Jimenez R., Dunlop J., 2004, Nature, 428, 625

Heinz S., Brüggen M., Young A., Levesque E., 2006, MNRAS, 373, L65

Hernquist L., 1989, Nature, 340, 687

Hicks A. K., Mushotzky R., 2005, ApJ, 635, L9

Hogg D. W., Baldry I. K., Blanton M. R., Eisenstein D. J., 2002, ArXiv Astrophysics e-prints

Hogg D. W. et al., 2002, AJ, 124, 646

Hopkins A. M., Beacom J. F., 2006, ApJ, 651, 142

Hopkins P. F., Hernquist L., Cox T. J., Robertson B., Springel V., 2006, ApJS, 163, 50

Hopkins P. F., Cox T. J., Kereš D., Hernquist L., 2008, ApJS, 175, 390

Hopkins P. F., Cox T. J., Dutta S. N., Hernquist L., Kormendy J., Lauer T. R., 2009, ApJS, 181, 135

Hopkins P. F., Somerville R. S., Cox T. J. et al., 2009, MNRAS, 397, 802

Hopkins P. F., Bundy K., Hernquist L., Wuyts S., Cox T. J., 2010, MNRAS, 401, 1099

Hubble E. P., 1926, ApJ, 64, 321

Hutchings J. B., Johnson I., Pyke R., 1988, ApJS, 66, 361

Johansson P. H., Naab T., Ostriker J. P., 2009, ApJ, 697, L38

Jones C., Forman W., Vikhlinin A., Markevitch M., David L., Warmflash A., Murray S., Nulsen P. E. J., 2002, ApJ, 567, L115

Jubelgas M., Springel V., Dolag K., 2004, MNRAS, 351, 423

Juneau S., Glazebrook K., Crampton D. et al., 2005, ApJ, 619, L135

Jungwiert B., Combes F., Palouš J., 2001, A&A, 376, 85

Katz N. S., 1989, PhD thesis, Princeton Univ., NJ.

Katz N., Hernquist L., Weinberg D. H., 1992, ApJ, 399, L109

Katz N., Weinberg D. H., Hernquist L., 1996, ApJS, 105, 19

Kauffmann G., White S. D. M., Guiderdoni B., 1993, MNRAS, 264, 201

Kauffmann G. et al., 2003, MNRAS, 341, 33

Kauffmann G., Heckman T. M., Tremonti C. et al., 2003a, MNRAS, 346, 1055

Kauffmann G., Heckman T. M., White S. D. M. et al., 2003c, MNRAS, 341, 54

Kaviraj S., Schawinski K., Devriendt J. E. G. et al., 2007, ApJS, 173, 619

Kennicutt Jr. R. C., 1998, ApJ, 498, 541

Kereš D., Katz N., Weinberg D. H., Davé R., 2005, MNRAS, 363, 2

Kereš D., Hernquist L., 2009, ApJ, 700, L1

Kereš D., Katz N., Fardal M., Davé R., Weinberg D. H., 2009, MNRAS, 395, 160

Kereš D., Katz N., Davé R., Fardal M., Weinberg D. H., 2009a, MNRAS, 396, 2332

Kewley L. J., Ellison S. L., 2008, ApJ, 681, 1183

Khochfar S., Ostriker J. P., 2008, ApJ, 680, 54

Kimm T., Somerville R. S., Yi S. K. et al., 2009, MNRAS, 394, 1131

Komatsu E. et al., 2009, ApJS, 180, 330

Kormendy J., Richstone D., 1995, ARA&A, 33, 581

Kriek M., van der Wel A., van Dokkum P. G., Franx M., Illingworth G. D., 2008, ApJ, 682, 896

Lake G., Carlberg R. G., 1988, AJ, 96, 1581

Larson R. B., Tinsley B. M., Caldwell C. N., 1980, ApJ, 237, 692

Lauer T. R., Faber S. M., Gebhardt K. et al., 2005, AJ, 129, 2138

Levine R., Gnedin N. Y., Hamilton A. J. S., 2010, ApJ, 716, 1386

Lu Y., Kereš D., Katz N., Mo H. J., Fardal M., Weinberg M. D., 2010, ArXiv e-prints

Machacek M., Nulsen P. E. J., Jones C., Forman W. R., 2006, ApJ, 648, 947

Madau P., Pozzetti L., Dickinson M., 1998, ApJ, 498, 106

Madgwick D. S., Lahav O., Baldry I. K. et al., 2002, MNRAS, 333, 133

Magorrian J., Tremaine S., Richstone D. et al., 1998, AJ, 115, 2285

Maiolino R., Nagao T., Grazian A. et al., 2008, A&A, 488, 463

Maller A. H., Katz N., Kereš D., Davé R., Weinberg D. H., 2006, ApJ, 647, 763

Maller A. H., Berlind A. A., Blanton M. R., Hogg D. W., 2009, ApJ, 691, 394

Marchesini D. et al., 2010, ApJ, 725, 1277

Martig M., Bournaud F., Teyssier R., Dekel A., 2009, ApJ, 707, 250

Martin C. L., 2005, ApJ, 621, 227

Mathews W. G., 2009, ApJ, 695, L49

McCarthy I. G. et al., 2010, MNRAS, 406, 822

McGaugh S. S., Schombert J. M., de Blok W. J. G., Zagursky M. J., 2009, ArXiv e-prints

McKee C. F., Ostriker J. P., 1977, ApJ, 218, 148

McLure R. J., Kukula M. J., Dunlop J. S., Baum S. A., O'Dea C. P., Hughes D. H., 1999, MNRAS, 308, 377

McNamara B. R. et al., 2000, ApJ, 534, L135

McNamara B. R., Nulsen P. E. J., Wise M. W., Rafferty D. A., Carilli C., Sarazin C. L., Blanton E. L., 2005, Nature, 433, 45

McNamara B. R., Rafferty D. A., Bîrzan L. et al., 2006, ApJ, 648, 164

McNamara B. R., Rohanizadegan M., Nulsen P. E. J., 2010, ArXiv e-prints

Mendygral P. J., O'Neill S. M., Jones T. W., 2011, ApJ, 730, 100

Mihos J. C., Hernquist L., 1996, ApJ, 464, 641

Mittal R., Hudson D. S., Reiprich T. H., Clarke T., 2009, A&A, 501, 835

Moore B., Lake G., Katz N., 1998, ApJ, 495, 139

Morsony B. J., Heinz S., Brüggen M., Ruszkowski M., 2010, MNRAS, 407, 1277

Moster B. P., Macciò A. V., Somerville R. S., Naab T., Cox T. J., 2011, MNRAS, 1064

Mo H. J., Mao S., White S. D. M., 1998, MNRAS, 295, 319

Mulchaey J. S., Jeltema T. E., 2010, ApJ, 715, L1

Murante G. et al., 2004, ApJ, 607, L83

Murray N., Quataert E., Thompson T. A., 2005, ApJ, 618, 569

Naab T., Johansson P. H., Ostriker J. P., 2009, ApJ, 699, L178

Narayan R., Quataert E., 2005, Science, 307, 77

Nulsen P. E. J., Jones C., Forman W. R., David L. P., McNamara B. R., Rafferty D. A., Bîrzan L., Wise M. W., 2007, in Heating versus Cooling in Galaxies and Clusters of Galaxies, H. Böhringer, G. W. Pratt, A. Finoguenov, & P. Schuecker , ed., pp. 210–+

Ocvirk P., Pichon C., Teyssier R., 2008, MNRAS, 390, 1326

Oemler A. J., 1974, ApJ, 194, 10

Oke J. B., 1974, ApJS, 27, 21

Oppenheimer B. D., Davé R., 2006, MNRAS, 373, 1265

—, 2008, MNRAS, 387, 577

—, 2009, MNRAS, 395, 1875

Oppenheimer B. D., Davé R., Finlator K., 2009, MNRAS, 396, 729

Oppenheimer B. D., Davé R., Kereš D., Fardal M., Katz N., Kollmeier J. A., Weinberg D. H., 2010, MNRAS, 406, 2325

Oser L., Naab T., Ostriker J. P., Johansson P. H., 2011, ArXiv e-prints

Padmanabhan N., Schlegel D. J., Finkbeiner D. P. et al., 2008, ApJ, 674, 1217

Parrish I. J., Quataert E., Sharma P., 2009, ApJ, 703, 96

Peebles P. J. E., 1982, ApJ, 263, L1

Peterson J. R., Fabian A. C., 2006, Phys. Rep., 427, 1

Phleps S., Peacock J. A., Meisenheimer K., Wolf C., 2006, A&A, 457, 145

Postman M., Geller M. J., 1984, ApJ, 281, 95

Pozzetti L., Cimatti A., Zamorani G. et al., 2003, A&A, 402, 837

Press W. H., Schechter P., 1974, ApJ, 187, 425

Quataert E., Narayan R., 2000, ApJ, 528, 236

Quilis V., Moore B., Bower R., 2000, Science, 288, 1617

Quillen A. C. et al., 2008, ApJS, 176, 39

Quintero A. D., Hogg D. W., Blanton M. R. et al., 2004, ApJ, 602, 190

Randall S. W. et al., 2010, ArXiv e-prints

Rees M. J., Ostriker J. P., 1977, MNRAS, 179, 541

Richstone D. O., 1976, ApJ, 204, 642

Richstone D., Ajhar E. A., Bender R. et al., 1998, Nature, 395, A14+

Robertson B., Bullock J. S., Cox T. J., Di Matteo T., Hernquist L., Springel V., 2006, ApJ, 645, 986

Rosati P., Borgani S., Norman C., 2002, ARA&A, 40, 539

Rudnick G. et al., 2009, ApJ, 700, 1559

Rupke D. S., Veilleux S., Sanders D. B., 2005, ApJS, 160, 115

Ruszkowski M., Brüggen M., Begelman M. C., 2004, ApJ, 615, 675

Ruszkowski M., Brüggen M., Begelman M. C., 2004a, ApJ, 611, 158

Ruszkowski M., Oh S. P., 2010, ApJ, 713, 1332

Ruszkowski M., Lee D., Bruggen M., Parrish I., Oh S. P., 2010, ArXiv e-prints

Salomé P. et al., 2006, A&A, 454, 437

Sanders D. B., Mirabel I. F., 1996, ARA&A, 34, 749

Sanders J. S., Fabian A. C., 2007, MNRAS, 381, 1381

—, 2008, MNRAS, 390, L93

Scannapieco E., Bildsten L., 2005, ApJ, 629, L85

Scannapieco E., Pichon C., Aracil B., Petitjean P., Thacker R. J., Pogosyan D., Bergeron J., Couchman H. M. P., 2006, MNRAS, 365, 615

Scannapieco E., Brüggen M., 2008, ApJ, 686, 927

Schawinski K., Kaviraj S., Khochfar S. et al., 2007, ApJS, 173, 512

Schawinski K., Virani S., Simmons B., Urry C. M., Treister E., Kaviraj S., Kushkuley B., 2009, ApJ, 692, L19

Schaye J., Dalla Vecchia C., Booth C. M. et al., 2009, ArXiv e-prints

Schaye J. et al., 2010, MNRAS, 402, 1536

Schmidt M., 1959, ApJ, 129, 243

Schmidt M., 1968, ApJ, 151, 393

Schweizer F., Seitzer P., 1992, AJ, 104, 1039

Searle L., Zinn R., 1978, ApJ, 225, 357

Sijacki D., Springel V., Di Matteo T., Hernquist L., 2007, MNRAS, 380, 877

Silk J., 1977, ApJ, 211, 638

Silk J., Rees M. J., 1998, A&A, 331, L1

Silverman J. D., Mainieri V., Lehmer B. D. et al., 2008, ApJ, 675, 1025

Silverman J. D. et al., 2009, ApJ, 696, 396

Simha V., Weinberg D. H., Davé R., Gnedin O. Y., Katz N., Kereš D., 2009, MNRAS, 399, 650

Smith E. P., Bohlin R. C., Bothun G. D., O'Connell R. W., Roberts M. S., Neff S. G., Smith A. M., Stecher T. P., 1997, ApJ, 478, 516

Soker N., 2006, New A, 12, 38

Somerville R. S., Primack J. R., Faber S. M., 2001, MNRAS, 320, 504

Somerville R. S., Hopkins P. F., Cox T. J., Robertson B. E., Hernquist L., 2008, MNRAS, 391, 481

Springel V., Hernquist L., 2003, MNRAS, 339, 289

—, 2005, ApJ, 622, L9

Springel V., Di Matteo T., Hernquist L., 2005, ApJ, 620, L79

Springel V., White S. D. M., Jenkins A. et al., 2005b, Nature, 435, 629

Springel V., 2005, MNRAS, 364, 1105

Strateva I. et al., 2001, AJ, 122, 1861

Stutz A. M., Papovich C., Eisenstein D. J., 2008, ApJ, 677, 828

Sun M., Jones C., Forman W., Vikhlinin A., Donahue M., Voit M., 2007, ApJ, 657, 197

Sun M., 2009, ApJ, 704, 1586

Sutherland R. S., Dopita M. A., 1993, ApJS, 88, 253

Sánchez-Blázquez P., Gibson B. K., Kawata D., Cardiel N., Balcells M., 2009, MNRAS, 1599

Sánchez S. F., Jahnke K., Wisotzki L. et al., 2004, ApJ, 614, 586

Taylor E. N., Franx M., van Dokkum P. G. et al., 2009, ApJ, 694, 1171

Teyssier R., Chapon D., Bournaud F., 2010, ApJ, 720, L149

Teyssier R., Moore B., Martizzi D., Dubois Y., Mayer L., 2011, MNRAS, 618

Thompson R. I., Weymann R. J., Storrie-Lombardi L. J., 2001, ApJ, 546, 694

Thompson R. I., 2002, ApJ, 581, L85

Thompson R. I., Eisenstein D., Fan X., Dickinson M., Illingworth G., 2006, ApJ, 647, 787

Toft S., van Dokkum P., Franx M., Thompson R. I., Illingworth G. D., Bouwens R. J., Kriek M., 2005, ApJ, 624, L9

Toft S. et al., 2007, ApJ, 671, 285

Toomre A., Toomre J., 1972, ApJ, 178, 623

Totani T., 2005, New Astronomy Review, 49, 205

Trager S. C., Worthey G., Faber S. M., Burstein D., Gonzalez J. J., 1998, ApJS, 116, 1

Trager S. C., Faber S. M., Worthey G., González J. J., 2000, AJ, 120, 165

Trager S. C., Faber S. M., Dressler A., 2008, MNRAS, 386, 715

Tremaine S., Gebhardt K., Bender R. et al., 2002, ApJ, 574, 740

Tremonti C. A., Heckman T. M., Kauffmann G. et al., 2004, ApJ, 613, 898

Tremonti C. A., Moustakas J., Diamond-Stanic A. M., 2007, ApJ, 663, L77

Trump J. R. et al., 2006, ApJS, 165, 1

Urrutia T., Lacy M., Becker R. H., 2008, ApJ, 674, 80

van der Wel A., Holden B. P., Zirm A. W., Franx M., Rettura A., Illingworth G. D., Ford H. C., 2008, ApJ, 688, 48

van der Wel A., Bell E. F., Holden B. P., Skibba R. A., Rix H.-W., 2010, ApJ, 714, 1779

van Dokkum P. G. et al., 2008, ApJ, 677, L5

van Dokkum P. G. et al., 2010, ApJ, 709, 1018

Vernaleo J. C., Reynolds C. S., 2006, ApJ, 645, 83

Voit G. M., Donahue M., 2005, ApJ, 634, 955

Voit G. M., 2005, Reviews of Modern Physics, 77, 207

Wang B., Heckman T. M., 1996, ApJ, 457, 645

Weiner B. J. et al., 2005, ApJ, 620, 595

Weinmann S. M., van den Bosch F. C., Yang X., Mo H. J., 2006, MNRAS, 366, 2

Weinmann S. M., Kauffmann G., van den Bosch F. C., Pasquali A., McIntosh D. H., Yang X., Guo Y., 2009, MNRAS, 394, 1213

Whitaker K. E. et al., 2010, ApJ, 719, 1715

White S. D. M., 1978, MNRAS, 184, 185

White S. D. M., Rees M. J., 1978, MNRAS, 183, 341

White S. D. M., Frenk C. S., Davis M., Efstathiou G., 1987, ApJ, 313, 505

White S. D. M., Frenk C. S., 1991, ApJ, 379, 52

Williams R. J., Quadri R. F., Franx M., van Dokkum P., Labbé I., 2009, ApJ, 691, 1879

Willmer C. N. A., Faber S. M., Koo D. C. et al., 2006, ApJ, 647, 853

Woods D. F., Geller M. J., Barton E. J., 2006, AJ, 132, 197

Xue Y. Q. et al., 2010, ApJ, 720, 368

Yang Y., Zabludoff A. I., Davé R., Eisenstein D. J., Pinto P. A., Katz N., Barton E. J., 2006, ApJ, 640, 539

Yang Y., Zabludoff A. I., Zaritsky D., Mihos J. C., 2008, ApJ, 688, 945

Yi S. K., Yoon S., Kaviraj S. et al., 2005, ApJ, 619, L111

Zabludoff A. I., Zaritsky D., Lin H., Tucker D., Hashimoto Y., Shectman S. A., Kirshner R. P., 1996, ApJ, 466, 104

Zakamska N. L., Narayan R., 2003, ApJ, 582, 162

Zehavi I., Zheng Z., Weinberg D. H. et al., 2005, ApJ, 630, 1

Zwicky I. F., 1942, ApJ, 95, 555